Supplementary Information for

Hydroxyl-radical-specific cascade photogeneration for oxygen-chain photocatalytic therapy

Qiang Liu,[a] Chenxu Yan,*[a] Xie Li,[b] Haiyang Huang,[a] Zheyu Fan,[b] Jizhan Zhang,[a] Weiwei Zhang,[ac] Ping Shi,[b] Yuzheng Zhao,[b] Zhiqian Guo,*[ab] and Wei-Hong Zhu [ac]

[a] Q. Liu, Dr. C. Yan, H. Huang, J. Zhang, Prof. Dr. W. Zhang, Prof. Dr. W.-H. Zhu, Prof. Dr. Z. Guo
Key Laboratory for Advanced Materials and Joint International Research Laboratory of Precision Chemistry and Molecular Engineering, Shanghai Key Laboratory of Functional Materials Chemistry, Feringa Nobel Prize Scientist Joint Research Center, Institute of Fine Chemicals, Frontiers Science Center for Materiobiology and Dynamic Chemistry, School of Chemistry and Molecular Engineering, East China University of Science and Technology, Shanghai 200237, China. E-mail: chenxuyan@ecust.edu.cn; guozq@ecust.edu.cn

[b] Dr. X. Li, Z. Fan, Prof. Dr. P. Shi, Prof. Dr. Y. Zhao, Prof. Dr. Z. Guo
Optogenetics & Synthetic Biology Interdisciplinary Research Center, Shanghai Frontiers Science Center of Optogenetic Techniques for Cell Metabolism, State Key Laboratory of Bioreactor Engineering, School of Pharmacy, East China University of Science and Technology, Shanghai 200237, China.

[c] Prof. Dr. W. Zhang, Prof. Dr. W.-H. Zhu
State Key Laboratory of Green Chemical Engineering and Industrial Catalysis, Center of Photosensitive Chemicals Engineering, East China University of Science and Technology, Shanghai 200237, China.

Contents

1. Experimental section

Materials and general methods

Unless specially stated, all solvents and chemicals were purchased from commercial suppliers in analytical grade and used without further purification. The ^{1}H NMR and ^{13}C NMR spectra were recorded on a Bruker AVANCE III 400MHz. High-resolution mass spectrometry (HRMS) data were obtained with a Thermo Fisher Q EXACTIVE Plus. Absorption spectra were collected on a Varian Cary 500 spectrophotometer, and fluorescence spectra measurements were performed on a Varian Cary Eclipse fluorescence spectrophotometer or a FLS1000 photoluminescence spectrometer. The single-crystal data were obtained with a Bruker D8 Venture X-Ray Diffractometer. Particle size was measured by dynamic light scattering with a Malvern Zetasizer Nano ZSE. Confocal fluorescence images were taken on a confocal laser scanning microscope (LEICA TCS SP8). *In vitro* photodynamic and photothermal experiments were implemented by a 635 nm laser (Beijing Blueprint Photoelectric Technology Co., Ltd.). Temperature change was monitored by a FOTRIC280 thermal imager. Cellular photodynamic experiments were implemented by a 660 nm laser (Beijing NBET Technology Co., Ltd.). ESR signals were measured with a Bruker EMX-8/2.7. Electrochemistry tests were taken on a CHI760E (CH Instruments Ins). Mass spectrometry data of gases were obtained with an Agilent 7890B-5977B. Flow cytometric analysis was carried out with a CytoFLEX Flow Cytometers (Beckman, USA). NIR-II fluorescence images were measured with a NIR-II imaging system MARS (ARTEMIS INTELLIGENT IMAGING, China). *In vivo* and *ex vivo* NIR-I fluorescence images were measured with an IVIS Lumina Series III (PerkinElmer, USA). Photoacoustic imaging was performed under a 3D optoacoustic imaging system (LOIS-3D, TomoWave Suzhou Medical Imaging Co., Ltd, China).

Synthesis

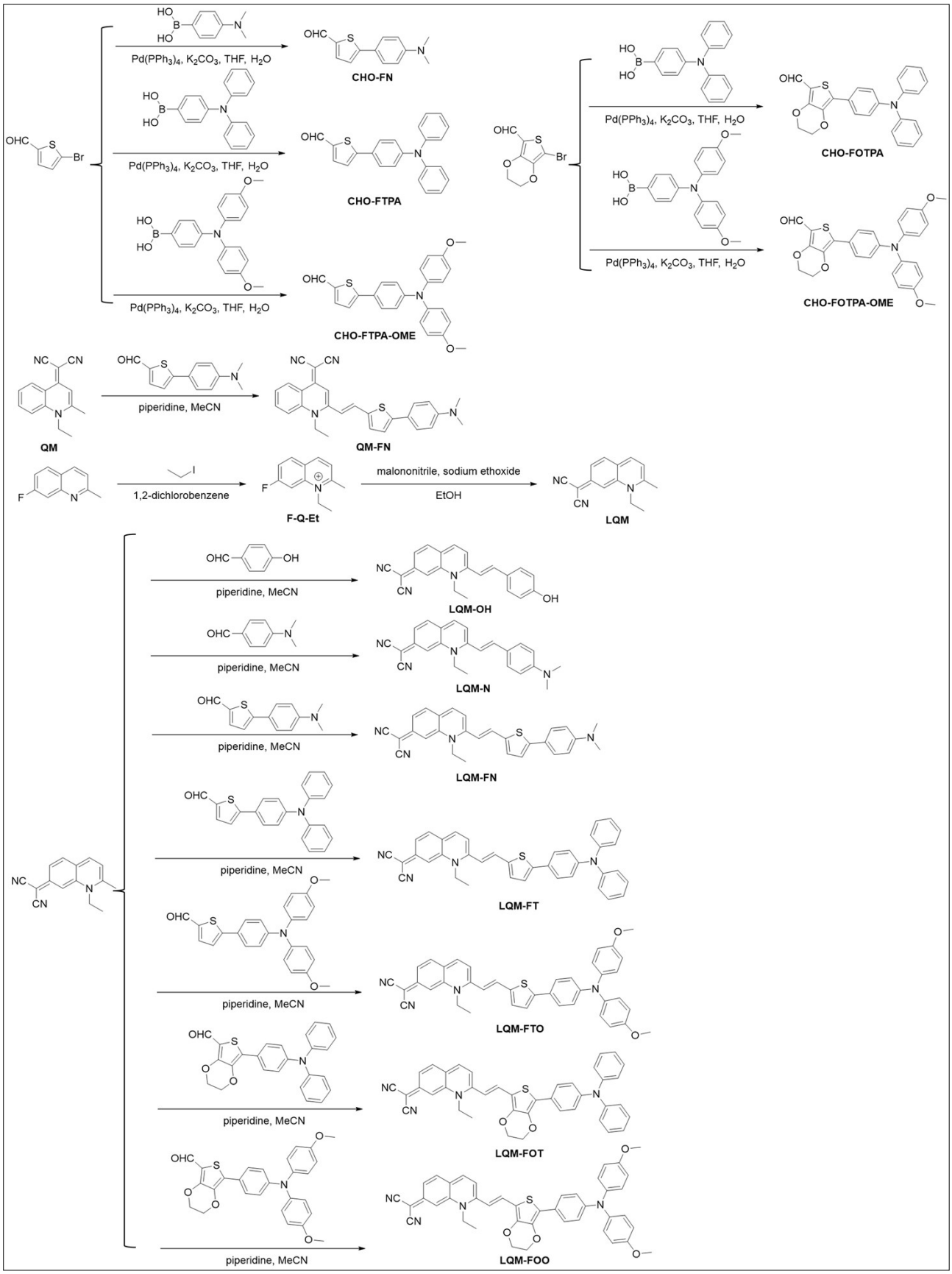

Figure S1. Synthesis route of LQM-Fluors.

Synthesis of F-Q-Et

7-Fluoro-2-Methylquinoline (1.00 g, 6.20 mmol) and iodoethane (2.90 g, 18.61 mmol) were dissolved in anhydrous 1,2-dichlorobenzene (3 mL). Then the mixture was stirred for 8 h at 140 °C under an argon atmosphere. The mixture was filtered after cooling to room temperature, and the filter cake was washed with 1,2-dichlorobenzene (5 mL × 3) before drying to afford F-Q-Et as a green solid (849 mg): Yield 43%.^{1}H NMR (400 MHz, DMSO-d_6, ppm) δ: 9.12 (d, J = 8.6 Hz, 1H, Ph-H), 8.52-8.59 (m, 2H, Ph-H), 8.11 (d, J = 8.5 Hz, 1H, Ph-H), 7.98 (td, J_1 = 2.2 Hz, J_2 = 8.7 Hz, 1H, Ph-H), 4.96 (q, J = 7.3 Hz, 2H, -NC***H***$_2$CH$_3$), 3.11 (s, 3H, -C***H***$_3$), 1.50 (t, J = 7.3 Hz, 3H, -NCH$_2$C***H***$_3$); ^{13}C NMR (100 MHz, DMSO-d_6, ppm) δ: 166.75, 164.22, 161.44, 145.49, 139.71, 139.58, 133.97, 133.86, 125.69, 125.00, 119.35, 119.10, 105.24, 104.96, 47.60, 22.38, 13.19; ^{19}F NMR (565 MHz, DMSO-d_6, ppm) δ: -98.52 (dd, J_1 = 7.9 Hz, J_2 = 17.5 Hz, 1F); Mass spectrometry (ESI-MS, m/z): [M - I]$^+$ calcd. for [$C_{12}H_{13}NFI$ - I]$^+$ 190.1027; found, 190.1021.

Synthesis of LQM

F-Q-Et (100 mg, 0.32 mmol) and malononitrile (52 mg, 0.79 mmol) were dissolved in anhydrous ethanol (1.2 mL). Then sodium ethoxide (64 mg, 0.94 mmol, dissolved in 1.2 mL anhydrous ethanol) was added dropwise at 0 °C. Then the mixture was stirred for 24 h at room temperature under an argon atmosphere. The solvent was removed under reduced pressure, and then the crude product was purified by silica gel chromatography (dichloromethane : methanol = 50:3, v:v) to afford LQM as a red solid (23 mg): Yield 31%.^{1}H NMR (400 MHz, DMSO-d_6, ppm) δ: 8.41 (d, J = 7.9 Hz, 1H, Ph-H), 7.82 (d, J = 8.9 Hz, 1H, Ph-H), 7.30-7.35 (m, 2H, Ph-H), 6.98 (s, 1H, Ph-H), 4.56 (q, J = 7.2 Hz, 2H, -NC***H***$_2$CH$_3$), 2.85 (s, 3H, -C***H***$_3$), 1.47 (t, J = 7.2 Hz, 3H, -NCH$_2$C***H***$_3$); ^{13}C NMR (100 MHz, DMSO-d_6, ppm) δ: 153.82, 151.92, 141.42, 140.86, 129.77, 124.92, 124.64, 120.99, 120.70, 115.96, 98.46, 45.14, 21.93, 12.60; Mass spectrometry (NSI-MS, m/z): [M + H]$^+$ calcd. for [$C_{15}H_{13}N_3$ + H]$^+$ 236.1182; found, 236.1172.

Synthesis of LQM-N

LQM (100 mg, 0.43 mmol) and *p*-dimethylaminobenzaldehyde (76 mg, 0.51 mmol) were dissolved in anhydrous acetonitrile (20 mL). Then piperidine (1.00 mL) was added. Then the mixture was refluxed for 24 h under an argon atmosphere. The solvent was removed under reduced pressure, and then the crude product was purified by silica gel chromatography (dichloromethane : methanol = 50:3, v:v) to afford LQM-N as a black solid (80 mg): Yield 51%.^{1}H NMR (400 MHz, DMSO-d_6, ppm) δ: 8.33 (d, J = 8.5 Hz, 1H, Ph-H), 7.87 (d, J = 15.5 Hz, 1H, alkene-H), 7.73-7.89 (m, 4H, Ph-H), 7.30 (d, J = 15.5 Hz, 1H, alkene-H), 7.25 (dd, J_1 = 1.4 Hz, J_2 = 8.7 Hz, 1H, Ph-H), 6.97 (s, 1H, Ph-H), 6.78 (d, J = 9.0 Hz, 2H, Ph-H), 4.67 (q, J = 6.7 Hz, 2H, -NC***H***$_2$CH$_3$), 3.04 (s, 6H, -N(C***H***$_3$)$_2$), 1.52 (t, J = 6.7 Hz, 3H, -NCH$_2$C***H***$_3$); ^{13}C NMR (100 MHz, DMSO-d_6, ppm) δ: 153.01, 151.99, 150.88, 144.82, 140.60, 140.39, 130.75, 130.22, 122.64, 122.47, 121.62, 113.66, 112.01, 111.72, 99.29, 54.88, 44.82, 12.68; Mass spectrometry (NSI-MS, m/z): [M + H]$^+$ calcd. for [$C_{24}H_{22}N_4$ + H]$^+$ 367.1917; found, 367.1912.

Synthesis of CHO-FN

5-bromo-2-thiophencarboxaldehyde (1.16 g, 6.11 mmol), 4-(dimethylamino)benzene-boronic acid (1.20 g, 7.27 mmol) and tetrakis(triphenylphosphine)palladium (353 mg, 0.31 mmol) were dissolved in anhydrous tetrahydrofuran (12 mL). Then aqueous solution of potassium carbonate (2 M, 5.20 mL) was added under an argon atmosphere. Then the mixture was stirred for 20 h at 70 °C under an argon atmosphere. After cooling to room temperature, the mixture was filtered, washed with tetrahydrofuran (5 mL × 3) and deionized water (5 mL × 3), and evaporated to dryness to afford CHO-FN as a yellow solid (1.37 g): Yield 97%.^{1}H NMR (400 MHz, $CDCl_3$, ppm) δ: 9.82 (s, 1H, -C***H***O), 7.68 (d, J = 4.0 Hz, 1H, thioph-H), 7.55-7.58 (m, 2H, Ph-H), 7.24 (d, J = 4.0 Hz, 1H, thioph-H), 6.70-6.74 (m, 2H, Ph-H), 3.03 (s, 6H, -N(C***H***$_3$)$_2$); ^{13}C NMR (100 MHz, $CDCl_3$, ppm) δ: 182.39, 156.07, 151.16, 140.09, 138.01, 127.38, 121.37, 120.84, 112.22, 40.17; Mass spectrometry (NSI-MS, m/z): [M + H]$^+$ calcd. for [$C_{13}H_{13}NOS$ + H]$^+$ 232.0791; found, 232.0785.

Synthesis of LQM-FN

LQM (100 mg, 0.43 mmol) and CHO-FN (118 mg, 0.51 mmol) were dissolved in anhydrous acetonitrile (20 mL). Then piperidine (1.00 mL) was added. Then the mixture was refluxed for 24 h under an argon atmosphere. The solvent was removed under reduced pressure, and then the crude product was purified by silica gel chromatography (dichloromethane : methanol = 50:3, v:v) to afford LQM-FN as a black solid (130 mg): Yield 68%.^{1}H NMR (400 MHz, DMSO-d_6, ppm) δ: 8.39 (d, J = 8.4 Hz, 1H, Ph-H), 8.10 (d, J = 15.4 Hz, 1H, alkene-H), 7.81 (d, J = 3.2 Hz, 1H, thioph-H), 7.79 (d, J = 2.8 Hz, 1H, Ph-H), 7.58-7.60 (m, 3H, Ph-H), 7.44 (d, J = 3.2 Hz, 1H, thioph-H), 7.29 (d, J = 8.9 Hz, 1H, Ph-H), 7.17 (d, J = 15.4 Hz, 1H, alkene-H), 6.97 (s, 1H, Ph-H), 6.78 (d, J = 8.9 Hz, 2H, Ph-H), 4.65 (q, J = 7.9 Hz, 2H, -NC***H***$_2$CH$_3$), 2.98 (s, 6H, -N(C***H***$_3$)$_2$), 1.53 (t, J = 7.9 Hz, 3H, -NCH$_2$C***H***$_3$); Mass spectrometry (ESI-MS, m/z): $[M + H]^+$ calcd. for $[C_{28}H_{24}N_4S + H]^+$ 449.1794; found, 449.1788.

Synthesis of QM-FN

QM (150 mg, 0.64 mmol) and CHO-FN (147 mg, 0.64 mmol) were dissolved in anhydrous acetonitrile (30 mL). Then piperidine (1.50 mL) was added. Then the mixture was refluxed for 24 h under an argon atmosphere. The solvent was removed under reduced pressure, and then the crude product was purified by silica gel chromatography (dichloromethane : methanol = 50:3, v:v) to afford QM-FN as a red solid (184 mg): Yield 64%.^{1}H NMR (400 MHz, DMSO-d_6, ppm) δ: 8.93 (d, J = 7.8 Hz, 1H, Ph-H), 8.09 (d, J = 9.0 Hz, 1H, Ph-H), 7.93 (t, J = 7.0 Hz, 1H, Ph-H), 7.67 (d, J = 15.4 Hz, 1H, alkene-H), 7.55-7.62 (m, 4H, Ph-H, thioph-H), 7.38 (d, J = 3.8 Hz, 1H, thioph-H), 7.07 (d, J = 15.4 Hz, 1H, alkene-H), 7.04 (s, 1H, Ph-H), 6.77 (d, J = 7.7 Hz, 2H, Ph-H), 4.55 (q, J = 7.2 Hz, 2H, -NC***H***$_2$CH$_3$), 2.97 (s, 6H, -N(C***H***$_3$)$_2$), 1.42 (t, J = 7.2 Hz, 3H, -NCH$_2$C***H***$_3$); Mass spectrometry (NSI-MS, m/z): $[M + H]^+$ calcd. for $[C_{28}H_{24}N_4S + H]^+$ 449.1794; found, 449.1777.

Synthesis of LQM-OH

LQM (100 mg, 0.43 mmol) and 4-hydroxybenzaldehyde (62 mg, 0.51 mmol) were dissolved in anhydrous acetonitrile (20 mL). Then piperidine (1.00 mL) was added. Then the mixture was refluxed for 24 h under an argon atmosphere. The solvent was removed under reduced pressure, and then the crude product was purified by silica gel chromatography (dichloromethane : methanol = 50:3, v:v) to afford LQM-OH as a black solid (97 mg): Yield 67%.^{1}H NMR (400 MHz, DMSO-d_6, ppm) δ: 10.15 (s, 1H, -O***H***), 8.40 (d, J = 8.4 Hz, 1H, Ph-H), 7.75-7.83 (m, 5H, Ph-H, alkene-H), 7.41 (d, J = 15.7 Hz, 1H, alkene-H), 7.29 (dd, J_1 = 1.0 Hz, J_2 = 8.8 Hz, 1H, Ph-H), 6.98 (s, 1H, Ph-H), 6.88 (d, J = 8.6 Hz, 2H, Ph-H), 4.69 (q, J = 6.8 Hz, 2H, -NC***H***$_2$CH$_3$), 1.52 (t, J = 6.8 Hz, 3H, -NCH$_2$C***H***$_3$); ^{13}C NMR (100 MHz, DMSO-d_6, ppm) δ: 160.11, 152.73, 151.27, 143.75, 141.20, 140.42, 130.76, 130.33, 126.37, 123.20, 122.80, 121.35, 115.85, 115.10, 114.07, 99.03, 45.16, 12.69; Mass spectrometry (ESI-MS, m/z): $[M - H]^-$ calcd. for $[C_{22}H_{17}ON_3 - H]^-$ 338.1288; found, 338.1296.

Synthesis of CHO-FTPA

5-bromo-2-thiophencarboxaldehyde (100 mg, 0.53 mmol), 4-(diphenylamino)phenylboronic acid (183 mg, 0.63 mmol) and tetrakis(triphenylphosphine)palladium (31 mg, 0.03 mmol) were dissolved in anhydrous tetrahydrofuran (1 mL). Then aqueous solution of potassium carbonate (2 M, 0.46 mL) was added under an argon atmosphere. Then the mixture was stirred for 20 h at 70 °C under an argon atmosphere. After cooling to room temperature, the mixture was filtered through Celite. Thereafter, the filtrate was extracted with dichloromethane (10 mL × 3). The combined organic phases were dried over Na_2SO_4, filtered, and concentrated under reduced pressure. The crude product was purified by silica gel chromatography (hexane : ethyl acetate = 3:1, v:v) to afford CHO-FTPA as a yellow solid (167 mg): Yield 89%.^{1}H NMR (400 MHz, $CDCl_3$, ppm) δ: 9.85 (s, 1H, -C***H***O), 7.70 (d, J = 4.0 Hz, 1H, thioph-H), 7.50-7.53 (m, 2H, Ph-H), 7.27-7.32 (m, 5H, Ph-H, thioph-H), 7.12-7.15 (m, 4H, Ph-H), 7.04-7.11 (m, 4H, Ph-H); ^{13}C NMR (100 MHz, $CDCl_3$, ppm) δ: 182.62, 154.62, 149.16, 146.97, 141.30, 137.73, 129.59, 127.18, 126.12, 125.09, 123.80, 122.78, 122.28; Mass spectrometry (ESI-MS, m/z): $[M + H]^+$ calcd. for $[C_{23}H_{17}ONS + H]^+$ 356.1104; found, 356.1097.

Synthesis of LQM-FT

LQM (119 mg, 0.51 mmol) and CHO-FTPA (180 mg, 0.51 mmol) were dissolved in anhydrous acetonitrile (25 mL). Then piperidine (1.25 mL) was added. Then the mixture was refluxed for 24 h under an argon atmosphere. The solvent was removed under reduced pressure, and then the crude product was purified by silica gel chromatography (dichloromethane : methanol = 50:3, v:v) to afford LQM-FT as a black solid (171 mg): Yield 59%.^{1}H NMR (400 MHz, DMSO-d_6, ppm) δ: 8.38 (d, J = 8.3 Hz, 1H, Ph-H), 8.06 (d, J = 15.3 Hz, 1H, alkene-H), 7.76-7.80 (m, 2H, Ph-H), 7.62-7.64 (m, 3H, Ph-H, thioph-H), 7.52 (d, J = 3.4 Hz, 1H, thioph-H), 7.36 (t, J = 7.6 Hz, 4H, Ph-H), 7.28 (d, J = 8.7 Hz, 1H, Ph-H), 7.21 (d, J = 15.3 Hz, 1H, alkene-H), 7.07-7.14 (m, 6H, Ph-H), 6.95-6.98 (m, 3H, Ph-H), 4.64 (q, J = 6.8 Hz, 2H, -NC***H***$_2$CH$_3$), 1.52 (t, J = 6.8 Hz, 3H, -NCH$_2$C***H***$_3$); ^{13}C NMR (100 MHz, DMSO-d_6, ppm) δ: 151.56, 147.75, 146.53, 141.06, 140.51, 138.40, 135.95, 133.86, 130.31, 129.79, 126.69, 126.28, 124.81, 123.95, 123.46, 122.20, 121.27, 116.34, 114.14, 98.96, 45.17, 12.65; Mass spectrometry (ESI-MS, m/z): $[M + H]^+$ calcd. for $[C_{38}H_{28}N_4S + H]^+$ 573.2107; found, 573.2093.

Synthesis of CHO-FOTPA

7-bromo-2,3-dihydrothieno[3,4-b][1,4]dioxine-5-carbaldehyde (100 mg, 0.40 mmol), 4-(diphenylamino)phenylboronic acid (139 mg, 0.48 mmol) and tetrakis(triphenylphosphine)palladium (23 mg, 0.02 mmol) were dissolved in anhydrous tetrahydrofuran (1 mL). Then aqueous solution of potassium carbonate (2 M, 0.35 mL) was added under an argon atmosphere. Then the mixture was stirred for 20 h at 70 °C under an argon atmosphere. After cooling to room temperature, the mixture was filtered through Celite. Thereafter, the filtrate was extracted with dichloromethane (10 mL × 3). The combined organic phases were dried over Na_2SO_4, filtered, and concentrated under reduced pressure. The crude product was purified by silica gel chromatography (hexane : dichloromethane = 1:2, v:v) to afford CHO-FOTPA as a yellow solid (100 mg): Yield 60%.^{1}H NMR (400 MHz, $CDCl_3$, ppm) δ: 9.90 (s, 1H, -C***H***O), 7.64 (d, J = 8.7 Hz, 2H, Ph-H), 7.26-7.30 (m, 4H, Ph-H), 7.12 (d, J = 7.9 Hz, 4H, Ph-H), 7.04-7.09 (m, 4H, Ph-H), 4.40 (t, J = 5.1 Hz, 2H, -OC***H***$_2$CH$_2$O-), 4.35 (t, J = 5.1 Hz, 2H, -OCH$_2$C***H***$_2$O-); ^{13}C NMR (100 MHz, $CDCl_3$, ppm) δ: 179.48, 149.14, 148.38, 147.04, 136.95, 129.48, 127.89, 124.94, 123.79, 122.34, 114.76, 65.14, 64.53; Mass spectrometry (ESI-MS, m/z): $[M + H]^+$ calcd. for $[C_{25}H_{19}O_3NS + H]^+$ 414.1158; found, 414.1153.

Synthesis of LQM-FOT

LQM (48 mg, 0.21 mmol) and CHO-FOTPA (85 mg, 0.21 mmol) were dissolved in anhydrous acetonitrile (10 mL). Then piperidine (0.50 mL) was added. Then the mixture was refluxed for 24 h under an argon atmosphere. The solvent was removed under reduced pressure, and then the crude product was purified by silica gel chromatography (dichloromethane : methanol = 50:3, v:v) to afford LQM-FOT as a black solid (80 mg): Yield 62%.^{1}H NMR (400 MHz, $CDCl_3$, ppm) δ: 7.85 (d, J = 8.2 Hz, 1H, Ph-H), 7.61-7.64 (m, 2H, Ph-H), 7.53 (d, J = 15.3 Hz, 1H, alkene-H), 7.39-7.45 (m, 2H, Ph-H), 7.27-7.31 (m, 4H, Ph-H), 7.24 (d, J = 8.3 Hz, 1H, Ph-H), 7.12-7.15 (m, 4H, Ph-H), 7.05-7.08 (m, 4H, Ph-H), 6.94 (d, J = 15.3 Hz, 1H, alkene-H), 6.94 (s, 1H, Ph-H), 4.50 (q, J = 7.3 Hz, 2H, -NC***H***$_2$CH$_3$), 4.42-4.44 (m, 2H, -OC***H***$_2$CH$_2$O-), 4.38-4.39 (m, 2H, -OCH$_2$C***H***$_2$O-), 1.66 (t, J = 7.3 Hz, 3H, -NCH$_2$C***H***$_3$); ^{13}C NMR (100 MHz, $CDCl_3$, ppm) δ: 153.41, 151.27, 147.84, 147.08, 144.51, 141.11, 139.47, 137.85, 131.44, 129.51, 127.34, 125.25, 124.91, 123.80, 123.35, 122.47, 121.71, 121.33, 112.90, 112.12, 98.91, 65.23, 64.64, 44.00, 12.90; Mass spectrometry (ESI-MS, m/z): $[M + H]^+$ calcd. for $[C_{40}H_{30}O_2N_4S + H]^+$ 631.2162; found, 631.2157.

Synthesis of CHO-FTPA-OME

5-bromo-2-thiophencarboxaldehyde (200 mg, 1.05 mmol), (4-(bis(4-methoxyphenyl)amino)phenyl)boronic acid (437 mg, 1.25 mmol) and tetrakis(triphenylphosphine)palladium (61 mg, 0.05 mmol) were dissolved in anhydrous tetrahydrofuran (2 mL). Then aqueous solution of potassium carbonate (2 M, 0.90 mL) was added under an argon atmosphere. Then the mixture was stirred for 20 h at 70 °C under an argon atmosphere. After cooling to room temperature, the mixture was filtered through Celite. Thereafter, the filtrate was extracted with

dichloromethane (10 mL × 3). The combined organic phases were dried over Na_2SO_4, filtered, and concentrated under reduced pressure. The crude product was purified by silica gel chromatography (hexane : ethyl acetate = 4:1, v:v) to afford CHO-FTPA-OME as a yellow solid (424 mg): Yield 97%.^{1}H NMR (400 MHz, $CDCl_3$, ppm) δ: 9.85 (s, 1H, -C***H***O), 7.71 (d, *J* = 4.0 Hz, 1H, thioph-H), 7.48 (d, *J* = 8.8 Hz, 2H, Ph-H), 7.28 (d, *J* = 4.0 Hz, 1H, thioph-H), 7.11-7.13 (m, 4H, Ph-H), 6.87-6.93 (m, 6H, Ph-H), 3.83 (s, 6H, -OC***H***$_3$); ^{13}C NMR (100 MHz, $CDCl_3$, ppm) δ: 182.57, 156.53, 155.14, 150.01, 140.78, 139.88, 137.99, 137.89, 127.21, 124.22, 122.27, 119.30, 114.91, 55.60; Mass spectrometry (ESI-MS, m/z): $[M + H]^+$ calcd. for $[C_{25}H_{21}O_3NS + H]^+$ 416.1315; found, 416.1313.

Synthesis of LQM-FTO

LQM (297 mg, 1.26 mmol) and CHO-FTPA-OME (524 mg, 1.26 mmol) were dissolved in anhydrous acetonitrile (60 mL). Then piperidine (3.00 mL) was added. Then the mixture was refluxed for 24 h under an argon atmosphere. The solvent was removed under reduced pressure, and then the crude product was purified by silica gel chromatography (dichloromethane : methanol = 50:3, v:v) to afford LQM-FTO as a black solid (402 mg): Yield 50%.^{1}H NMR (400 MHz, DMSO-d_6, ppm) δ: 8.37 (d, *J* = 8.4 Hz, 1H, Ph-H), 8.05 (d, *J* = 15.3 Hz, 1H, alkene-H), 7.76 (t, *J* = 8.2 Hz, 2H, Ph -H), 7.60 (d, *J* = 3.7 Hz, 1H, thioph-H), 7.53 (d, *J* = 8.6 Hz, 2H, Ph-H), 7.44 (d, *J* = 3.7 Hz, 1H, thioph-H), 7.27 (d, *J* = 8.7 Hz, 1H, Ph-H), 7.15 (d, *J* = 15.3 Hz, 1H, alkene-H), 7.08 (d, *J* = 8.8 Hz, 4H, Ph-H), 6.95 (d, *J* = 8.9 Hz, 5H, Ph-H), 6.75 (d, *J* = 8.6 Hz, 2H, Ph-H), 4.62 (q, *J* = 7.0 Hz, 2H, -NC***H***$_2$CH$_3$), 3.76 (s, 6H, -OC***H***$_3$), 1.51 (t, *J* = 7.0 Hz, 3H, -NCH$_2$C***H***$_3$); ^{13}C NMR (100 MHz, DMSO-d_6, ppm) δ: 156.71, 152.07, 151.81, 149.41, 148.83, 141.43, 140.97, 139.73, 138.25, 136.51, 134.59, 134.45, 130.88, 130.77, 127.83, 127.14, 127.01, 124.42, 123.82, 123.34, 121.81, 118.82, 116.19, 115.55, 114.41, 99.48, 55.64, 45.63, 13.13; Mass spectrometry (ESI-MS, m/z): $[M + H]^+$ calcd. for $[C_{40}H_{32}O_2N_4S + H]^+$ 633.2319; found, 633.2315.

Synthesis of CHO-FOTPA-OME

7-bromo-2,3-dihydrothieno[3,4-b][1,4]dioxine-5-carbaldehyde (200 mg, 0.81 mmol), (4-(bis(4-methoxyphenyl)amino)phenyl)boronic acid (335 mg, 0.96 mmol) and tetrakis(triphenylphosphine)palladium (47 mg, 0.04 mmol) were dissolved in anhydrous tetrahydrofuran (2 mL). Then aqueous solution of potassium carbonate (2 M, 0.69 mL) was added under an argon atmosphere. Then the mixture was stirred for 20 h at 70 °C under an argon atmosphere. After cooling to room temperature, the mixture was filtered through Celite. Thereafter, the filtrate was extracted with dichloromethane (10 mL × 3). The combined organic phases were dried over Na_2SO_4, filtered, and concentrated under reduced pressure. The crude product was purified by silica gel chromatography (hexane : ethyl acetate = 2:1, v:v) to afford CHO-FOTPA-OME as a yellow solid (287 mg): Yield 75%.^{1}H NMR (400 MHz, $CDCl_3$, ppm) δ: 9.90 (s, 1H, -C***H***O), 7.59-7.62 (m, 2H, Ph-H), 7.08-7.12 (m, 4H, Ph-H), 6.89-6.93 (m, 2H, Ph-H), 6.85-6.88 (m, 4H, Ph-H), 4.40-4.42 (m, 2H, -OC***H***$_2$CH$_2$O-), 4.36-4.37 (m, 2H, -OCH$_2$C***H***$_2$O-), 3.82 (s, 6H, -OC***H***$_3$); ^{13}C NMR (100 MHz, $CDCl_3$, ppm) δ: 179.27, 156.42, 149.28, 140.00, 136.57, 130.11, 127.69, 127.22, 123.03, 119.23, 114.86, 114.32, 65.14, 64.48, 55.42; Mass spectrometry (ESI-MS, m/z): $[M + H]^+$ calcd. for $[C_{27}H_{23}O_5NS + H]^+$ 474.1370; found, 474.1362.

Synthesis of LQM-FOO

LQM (124 mg, 0.53 mmol) and CHO-FOTPA-OME (250 mg, 0.53 mmol) were dissolved in anhydrous acetonitrile (25 mL). Then piperidine (1.25 mL) was added. Then the mixture was refluxed for 24 h under an argon atmosphere. The solvent was removed under reduced pressure, and then the crude product was purified by silica gel chromatography (dichloromethane : methanol = 50:3, v:v) to afford LQM-FOO as a black solid (260 mg): Yield 71%.^{1}H NMR (400 MHz, DMSO-d_6, ppm) δ: 8.31 (d, *J* = 8.5 Hz, 1H, Ph-H), 7.85 (d, *J* = 15.2 Hz, 1H, alkene-H), 7.78 (t, *J* = 8.9 Hz, 2H, Ph-H), 7.56 (d, *J* = 8.8 Hz, 2H, Ph-H), 7.25 (d, *J* = 9.0 Hz, 1H, Ph-H), 7.10 (d, *J* = 15.2 Hz, 1H, alkene-H), 7.07 (d, *J* = 9.0 Hz, 4H, Ph-H), 6.95 (d, *J* = 8.9 Hz, 5H, Ph-H), 6.78 (d, *J* = 8.8 Hz, 2H, Ph-H), 4.56 (q, *J* = 7.3 Hz, 2H, -NC***H***$_2$CH$_3$), 4.48-4.49 (m, 2H, -OC***H***$_2$CH$_2$O-), 4.40-4.41 (m, 2H, -OCH$_2$C***H***$_2$O-), 3.76 (s, 6H, -OC***H***$_3$), 1.51 (t, *J* = 7.3 Hz, 3H, -NCH$_2$C***H***$_3$); ^{13}C NMR (100 MHz,

DMSO-d_6, ppm) δ: 156.64, 152.17, 151.59, 148.65, 145.23, 141.04, 140.94, 139.78, 138.08, 132.58, 130.76, 127.68, 127.59, 123.35, 123.25, 122.79, 121.94, 118.84, 115.52, 114.05, 113.72, 111.89, 99.48, 65.71, 65.05, 55.64, 12.87; Mass spectrometry (ESI-MS, m/z): $[M + H]^+$ calcd. for $[C_{42}H_{34}O_4N_4S + H]^+$ 691.2374; found, 691.2353.

Preparation of Photosensitizer@NPs and Photosensitizer@FA NPs

Photosensitizer@NPs were prepared according to previously reported protocols[1] with minor modifications: 1 mg photosensitizer, and 20 mg DSPE-PEG2000 polymer was dissolved in DMSO (1 mL) and stirred at room temperature (25 °C) for 10 min. Then this mixture was slowly added into sterilized water (10 mL) under an ultrasonic bath and stirred slightly for another 50 min. Subsequently, the solution was dialyzed against sterilized water for 24 h (molecular weight cutoff = 8000 Da) and sterilized water was exchanged for 4 times.

Photosensitizer@FA NPs were prepared using DSPE-PEG2000-FA polymer instead of DSPE-PEG2000 polymer, following a procedure similar to that used for Photosensitizer@NPs.

In vitro ROS detection

Total ROS was detected by 2',7'-Dichlorodihydrofluorescein (DCFH) in PBS buffer (pH = 7.4) solution.[2] When ROS is generated in the system, the DCFH will be oxidized and emit strong fluorescence centered at 526 nm, 10 μM of photosensitizers were dissolved in 3 mL PBS buffer containing 40 μM of DCFH. The mixture was then placed in a cuvette and irradiated with 635 nm laser or white light (only for QM-FN) at 50 mW/cm^2 (irradiation time of 1 min corresponding to energy dose of 3 J/cm^2). The fluorescence spectra change of sample was recorded by the fluorescence spectrofluorometer.

In vitro $^1O_2$ detection

The $^1O_2$ was detected by 9,10-anthracenediyl-bis(methylene)dimalonic acid (ABDA) in PBS buffer (pH = 7.4) solution.[2] When $^1O_2$ is generated in the system, the ABDA will be oxidized and the absorbance will decrease, 10 μM of photosensitizers were dissolved in 3 mL PBS buffer containing 40 μM of ABDA. The mixture was then placed in a cuvette and irradiated with 635 nm laser or white light (only for QM-FN) at 50 mW/cm^2 (irradiation time of 1 min corresponding to energy dose of 3 J/cm^2). The absorption spectra change of sample was recorded by the UV-Vis spectrophotometer.

In vitro $\cdot O_2^-$ detection

The $\cdot O_2^-$ was detected by Dihydroethidium (DHE) in PBS buffer (pH = 7.4) solution containing 0.5 mg/mL CT-DNA.[2] When $\cdot O_2^-$ is generated in the system, the DHE will be oxidized and emit strong fluorescence centered at 581 nm, 10 μM of photosensitizers were dissolved in 3 mL PBS buffer containing 40 μM of DHE. The mixture was then placed in a cuvette and irradiated with 635 nm laser or white light (only for QM-FN) at 50 mW/cm^2 (irradiation time of 1 min corresponding to energy dose of 3 J/cm^2). The fluorescence spectra change of sample was recorded by the fluorescence spectrofluorometer.

In vitro ·OH detection

The ·OH was detected by Hydroxyphenyl Fluorescein (HPF) in PBS buffer (pH = 7.4) solution.[3] When ·OH is generated in the system, the HPF will be oxidized and emit strong fluorescence centered at 516 nm, 10 μM of photosensitizers were dissolved in 3 mL PBS buffer containing 40 μM of HPF. The mixture was then placed in a cuvette and irradiated with 635 nm laser or white light (only for QM-FN) at 50 mW/cm^2 (irradiation time of 1 min corresponding to energy dose of 3 J/cm^2). The fluorescence spectra change of sample was recorded by the fluorescence spectrofluorometer.

NADH photocatalytic oxidation detection

The rate of photocatalytic oxidation of NADH by the photosensitizer was determined according to previously reported protocols[4] with minor modifications: 10 μM of photosensitizers were dissolved in 3 mL PBS buffer containing 100 μM of NADH. The mixture was then placed in a cuvette and irradiated with 635 nm laser or white light (only for QM-FN) at 50 mW/cm^2 (irradiation time of 1 min corresponding to energy dose of 3 J/cm^2). The absorption spectra change of NADH was recorded by the UV-Vis spectrophotometer.

Electron spin resonance (ESR) spectra

The free radical species generated by photosensitizers have been detected by ESR spectra according to previously reported protocols[4] with minor modifications: In 195 μL of water/dichloromethane solution, 100 μM photosensitizers and 5 μL of DMPO were added, shaken well and then placed under the light of 635 nm laser or white light at 0.3 W/cm^2 for 3 min (irradiation time of 1 min corresponding to energy dose of 18 J/cm^2), loaded into quartz glass tubes, sealed at both ends with vacuum sealing grease, and detected by paramagnetic resonance spectroscopy. The oxygen-free ESR experiments were repeated following the previous experimental procedure in an anaerobic glove box filled with nitrogen gas, and the reagents were deoxygenated before used.

Electrochemical Measurements

The electrochemical data of samples were recorded by the CHI760E electrochemical workstation. A standard three-electrode system was employed with a platinum foil and Ag/AgCl as the counter electrode and the reference electrode, respectively. For the preparation of the working electrodes, the samples (1.0 mg) were added into 20 μL 5% Nafion and 280 μL ethanol mixed solution and then sonicated for 1 hour, then the suspension (50 μL) was dropped onto indium tin oxide (ITO) glass and dried under ambient conditions. The electrolyte was Na_2SO_4 (0.2 M, pH = 6.8).

UV-vis diffuse-reflectance spectroscopy

The UV-vis diffuse reflectance spectra (DRS) of the samples were recorded on a UV-vis-NIR spectrophotometer (Lambda 1050+) equipped with an integrating sphere accessory. $BaSO_4$ powder was used as the reflectance standard. The reflectance data were converted into the Kubelka-Munk function, and the optical band gaps of the samples were calculated from Tauc plots.

Isotopic mass spectra measurement

The coumarin (0.1 mg mL^{-1}) was added in solution of photosensitizers in H_2O (0.5 mL) containing $H_2{}^{18}O$ (0.5 mL). Then the solution of photosensitizers were illuminated with 635 nm laser at 0.3 W/cm^2 for 10 min (irradiation time of 1 min corresponding to energy dose of 18 J/cm^2). Then the solution was used for mass spectra analysis.[5]

Theoretical calculation

The ground state geometric optimizations and frequency analysis were performed using the density functional theory (DFT) method while the excitation state calculations were investigated via Time-Dependent DFT (TD-DFT) with the Gaussian 16 program. All calculations employed CAM-B3LYP functional and CC-PVDZ basis set. The Electrostatic Potential (ESP) and hole-electron analysis were performed by Multiwfn.

Photothermal conversion efficiency determination

Photothermal conversion efficiency was determined according to previously reported protocols[6] with minor modifications: A 635 nm near-infrared (NIR) laser (Beijing Blueprint Photoelectric Technology Co., Ltd.) with various irradiation powers was used to stimulate the different concentrations of photosensitizers solution. The photothermal images of suspensions under laser irradiation were captured using an infrared thermal imaging system (FOTRIC280). The NIR laser source was paired with a 10 mm diameter laser module featuring adjustable power settings. The photothermal conversion efficiency was determined using the following equation:

$$\eta = \frac{hS(T_{max} - T_{surr}) - Q_0}{I(1 - 10^{-A_\lambda})}$$

where h is the heat transfer coefficient, S is the surface of the container, T_{max} and T_{surr} are the equilibrium temperature and ambient temperature, respectively. Q_0 is the heat associated with the light absorbance of the solvent, A_λ is the absorbance of photosensitizers solution at 635 nm, and I is the laser power density. According to the above equation, the η value of LQM-FOO, for a representative, was determined to be 70.10%.

Cell lines

The human renal tubular epithelial cell line Hk2 and human ovarian cancer cell line SKOV3 were purchased from Boster Biological Technology Co., Ltd. (Wuhan, China). All cells were propagated in T-75 flasks cultured at 37 °C under a humidified 5% CO_2 atmosphere in DMEM medium or McCoy's 5A medium (GIBCO/Invitrogen, Camarillo, CA, USA), which were supplemented with 10% fetal bovine serum (FBS, Biological Industry, Kibbutz Beit Haemek, Israel) and 1% penicillin-streptomycin (10,000 U mL^{-1} penicillin and 10 mg mL^{-1} streptomycin, Solarbio life science, Beijing, China).

Intracellular ROS detection

To simulate a hypoxic tumor environment, cells were cultured in an incubator at 37 °C in an atmosphere of 2% O_2, and the oxygen content in the chamber was monitored using an oxygen detector (Nuvair, O_2 Qucikstick).

The SKOV3 cells were seeded onto glass-bottom petri dishes with complete medium (1.5 mL) for 12 h. Then the cells were incubated with PBS, QM-FN@FA NPs, LQM-FN@FA NPs or LQM-FOO@FA NPs (10 μM) for 1 h, PBS (pH 7.4) was used to wash cells for three times to clean the extracellular photosensitizers. Then the cells were stained with 2',7'-Dichlorodihydrofluorescein Diacetate (DCFH-DA, 1 μM) in the dark. After 20 min incubation, PBS (pH 7.4) was used to wash cells for three times to clean the background. McCoy's 5A medium was added to culture cells. Finally, the cells were irradiation with 50 mW/cm^2 660 nm laser for 5 min (irradiation time of 1 min corresponding to energy dose of 3 J/cm^2) and scanned within 1 h under confocal microscopy at 488 nm excitation, the fluorescent channel at 525-580 nm was collected.

Intracellular ·OH detection

To simulate a hypoxic tumor environment, cells were cultured in an incubator at 37 °C in an atmosphere of 2% O_2, and the oxygen content in the chamber was monitored using an oxygen detector (Nuvair, O_2 Qucikstick).

The SKOV3 cells were seeded onto glass-bottom petri dishes with complete medium (1.5 mL) for 12 h. Then the cells were incubated with PBS, QM-FN@FA NPs, LQM-FN@FA NPs or LQM-FOO@FA NPs (10 μM) for 1 h, PBS (pH 7.4) was used to wash cells for three times to clean the extracellular photosensitizers. Then the cells were stained with Hydroxyphenyl Fluorescein (HPF, 2 μM) in the dark. After 30 min incubation, PBS (pH 7.4) was used to wash cells for three times to clean the background. McCoy's 5A medium was added to culture

cells. Finally, the cells were irradiation with 50 mW/cm^2 660 nm laser for 15 min (irradiation time of 1 min corresponding to energy dose of 3 J/cm^2) and scanned within 1 h under confocal microscopy at 450 nm excitation, the fluorescent channel at 510-580 nm was collected.

Live/dead cell staining

To simulate a hypoxic tumor environment, cells were cultured in an incubator at 37 °C in an atmosphere of 2% O_2, and the oxygen content in the chamber was monitored using an oxygen detector (Nuvair, O_2 Qucikstick).

The SKOV3 cells were seeded onto glass-bottom petri dishes with complete medium (1.5 mL) for 12 h. Then the cells were incubated with PBS, QM-FN@FA NPs, LQM-FN@FA NPs or LQM-FOO@FA NPs (10 μM) for 1 h, PBS (pH 7.4) was used to wash cells for three times to clean the extracellular photosensitizers. McCoy's 5A medium was added to culture cells, then the cells were irradiation with 50 mW/cm^2 660 nm laser for 15 min (irradiation time of 1 min corresponding to energy dose of 3 J/cm^2), and further cultured for 12 h. The cells were stained with calcein acetoxymethyl ester (calcein-AM) and propidium iodide (PI) for 20 min (2 μM for calcein-AM, 4.5 μM for PI). PBS (pH 7.4) was used to wash cells for three times to clean the background. McCoy's 5A medium was added to culture cells, the images were photographed by using a confocal laser scanning microscope. (calcein-AM: 488 nm as the excitation wavelength and fluorescent channel at 500-530 nm was collected; PI: 545 nm as the excitation wavelength and fluorescent channel at 590-640 nm was collected).

Apoptosis evaluation by flow cytometry

To simulate a hypoxic tumor environment, cells were cultured in an incubator at 37 °C in an atmosphere of 2% O_2, and the oxygen content in the chamber was monitored using an oxygen detector (Nuvair, O_2 Qucikstick).

The SKOV3 cells were inoculated and cultured in an incubator at 37 ℃ for 12 h. NPs are dispersed in McCoy's 5A at a concentration of 1 μM. SKOV3 cells were treated under different conditions: PBS only, PBS + laser, NPs only, NPs + laser (50 mW/cm^2, irradiation time of 1 min corresponding to energy dose of 3 J/cm^2). After treatment, the cells were further incubated for 12 h. Subsequently, all cells were collected centrifugally, washed with PBS, and then dispersed in 100 μL 1x Annexin V Binding Buffer solution. Next, all cells were stained with PI and Annexin-V-FITC for 15 minutes and finally analyzed by flow cytometry.

In vitro cytotoxicity assay

To simulate a hypoxic tumor environment, cells were cultured in an incubator at 37 °C in an atmosphere of 2% O_2, and the oxygen content in the chamber was monitored using an oxygen detector (Nuvair, O_2 Qucikstick).

The cell cytotoxicity to SKOV3 cells was measured by 3-(4,5-dimethylthiazol-2-yl)-2,5-diphenyltetrazolium bromide (MTT) assay. Cells were plated in 96 well plates in 0.1 mL volume of McCoy's 5A, at a density of 1×10^4 cells/well, and added with desired concentrations of QM-FN@FA NPs, LQM-FN@FA NPs or LQM-FOO@FA NPs. After incubation for 1 h, the cells were irradiation with 50 mW/cm^2 660 nm laser for 15 min (irradiation time of 1 min corresponding to energy dose of 3 J/cm^2) and further cultured for 24 h. The formazan blue crystal was dissolved by replacing the media with DMSO. The absorbance was measured with a Tecan GENios Pro multifunction reader (Tecan Group Ltd., Maennedorf, Switzerland). Each concentration was measured in triplicate and used in three independent experiments. The relative cell viability was calculated by the equation: cell viability (%) = ($OD_{treated}/OD_{control}$) × 100 %.

Animals

We have complied with all relevant ethical regulations for animal testing and research. BALB/c nude mice (4-week-old, female) were purchased from Nanjing MiceBion Biotechnology Co., Ltd. (Nanjing, China), and maintained under standard conditions. The mice were housed in sterile cages within laminar airflow hoods in a specific pathogen-free room with a 12-h light/12-h dark schedule and fed autoclaved

chow and water ad libitum at a room temperature of 20-24 °C and a relative humidity of 55%. Number of qualitative qualification: No.B202505288577. Production Permit No.: SCXK (Su) 2020-0009. All applicable institutional and governmental regulations concerning the ethical use of animals were followed. All animal care and experimental procedures were reviewed and approved by the East China University of Science and Technology Animal Studies Committee (ECUST-2023-026).

In vivo fluorescence imaging

BALB/c nude mice (n = 3) were inoculated with SKOV3 cells on their right flank by injecting 10^6 cells subcutaneously. When the tumors grew up to 6 mm in diameter, they were acquired background imaging and were intravenously injected with LQM-FN@FA NPs, LQM-FOO@NPs, or LQM-FOO@FA NPs (0.5 mg mL^{-1}, 200 μL). Fluorescence signals were recorded at different time points by IVIS Lumina Series III (PerkinElmer, USA). During the imaging process, the mice were kept on the imaging stage under anesthesia with 2.0% isoflurane gas in an oxygen flow (2.0 L min^{-1}). Equipment setup: field of view (FOV): D-12.5 cm; subject height: 1.5 cm; exposure time: auto; binning: medium; lens f/stop: 2.

Ex vivo fluorescence imaging

BALB/c nude mice (n = 3) were inoculated with SKOV3 cells on their right flank by injecting 10^6 cells subcutaneously. When the tumors grew up to 6 mm in diameter, they were intravenously injected with LQM-FN@FA NPs, LQM-FOO@NPs, or LQM-FOO@FA NPs (0.5 mg mL^{-1}, 200 μL). After injection for 12 h, the mice were sacrificed. The major organs (including the heart, liver, spleen, lung, kidney, stomach, intestine, muscle, and tumor) were excised and washed with PBS for *ex vivo* fluorescence imaging using IVIS Lumina Series III (PerkinElmer, USA). Equipment setup: field of view (FOV): D-12.5 cm; subject height: 1.5 cm; exposure time: auto; binning: medium; lens f/stop: 2.

Photothermal imaging

BALB/c nude mice (n = 3) were inoculated with SKOV3 cells on their right flank by injecting 10^6 cells subcutaneously. When the tumors grew up to 6 mm in diameter, QM-FN@FA NPs, LQM-FN@FA NPs or LQM-FOO@FA NPs (200 μM, 10 μL) solution was injected into the tumor of mice. The tumor sites were irradiated with the 635 nm laser at power density of 0.2 W/cm^2 for 5 min (irradiation time of 1 min corresponding to energy dose of 12 J/cm^2) and simultaneously imaged every 30 sec by a FOTRIC280 thermal imager.

2. Photophysical properties of photosensitizers

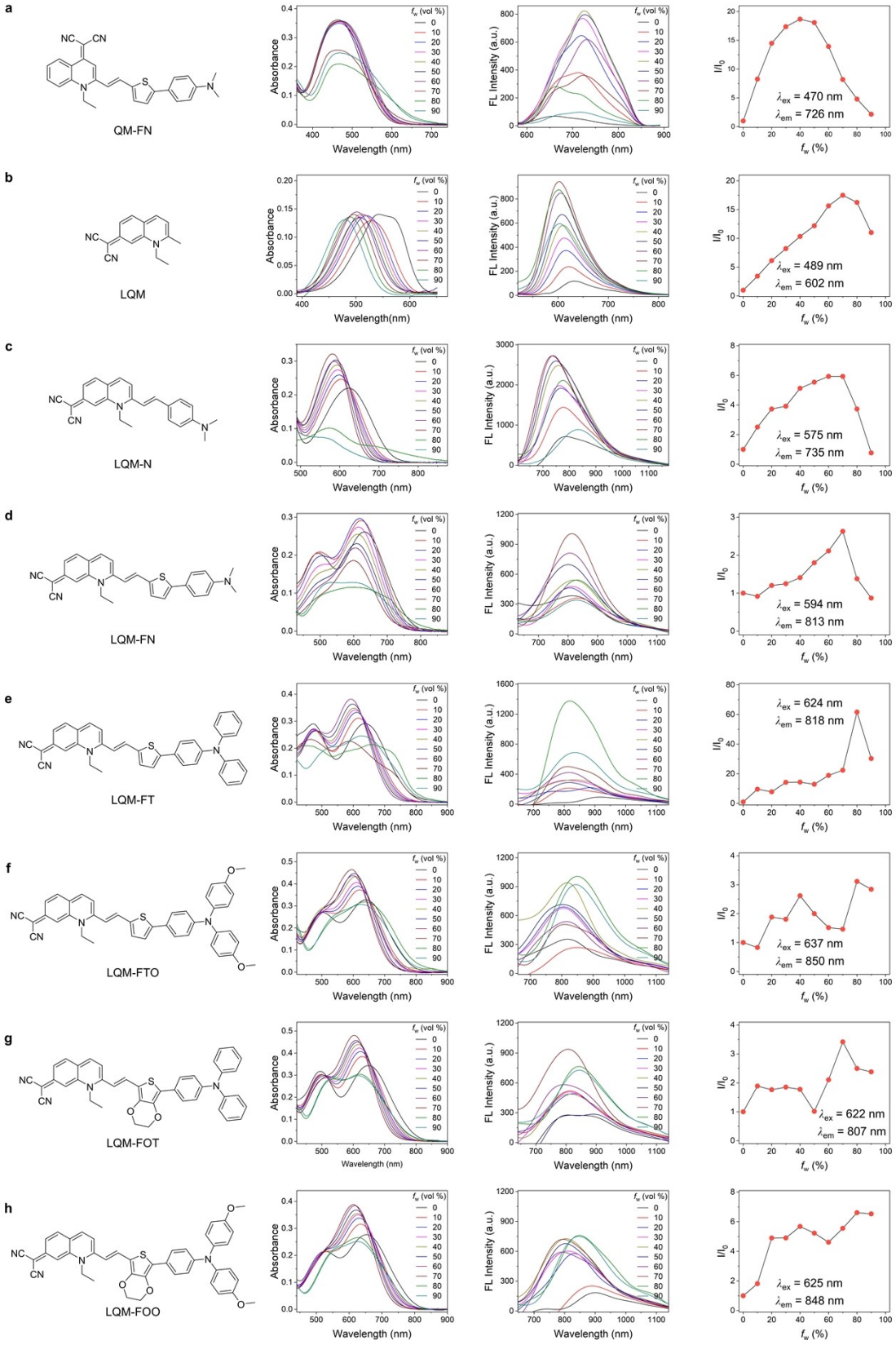

Figure S2. Chemical structure, absorption, fluorescence spectra, and variation in I/I_0 of QM-FN **(a)**, LQM **(b)**, LQM-N **(c)**, LQM-FN **(d)**, LQM-FT **(e)**, LQM-FTO **(f)**, LQM-FOT **(g)**, and LQM-FOO **(h)** (10 μM) in a water-tetrahydrofuran mixture with varying water fractions (f_w, v:v) . I_0 is the emission intensity of different photosensitizers (10 μM) in tetrahydrofuran.

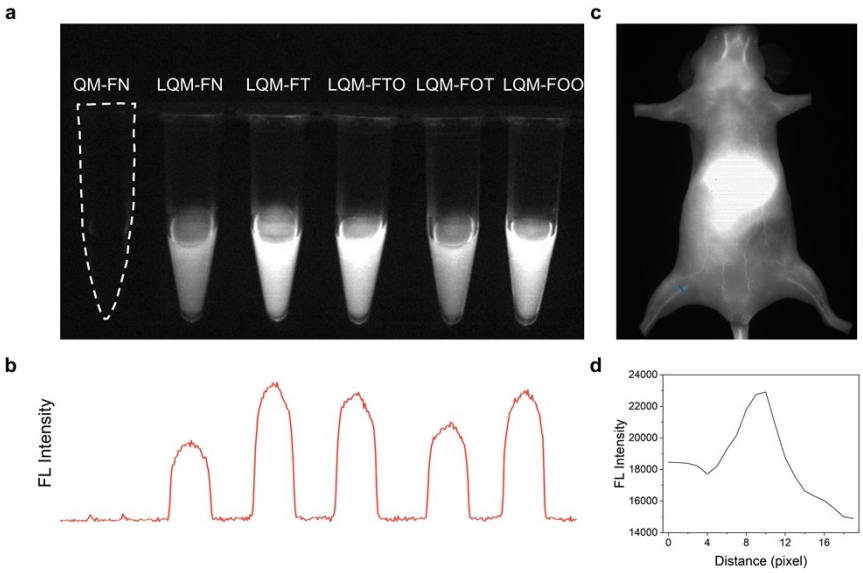

Figure S3. (a) NIR-II images of Eppendorf tubes containing QM-FN and LQM PSs (10 μM) in water (λ_{ex} = 755 nm, LP 900 nm filter). **(b)** Fluorescence intensity profiles extracted from the imaging results shown in panel a. **(c)** NIR-II images of mouse at 5 min after intravenous administration of LQM-FOO (200 μM, 200 μL, λ_{ex} = 755 nm, LP 900 nm filter). **(d)** Cross-sectional fluorescence intensity profiles along the blue line shown in panel c.

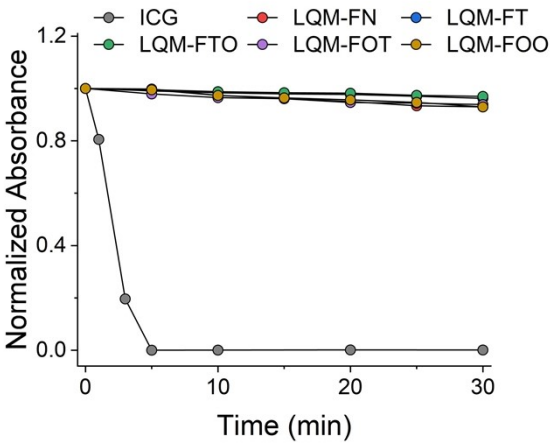

Figure S4. Time-dependent absorbance of ICG (10 μM, monitored at 790 nm), LQM-FN (10 μM, monitored at 602 nm), LQM-FT (10 μM, monitored at 598 nm), LQM-FTO (10 μM, monitored at 608 nm), LQM-FOT (10 μM, monitored at 605 nm) and LQM-FOO (10 μM, monitored at 624 nm) under illumination (Hamamatsu, LC8 Lightningcure, 300 W) in ethanol.

3. Single-crystal X-ray diffraction analysis of photosensitizers

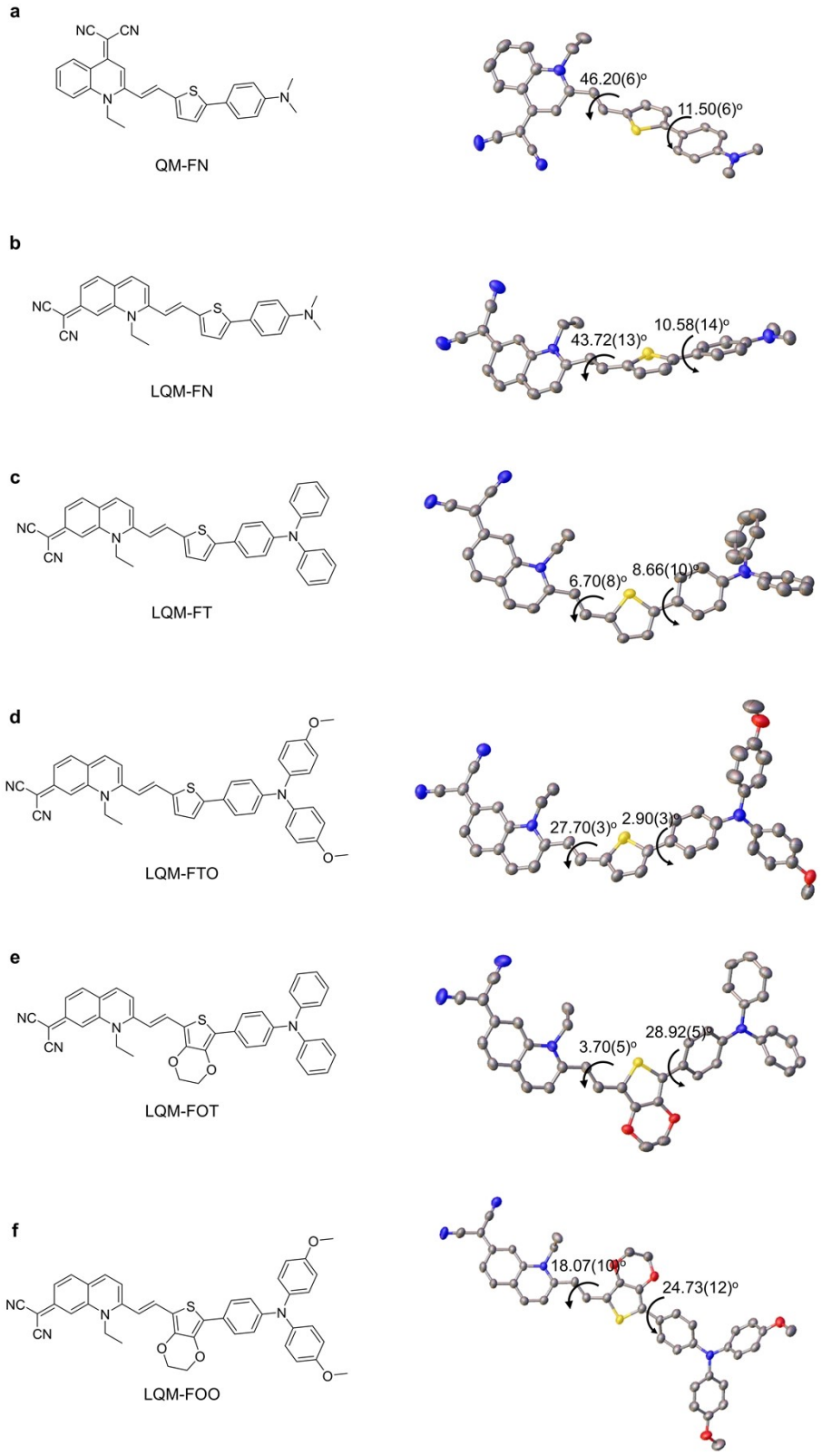

Figure S5. Chemical structure, and single-crystal X-ray structure of QM-FN **(a**, CCDC deposition number: 2482027**)**, LQM-FN **(b**, CCDC deposition number: 2482034**)**, LQM-FT **(c**, CCDC deposition number: 2482035**)**, LQM-FTO **(d**, CCDC deposition number: 2482032**)**, LQM-FOT **(e**, CCDC deposition number: 2482036**)**, and LQM-FOO **(f**, CCDC deposition number: 2482033**)**. Note: solvent molecules and H atoms are omitted for clarity.

4. *In vitro* photodynamic properties of photosensitizers

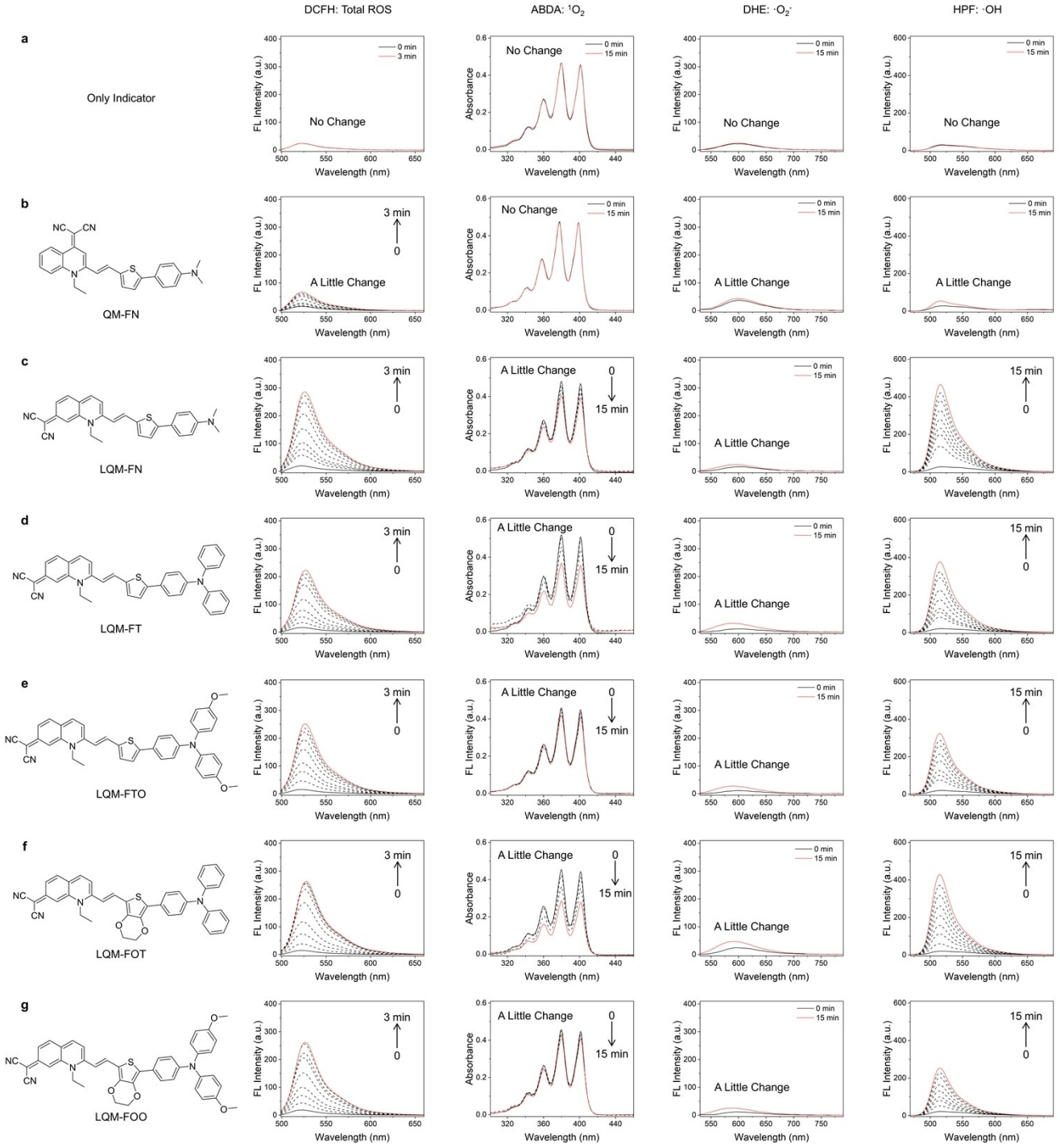

Figure S6. Chemical structure, total ROS detection (DCFH as indicator, 40 μM, λ_{ex} = 488 nm), $^1O_2$ detection (ABDA as indicator, 40 μM), $\cdot O_2^-$ detection (DHE as indicator, 40 μM, λ_{ex} = 510 nm) and ·OH detection (HPF as indicator, 40 μM, λ_{ex} = 450 nm) of only indicator **(a)**, QM-FN **(b)**, LQM-FN **(c)**, LQM-FT **(d)**, LQM-FTO **(e)**, LQM-FOT **(f)**, and LQM-FOO **(g)** (10 μM) after irradiation with a 635 nm laser or white light (only for QM-FN) for different durations (50 mW/cm^2, irradiation time of 1 min corresponding to energy dose of 3 J/cm^2).

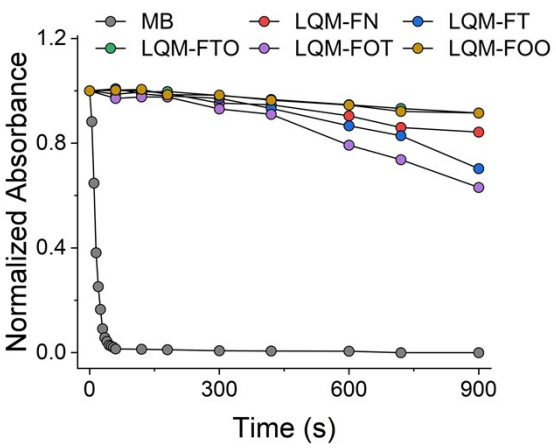

Figure S7. Normalized absorbance of ABDA (40 μM) during 635 nm laser irradiation (50 mW cm^{-2}, irradiation time of 1 min corresponding to energy dose of 3 J cm^{-2}) at different time points in the presence of different photosensitizers (10 μM).

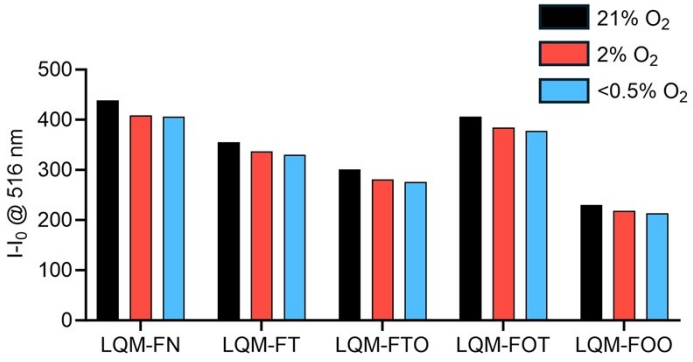

Figure S8. Changes in fluorescence intensity of HPF (monitored at 516 nm) under light irradiation (40 μM, 635 nm, 15 min, 50 mW cm^{-2}, irradiation time of 1 min corresponding to energy dose of 3 J cm^{-2}), in the presence of different photosensitizers (10 μM), under different O_2 content environments. I_0 is the emission intensity of HPF (40 μM) before irradiation. This indicates that LQM PSs can efficiently generate potent ·OH species even under O_2-deprived conditions.

5. Electron spin resonance (ESR) spectroscopy and ion chromatography

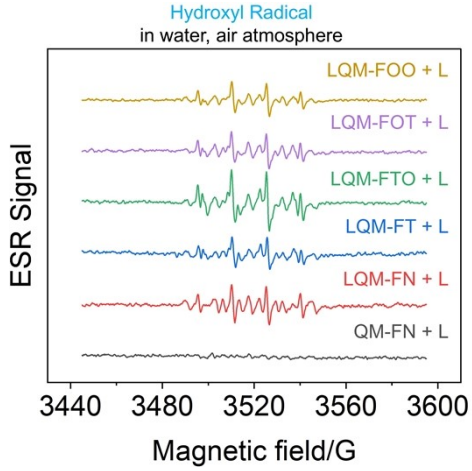

Figure S9. ESR signals of DMPO spin adducts confirming ·OH generation by LQM PSs upon irradiation under air in aqueous solution.

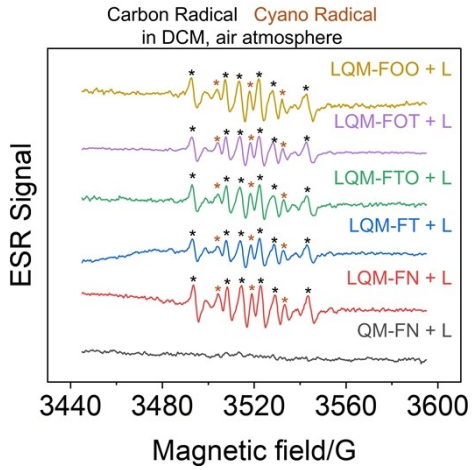

Figure S10. ESR signals of DMPO spin adducts confirming carbon-centered radicals and cyano radicals generation by LQM PSs upon irradiation in dichloromethane solution under air. Note: the black stars represent carbon-centered radicals, the brown stars represent cyano radicals.

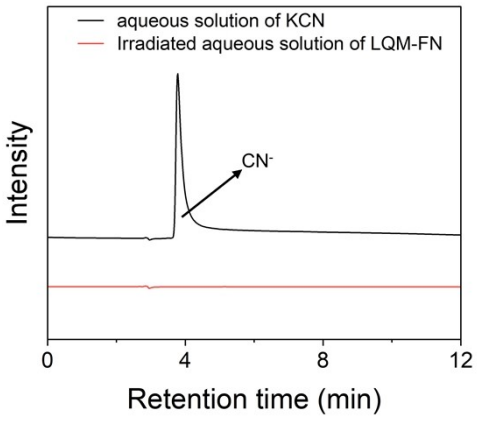

Figure S11. Ion chromatograms of an aqueous solution of KCN (1.0 mg L^{-1}, containing 0.002% KOH) and an irradiated aqueous solution of LQM-FN (200 μM, 635 nm, 0.8 W cm^{-2}, 20 min).

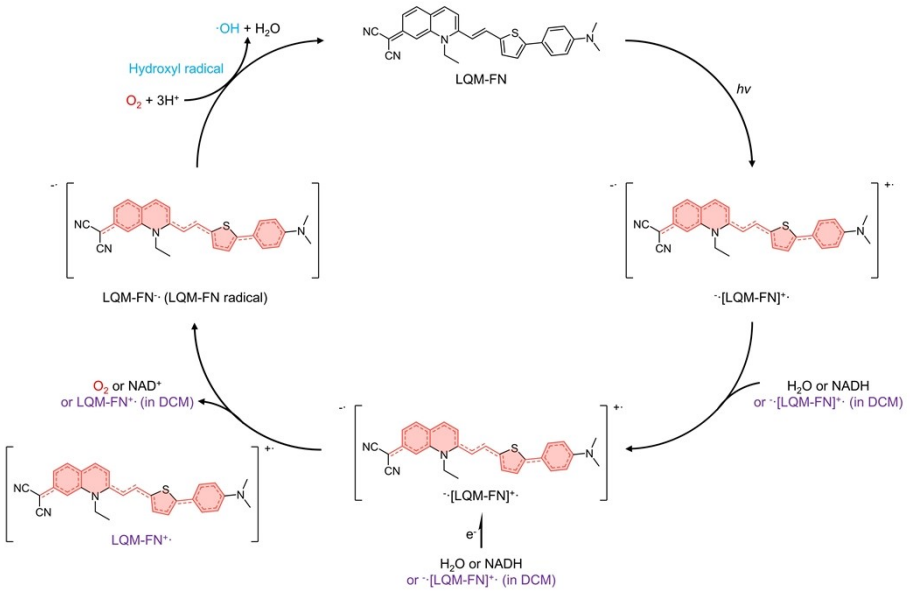

Figure S12. A possible mechanism for LQM PSs radical formation, H_2O oxidation (for O_2 production), and O_2 reduction (for ·OH generation) under light irradiation (LQM-FN as a representative example).

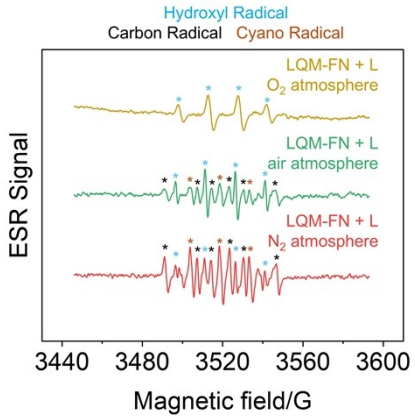

Figure S13. ESR spectra of LQM-FN upon irradiation under different atmospheres in aqueous solution. Note: the blue stars represent ·OH, the black stars represent carbon-centered radicals, the brown stars represent cyano radicals.

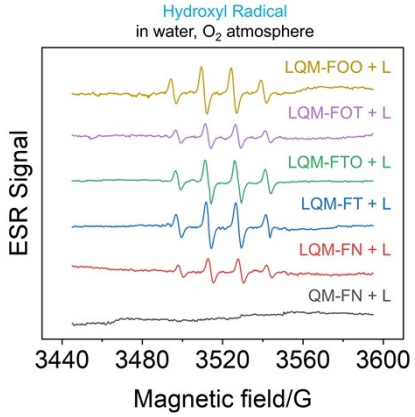

Figure S14. ESR spectra of QM-FN and LQM PSs upon irradiation under O_2 atmospheres in aqueous solution. All reagents were pre-saturated with O_2.

6. Measurement of photosensitizers' redox properties

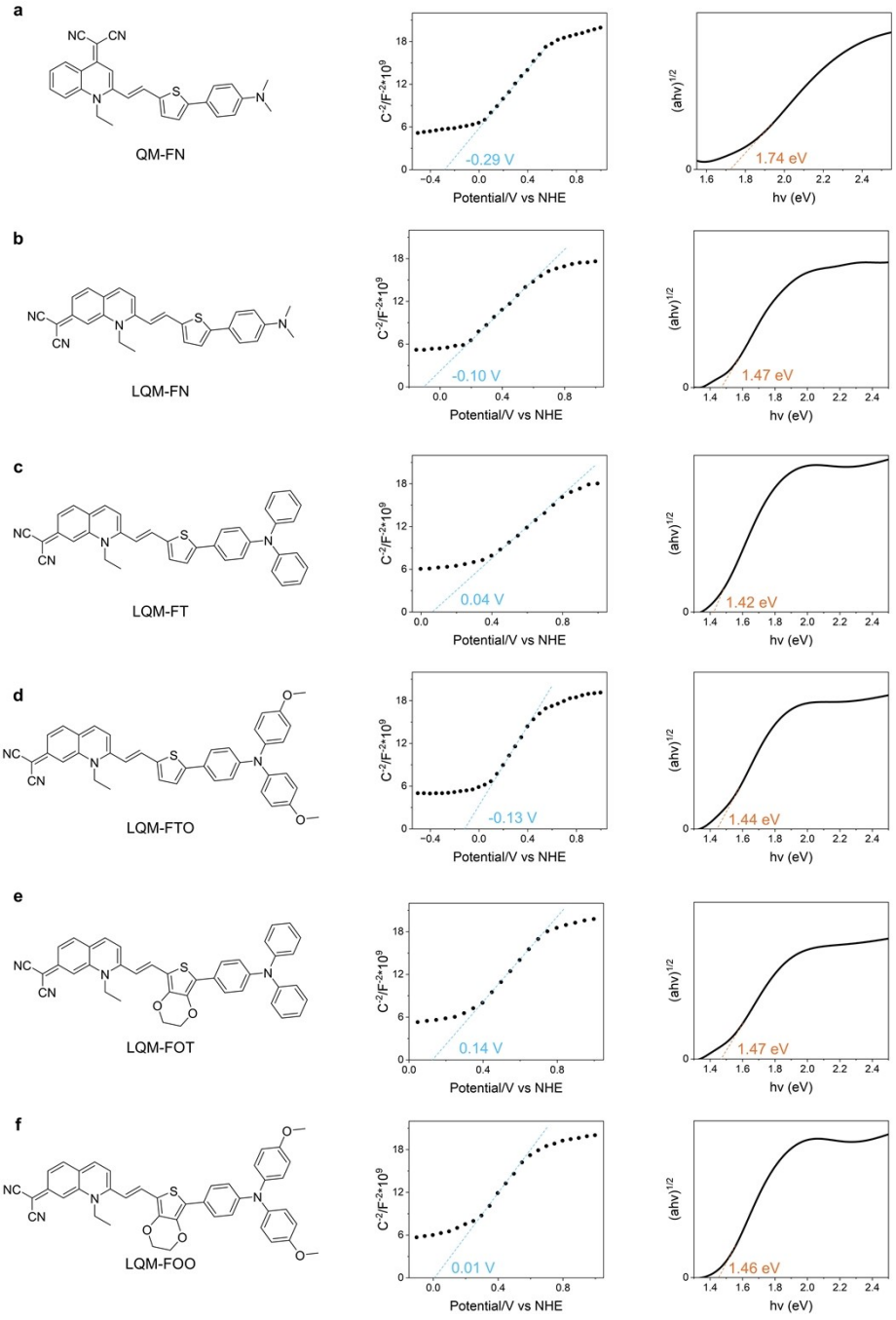

Figure S15. Chemical structure, Mott-Schottky plot, and Tauc plot curves of QM-FN **(a)**, LQM-FN **(b)**, LQM-FT **(c)**, LQM-FTO **(d)**, LQM-FOT **(e)**, and LQM-FOO **(f)**.

Probe	E_{VB} (vs NHE)	E_{CB} (vs NHE)
QM-FN	1.45 V	-0.29 V
LQM-FN	1.37 V	-0.10 V
LQM-FT	1.46 V	0.04 V
LQM-FTO	1.31 V	-0.13 V
LQM-FOT	1.61 V	0.14 V
LQM-FOO	1.47 V	0.01 V

Figure S16. Valence band and conduction band potentials of QM-FN, LQM-FN, LQM-FT, LQM-FTO, LQM-FOT, and LQM-FOO.

7. Theoretical calculation

PS	QM-FN	LQM-FN
D/Å[1]	0.59	1.82
Sr[2]	0.82	0.76
H/Å[3]	4.14	3.56
E_{coul}/eV[4]	4.11	4.17
HDI[5]	6.41	7.44
EDI[6]	5.74	6.91

Figure S17. Descriptor obtained from electron-hole analysis. [1]Distance between the electron and hole, with an increase in distance correlating to a more distinct charge separation. [2]A metric characterizing the overlap between the electron and hole, where a higher value denotes a more substantial overlap, conversely, a lower value implies a more pronounced charge separation. [3]A measure of the overall distribution scale of the electron and hole, with a smaller value implying a more focused distribution. [4]Exciton binding energy or coulombic attraction energy, which quantifies the attraction between the electron and hole. [5]Hole and [6]electron delocalization indices, respectively, where a higher value signifies a lower degree of delocalization.

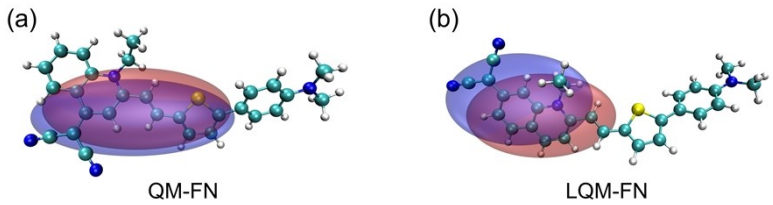

Figure S18. Chole (blue)-Cele (brown) function diagram in the T_1 state of **(a)** QM-FN and **(b)** LQM-FN. Note: The Chole-Cele diagram removes the distribution details, which avoids the problem that the general isosurfaces are interlaced and the distribution is complex, making the graph clearer.

8. Isotopic mass spectrometric determination of photocatalytically generated O_2 and ·OH

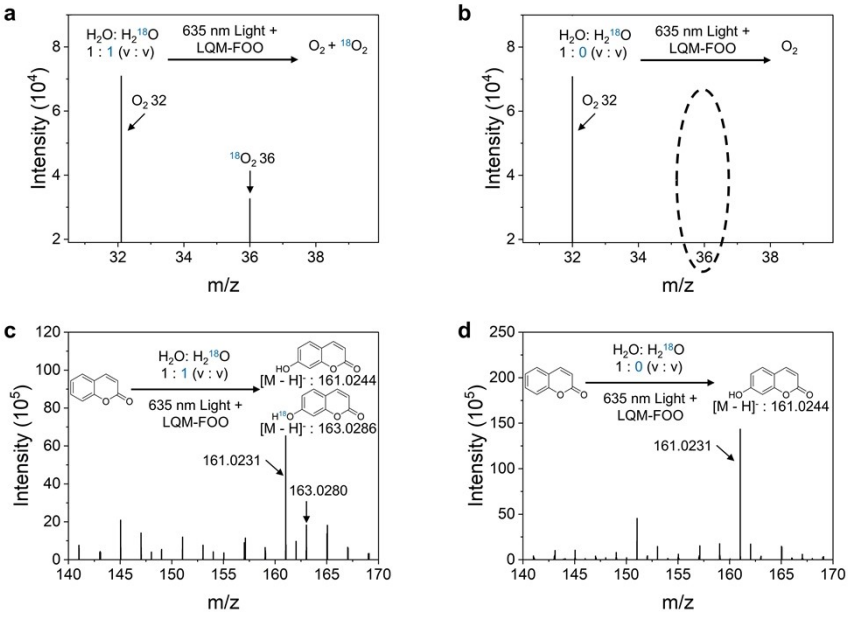

Figure S19. (a) Mass spectra of the photocatalytically generated $^{18}O_2$ products using LQM-FOO as the photosensitizer in H_2O containing $H_2{}^{18}O$ (v:v = 1:1). **(b)** Mass spectra confirming the absence of photocatalytically generated $^{18}O_2$ products using LQM-FOO as the photosensitizer in H_2O lacking $H_2{}^{18}O$ (v:v = 1:0). **(c)** Mass spectra of the products generated in the $\cdot{}^{18}OH$ with coumarin reaction using LQM-FOO as the photosensitizer in H_2O containing $H_2{}^{18}O$ (v:v = 1:1). **(d)** Mass spectra confirming the absence of products from the $\cdot{}^{18}OH$ with coumarin reaction using LQM-FOO as the photosensitizer in H_2O lacking $H_2{}^{18}O$ (v:v = 1:0).

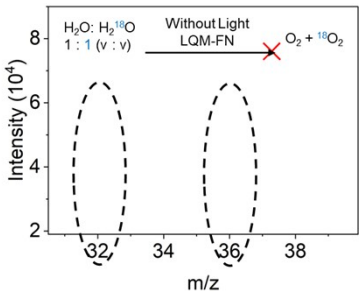

Figure S20. Mass spectra confirming the absence of photocatalytically generated $^{16}O_2$ and $^{18}O_2$ products using LQM-FN as the photosensitizer in H_2O containing $H_2{}^{18}O$ (v:v = 1:1).

9. *In vitro* NADH photocatalytic oxidation detection

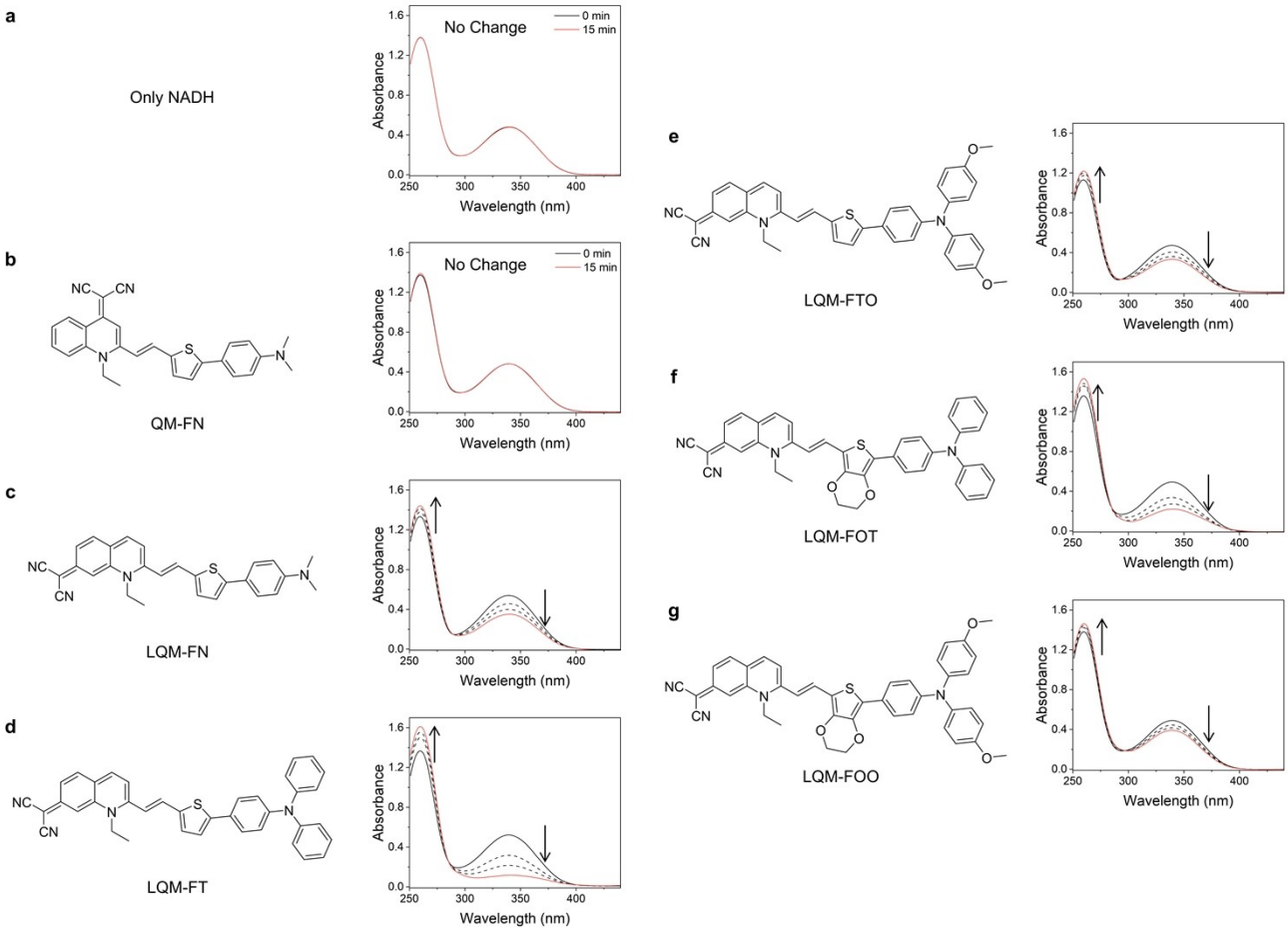

Figure S21. Chemical structure, absorption spectra change of only NADH **(a)**, and in the presence of QM-FN **(b)**, LQM-FN **(c)**, LQM-FT **(d)**, LQM-FTO **(e)**, LQM-FOT **(f)**, and LQM-FOO **(g)** (10 μM) after irradiation with a 635 nm laser or white light (only for QM-FN) for 15 min (50 mW/cm^2, irradiation time of 1 min corresponding to energy dose of 3 J/cm^2).

10. *In vitro* photothermal properties of photosensitizers

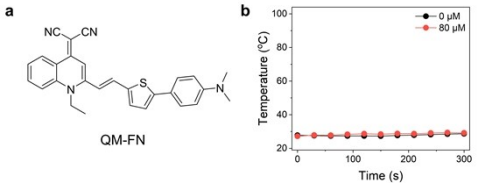

Figure S22. (a) Chemical structure of QM-FN. **(b)** Photothermal conversion of QM-FN (80 μM) under 635 nm laser irradiation (1.2 W cm^{-2}, irradiation time of 1 min corresponding to energy dose of 72 J cm^{-2}).

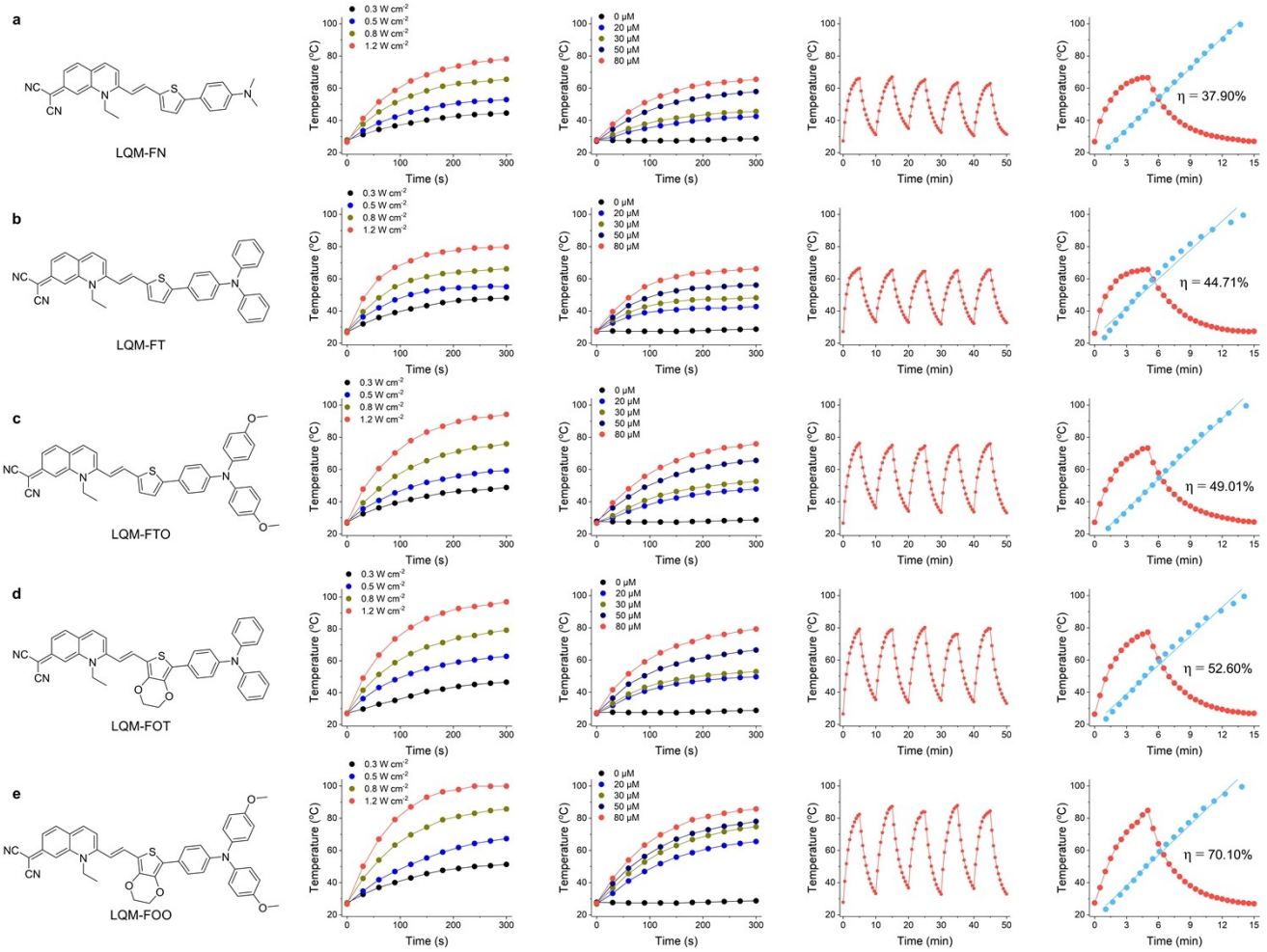

Figure S23. Chemical structure, photothermal conversion with different laser power (concentration of photosensitizer: 80 μM), photothermal conversion at different concentrations (laser power: 0.8 W cm^{-2}, irradiation time of 1 min corresponding to energy dose of 48 J cm^{-2}), photothermal stability study and photothermal conversion efficiency determination of LQM-FN **(a)**, LQM-FT **(b)**, LQM-FTO **(c)**, LQM-FOT **(d)**, and LQM-FOO **(e)** after irradiation with a 635 nm laser.

11. Evaluation of cellular uptake efficiency

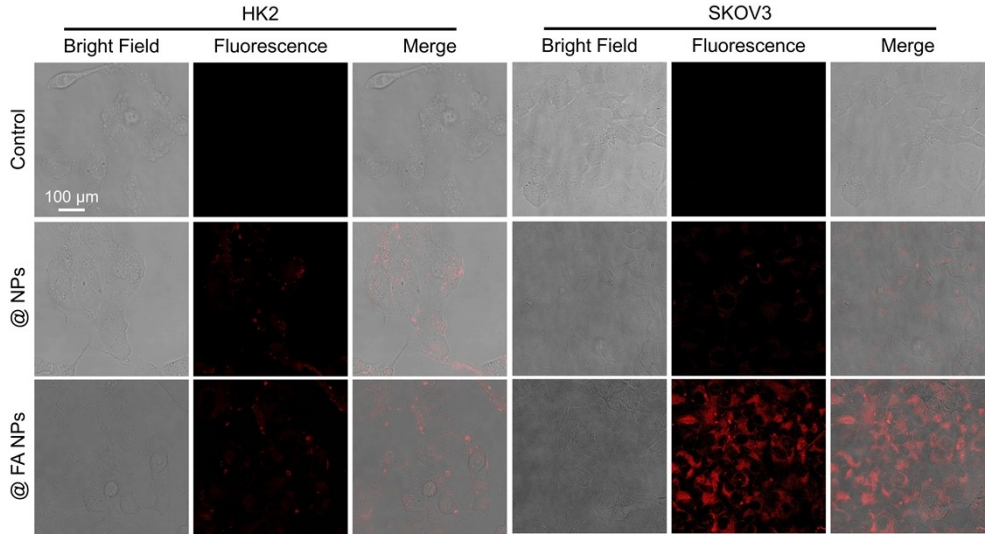

Figure S24. Confocal fluorescence images of HK2 and SKOV3 cells after 1 h incubation with LQM-FOO@NPs or LQM-FOO@FA NPs (10 μM), λ_{ex} = 635 nm, λ_{em} = 700-850 nm.

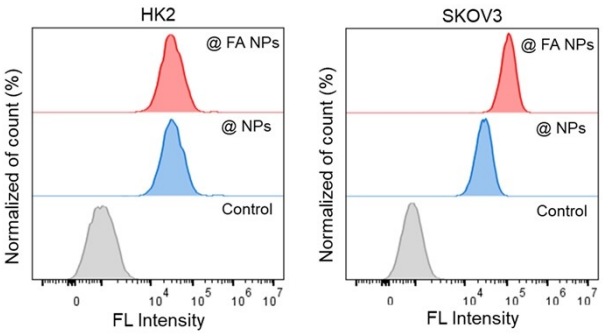

Figure S25. Cellular uptake efficiency evaluation by flow cytometry after 1 h incubation with LQM-FOO@NPs or LQM-FOO@FA NPs (10 μM), λ_{ex} = 638 nm, 763/43BP.

12. Intracellular NAD^+/NADH detection

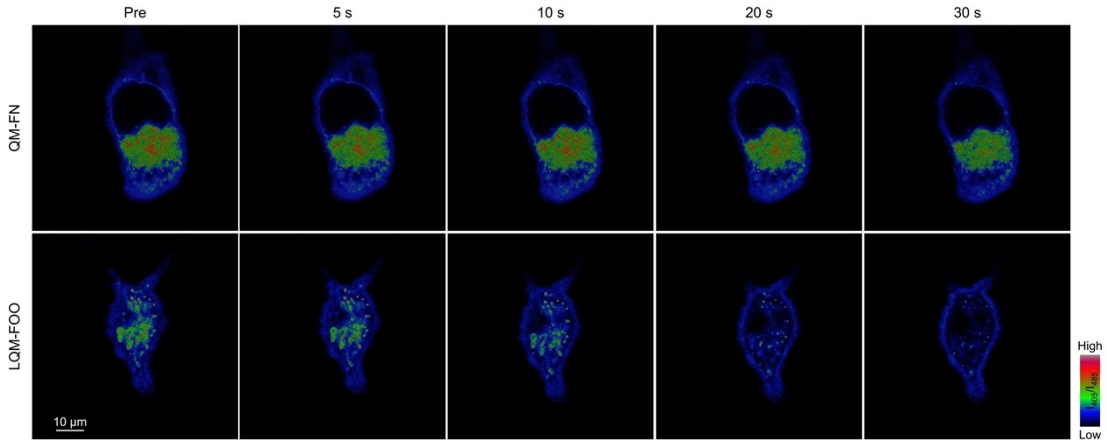

Figure S26. Detection of NAD^+/NADH ratio using SoNar after incubation with QM-FN or LQM-FOO (10 μM) upon irradiation (635 nm, 50 mW cm^{-2}, irradiation time of 1 min corresponding to energy dose of 3 J cm^{-2}) at different time points. Note: a low I_{405}/I_{485} ratio indicates a high NAD^+/NADH ratio.

13. Intracellular ROS detection

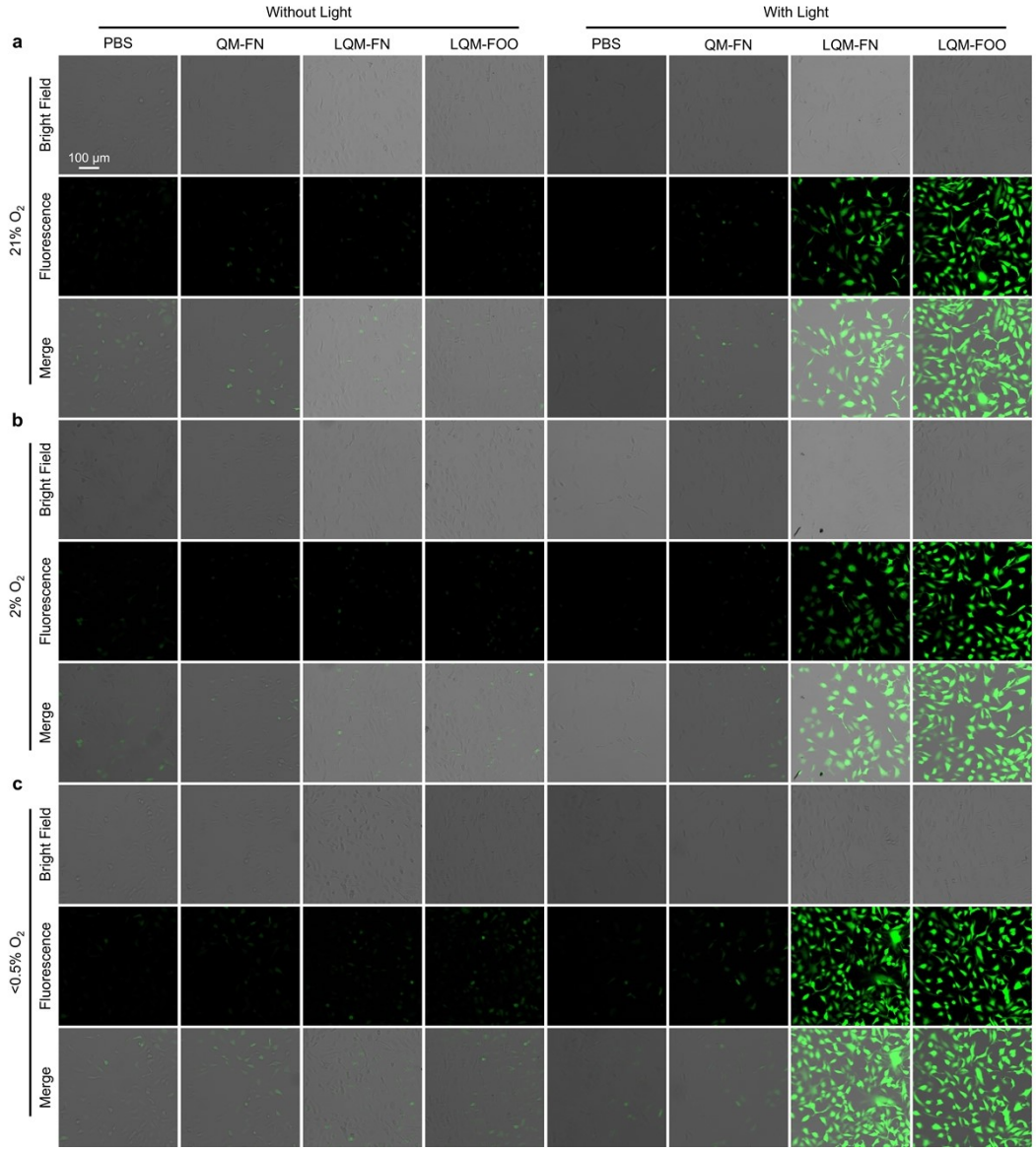

Figure S27. Detection of intracellular total ROS production (DCFH-DA as indicator, λ_{ex} = 488 nm, λ_{em} = 525-580 nm) after incubation with PBS, QM-FN@FA NPs, LQM-FN@FA NPs and LQM-FOO@FA NPs (10 μM), with or without 660 nm light irradiation (50 mW/cm^2 for 5 min, irradiation time of 1 min corresponding to energy dose of 3 J cm^{-2}), under 21% **(a)**, 2% **(b)**, and <0.5% O_2 **(c)** conditions.

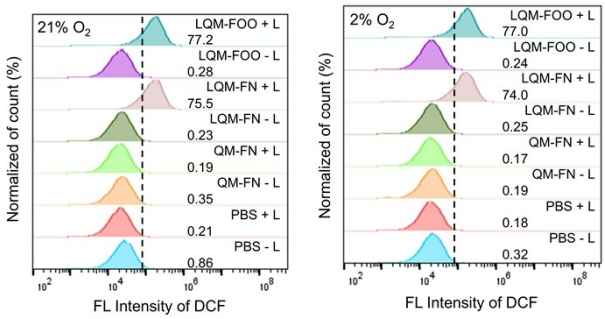

Figure S28. Flow cytometric analysis of intracellular total ROS production (DCFH-DA as indicator, λ_{ex} = 488 nm, 525/40BP) after incubation with PBS, QM-FN@FA NPs, LQM-FN@FA NPs and LQM-FOO@FA NPs (10 μM), with or without 660 nm light irradiation (50 mW/cm^2 for 5 min, irradiation time of 1 min corresponding to energy dose of 3 J cm^{-2}), under different oxygen content environment.

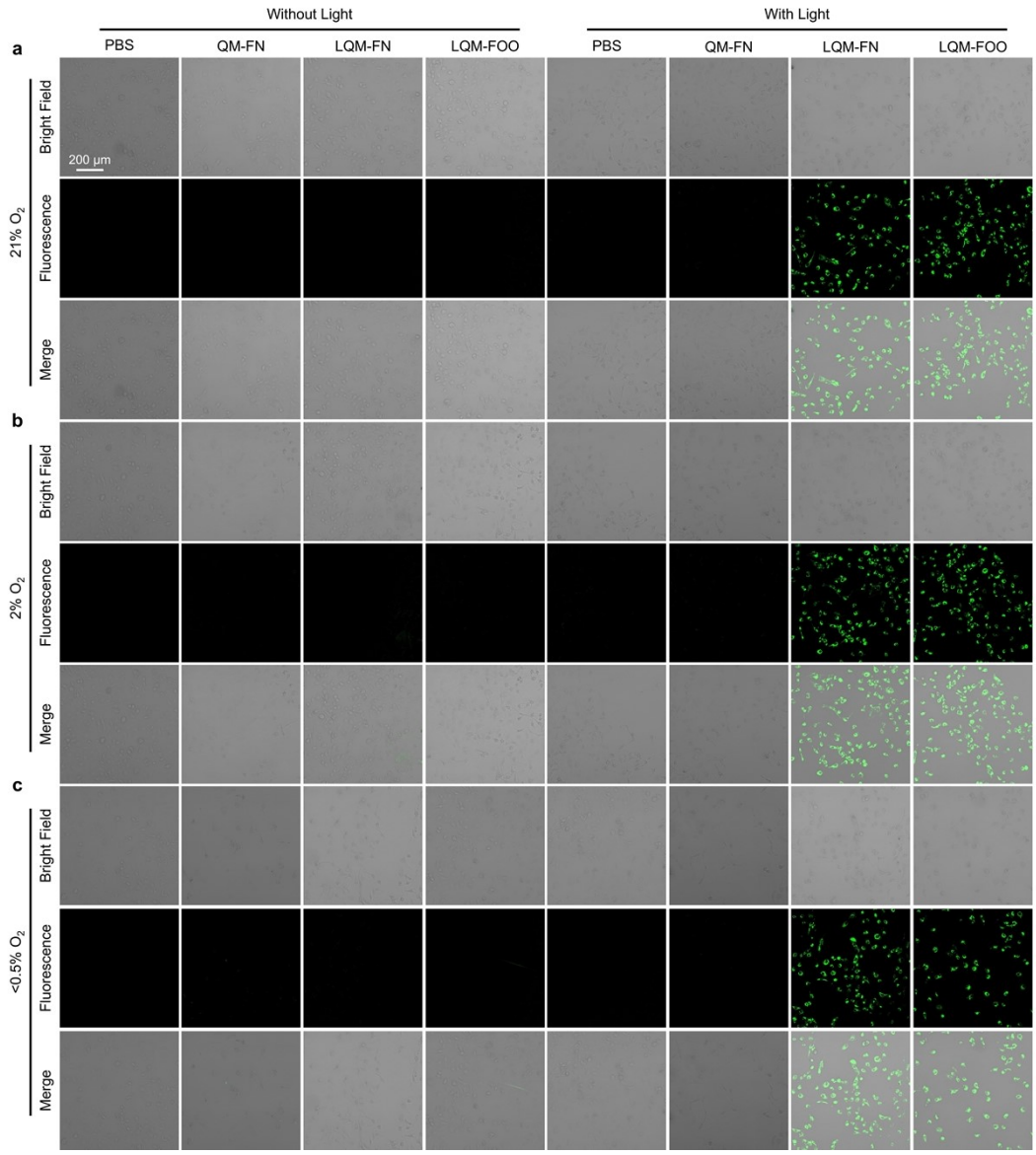

Figure S29. Detection of intracellular ·OH production (HPF as indicator, λ_{ex} = 450 nm, λ_{em} = 510-580 nm) after incubation with PBS, QM-FN@FA NPs, LQM-FN@FA NPs and LQM-FOO@FA NPs (10 μM), with or without 660 nm light irradiation (50 mW/cm^2 for 15 min, irradiation time of 1 min corresponding to energy dose of 3 J cm^{-2}), under 21% **(a)**, 2% **(b)**, and <0.5% O_2 **(c)** conditions.

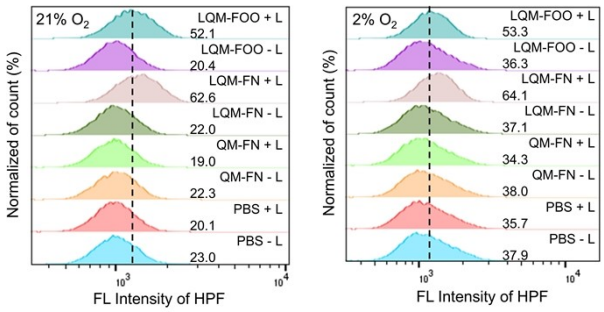

Figure S30. Flow cytometric analysis of intracellular ·OH production (HPF as indicator, λ_{ex} = 488 nm, 525/40BP) after incubation with PBS, QM-FN@FA NPs, LQM-FN@FA NPs and LQM-FOO@FA NPs (10 μM), with or without 660 nm light irradiation (50 mW/cm^2 for 15 min, irradiation time of 1 min corresponding to energy dose of 3 J cm^{-2}), under different oxygen content environment.

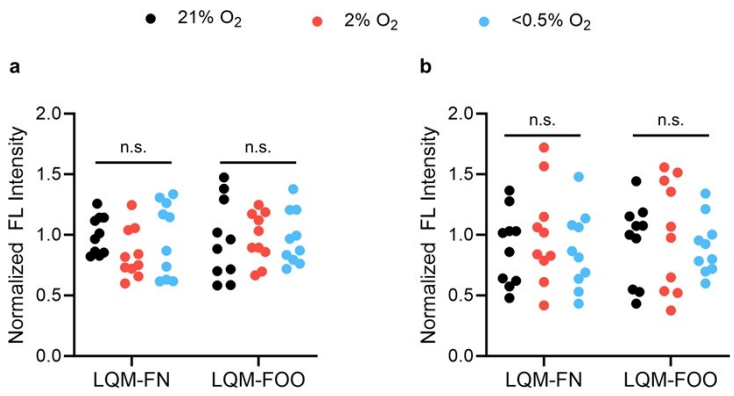

Figure S31. Normalized intracellular fluorescence intensities of DCFH **(a)** and HPF **(b)** after incubation with LQM-FN@FA NPs or LQM-FOO@FA NPs (10 μM) under different oxygen conditions upon 660 nm light irradiation. The maximum average fluorescence intensity of each group under different oxygen conditions was used as the normalization standard. Statistical significance (*P* value) is calculated by two-sided *t*-test. n.s.: not significant.

14. Evaluation of cancer cell killing efficiency

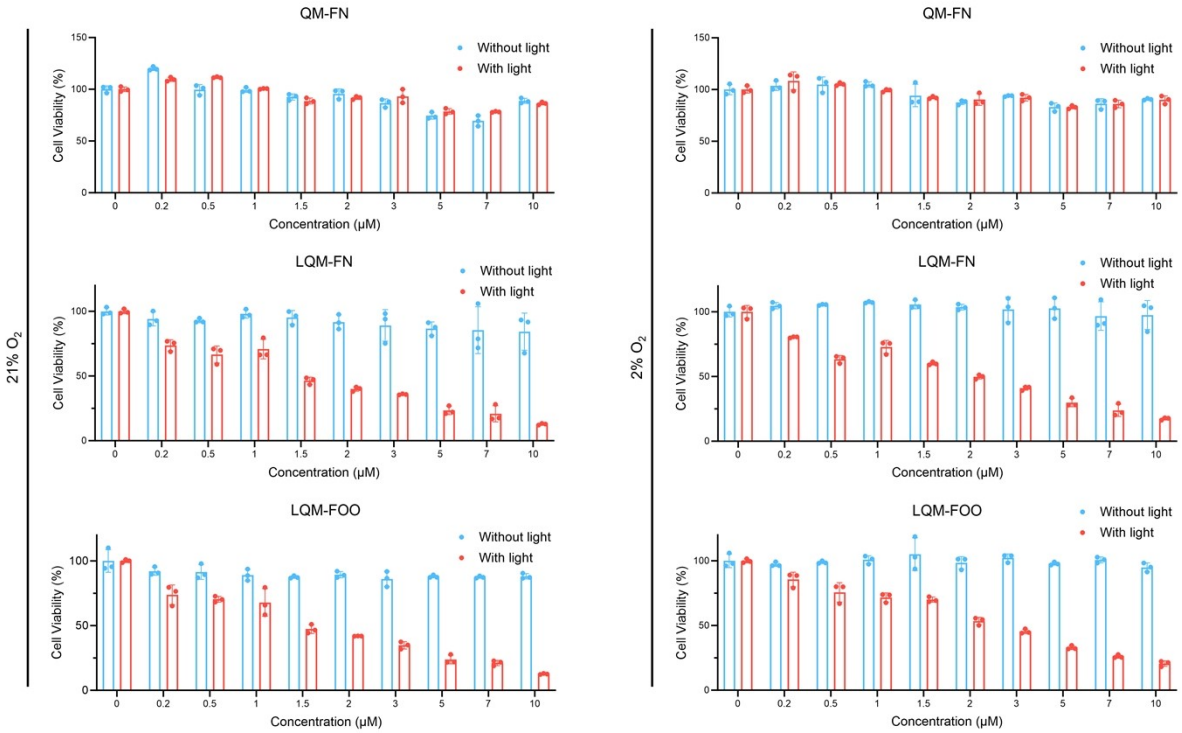

Figure S32. Evaluation of cancer cell killing efficiency by MTT assay after incubation with different concentrations of QM-FN@FA NPs, LQM-FN@FA NPs or LQM-FOO@FA NPs, with or without 660 nm light irradiation (50 mW/cm^2 for 15 min, irradiation time of 1 min corresponding to energy dose of 3 J cm^{-2}), under different oxygen content environment. Data are expressed as the mean ± SD of three independent experiments.

We further evaluated the cancer cell killing efficiency under an oxygen concentration below 0.5%. The experimental results demonstrated that LQM PSs retained robust cancer cell killing efficacy even under extremely hypoxic conditions:

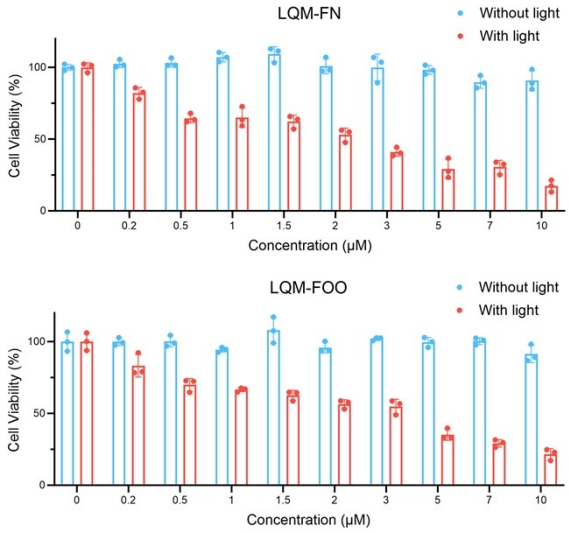

Figure S33. Evaluation of cancer cell killing efficiency by MTT assay after incubation with different concentrations of LQM-FN@FA NPs or LQM-FOO@FA NPs, with or without 660 nm light irradiation (50 mW/cm^2 for 15 min, irradiation time of 1 min corresponding to energy dose of 3 J cm^{-2}), under an oxygen concentration below 0.5%. Data are expressed as the mean ± SD of three independent experiments.

oxygen concentration	compound	IC_{50}(light, μM)	IC_{50}(dark, μM)	phototoxic indexes
21% O_2	LQM-FN	1.06	>512	>483
	LQM-FOO	1.18	>512	>433
2% O_2	LQM-FN	1.61	>512	>318
	LQM-FOO	2.42	>512	>211
<0.5% O_2	LQM-FN	1.85	>512	>276
	LQM-FOO	2.43	>512	>210

Figure S34. The photocytotoxicities and dark toxicities as well as the phototoxic indexes of LQM-FN and LQM-FOO in SKOV3 cells under different oxygen content environment.

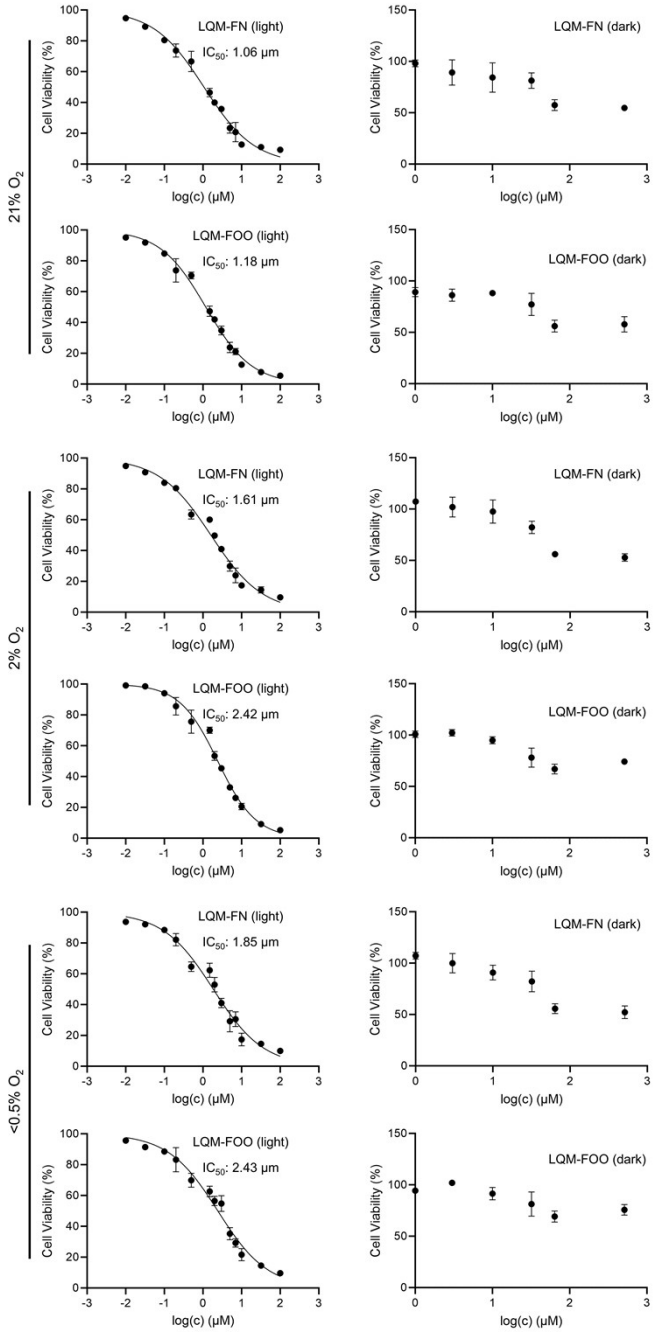

Figure S35. The data used to determine the IC_{50} values including the mathematical fits of LQM-FN and LQM-FOO in SKOV3 cells under different oxygen content environment.

15. Apoptosis evaluation by flow cytometry

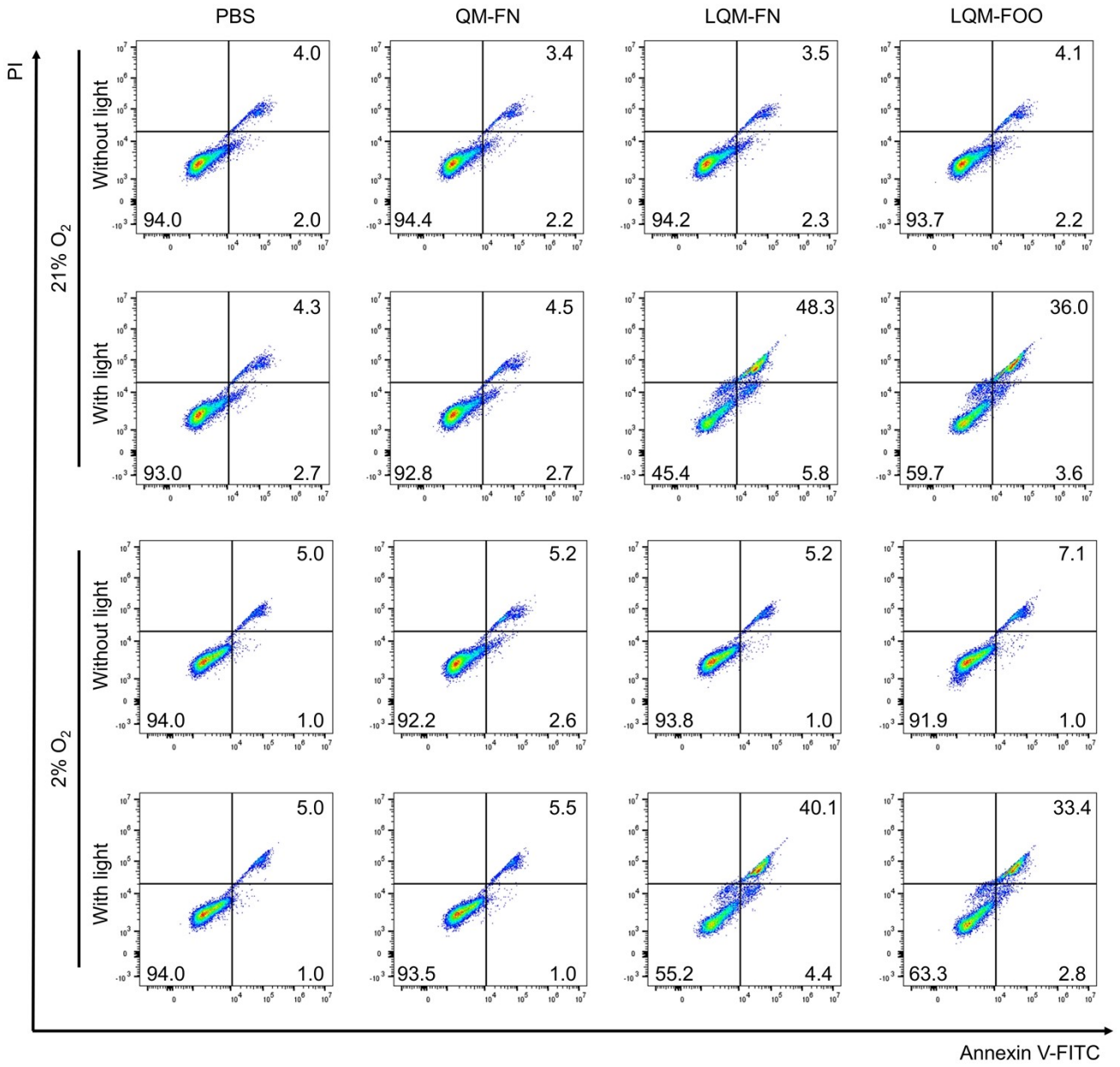

Figure S36. Apoptosis evaluation by flow cytometry after incubation with PBS, QM-FN@FA NPs, LQM-FN@FA NPs and LQM-FOO@FA NPs (1 μM), with or without 660 nm light irradiation (50 mW/cm^2 for 15 min, irradiation time of 1 min corresponding to energy dose of 3 J cm^{-2}), under different oxygen content environment.

16. Fluorescence imaging of mice

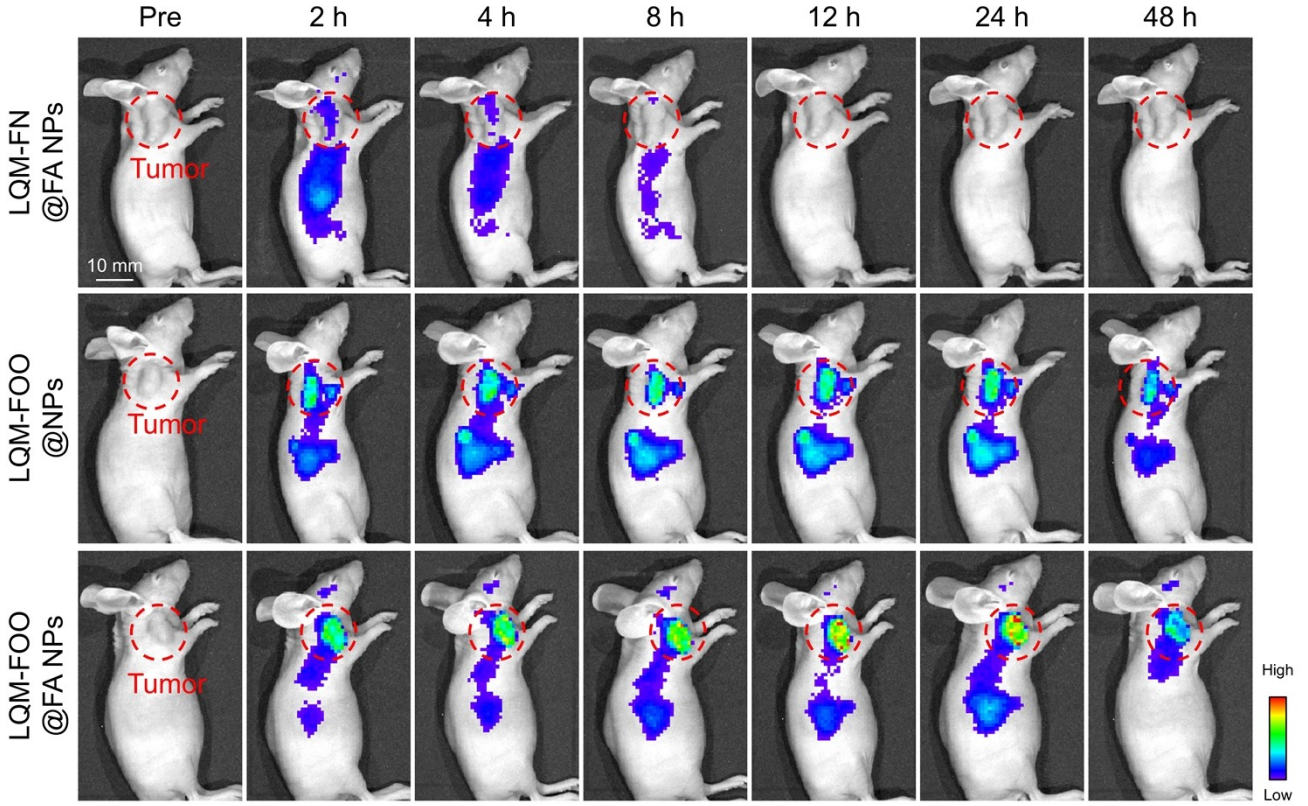

Figure S37. *In vivo* fluorescence imaging of SKOV3 xenograft tumor-bearing mice at different time points following intravenous administration of LQM-FN@FA NPs, LQM-FOO@NPs, or LQM-FOO@FA NPs (0.5 mg mL^{-1}, 200 μL, λ_{ex} = 600 ± 10 nm, λ_{em} = 845 ± 20 nm).

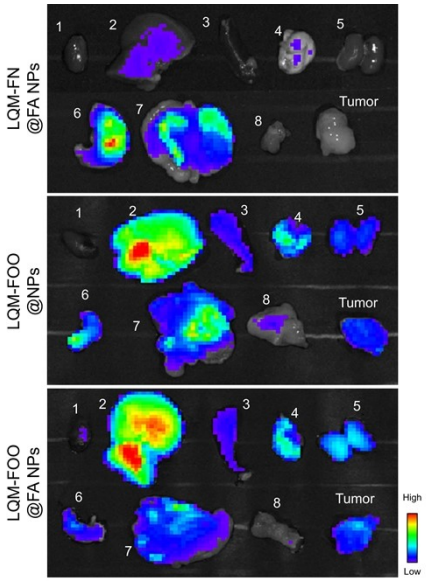

Figure S38. *Ex vivo* fluorescence imaging of the excised organs (1 heart, 2 liver, 3 spleen, 4 lung, 5 kidney, 6 stomach, 7 intestine, 8 muscle, and tumor) at 12 h after the intravenous injection of LQM-FN@FA NPs, LQM-FOO@NPs, or LQM-FOO@FA NPs (0.5 mg mL^{-1}, 200 μL, λ_{ex} = 600 ± 10 nm, λ_{em} = 845 ± 20 nm).

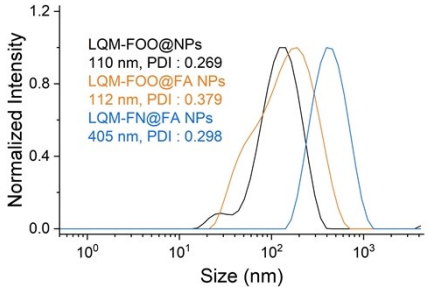

Figure S39. Particle size measurement by dynamic light scattering. The sizes of LQM-FOO@NPs, LQM-FOO@FA NPs and LQM-FN@FA NPs were determined to be 110 nm (PDI: 0.269), 112 nm (PDI: 0.379) and 405 nm (PDI: 0.298), respectively.

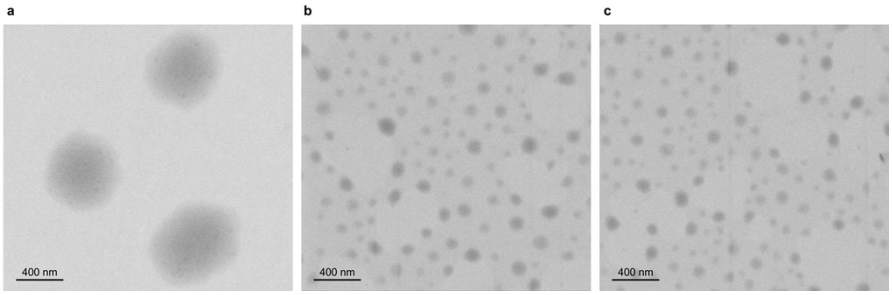

Figure S40. Transmission electron microscopy (TEM) images of LQM-FN@FA NPs **(a)**, LQM-FOO@FA NPs **(b)** and LQM-FOO@NPs **(c)**. This is consistent with the results obtained from dynamic light scattering characterization.

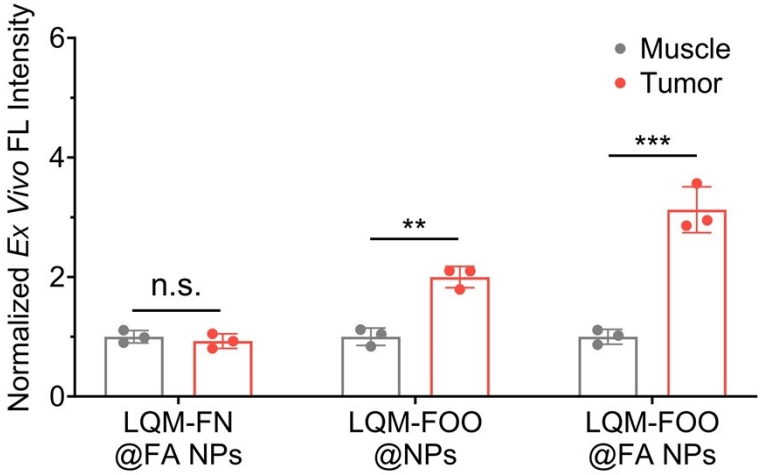

Figure S41. Normalized *ex vivo* fluorescent intensity in tumor and muscle tissues 12 hours after intravenous injection of LQM-FN@FA NPs, LQM-FOO@NPs, and LQM-FOO@FA NPs. Data are expressed as the mean ± SD of three independent mice. Statistical significance (*P* value) is calculated by two-sided *t*-test. n.s.: not significant, $^{**}P < 0.01$, $^{***}P < 0.001$.

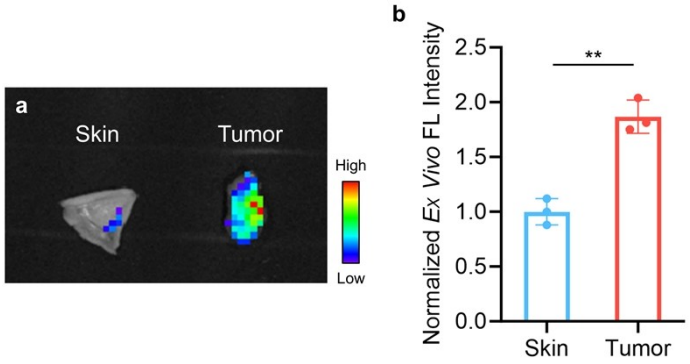

Figure S42. (a) *Ex vivo* fluorescence imaging of the excised organs (skin and tumor) at 12 h after the intravenous injection of LQM-FOO@FA NPs (0.5 mg mL^{-1}, 200 μL, λ_{ex} = 600 ± 10 nm, λ_{em} = 845 ± 20 nm). **(b)** Normalized *ex vivo* fluorescent intensity in tumor and skin tissues 12 hours after intravenous injection of LQM-FOO@FA NPs. Data are expressed as the mean ± SD of three independent mice. Statistical significance (*P* value) is calculated by two-sided *t*-test. $^{**}P < 0.01$. This result indicates that LQM-FOO@FA NPs exhibit excellent tumor-to-skin selectivity.

17. Photothermal imaging of mice

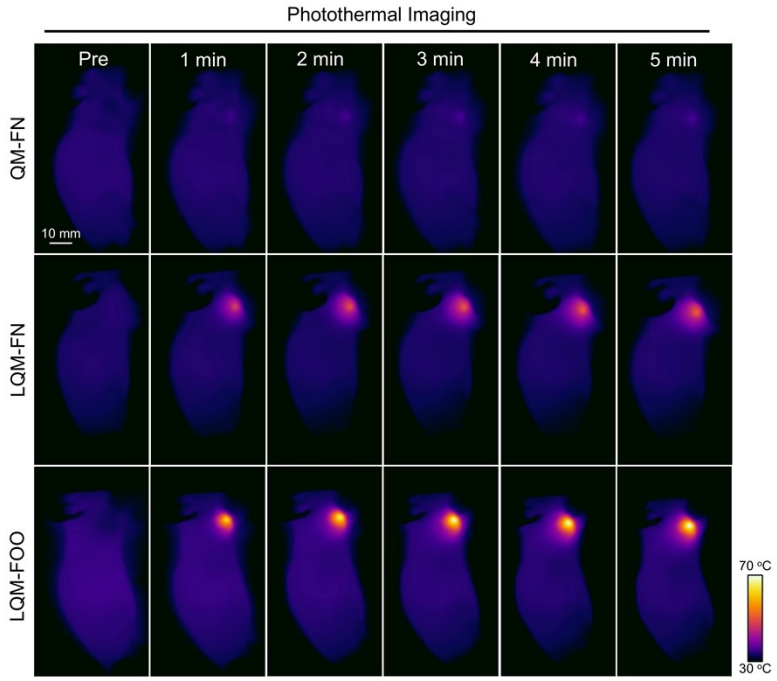

Figure S43. *In vivo* photothermal imaging of SKOV3 xenograft tumor-bearing mice at different time points following administration of QM-FN@FA NPs, LQM-FN@FA NPs, or LQM-FOO@FA NPs (under irradiation at 635 nm, 0.2 W cm^{-2}, irradiation time of 1 min corresponding to energy dose of 12 J cm^{-2}).

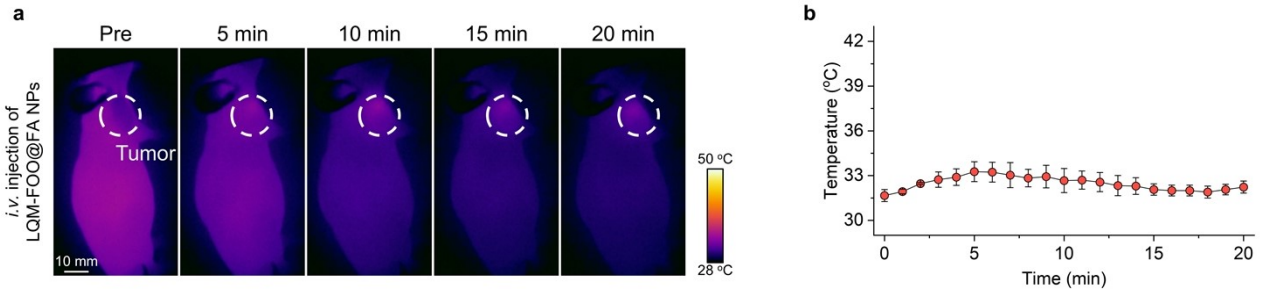

Figure S44. (a) *In vivo* photothermal imaging of SKOV3 xenograft tumor-bearing mice at different irradiation time points following intravenous administration of LQM-FOO@FA NPs for 48 h (0.5 mg mL^{-1}, 200 μL, under irradiation at 635 nm, 0.2 W cm^{-2}, irradiation time of 1 min corresponding to energy dose of 12 J cm^{-2}). **(b)** Temperature change profiles at different irradiation time points following intravenous administration of LQM-FOO@FA NPs for 48 h. Note: The body temperature of the mice may decrease during anesthesia. Data are expressed as the mean ± SD of three independent mice.

18. The light power density measurement setup and the emission spectrum of the used light source

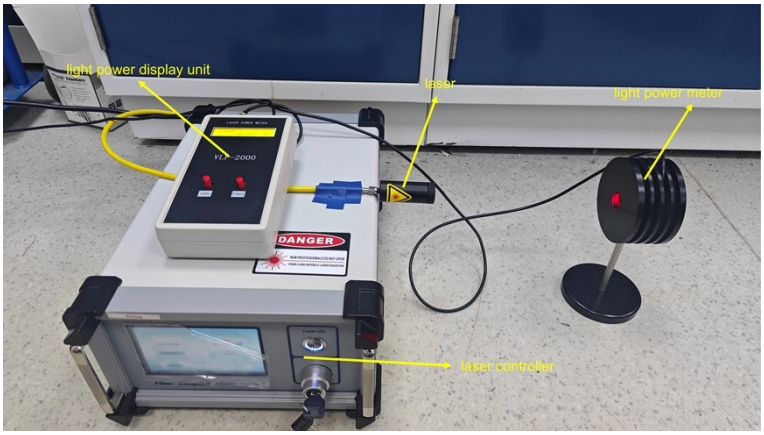

Figure S45. Photograph of light power density measurement setup. Taking cuvette-based experiments as an example, the distance between the cuvette and the laser source was fixed at 15 cm. Therefore, during calibration, both the laser output and the light power meter were aligned along the same horizontal line at this fixed distance of 15 cm to measure the corresponding light power density at the sample position. Specifically, in the cuvette experiments, the desired light power density was set to 50 mW cm^{-2}. Given that the laser spot size at the sample plane was circular with a radius of 0.5 cm, the irradiation area can be calculated as: $A = \pi r^2 = \pi \times 0.5 \times 0.5 = 0.785$ cm^2. Accordingly, the required light power was calculated as: $P = I \times A = 50$ mW $cm^{-2} \times 0.785$ $cm^2 = 39.3$ mW. Based on this calculation, we adjusted the laser controller until the light power meter displayed a power output of 39.3 mW, ensuring that the irradiance at the sample position reached the intended value for all subsequent experiments.

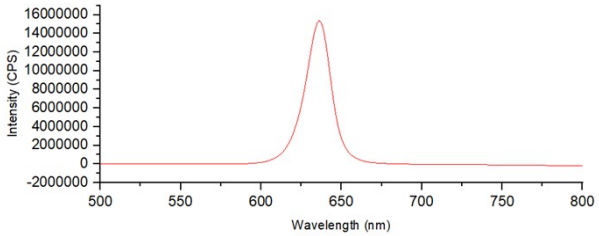

Figure S46. The emission spectrum of 635 nm laser (Beijing Blueprint Photoelectric Technology Co., Ltd.).

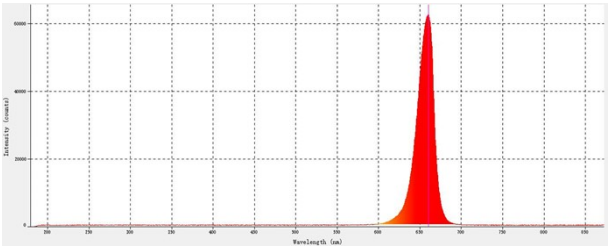

Figure S47. The emission spectrum of 660 nm laser (Beijing NBET Technology Co., Ltd.).

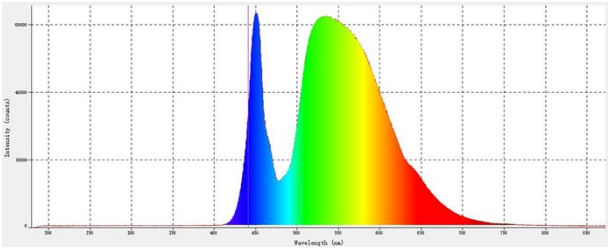

Figure S48. The emission spectrum of white light (Beijing NBET Technology Co., Ltd.).

19. Characterization of intermediate compounds, QM-FN, and LQM PSs

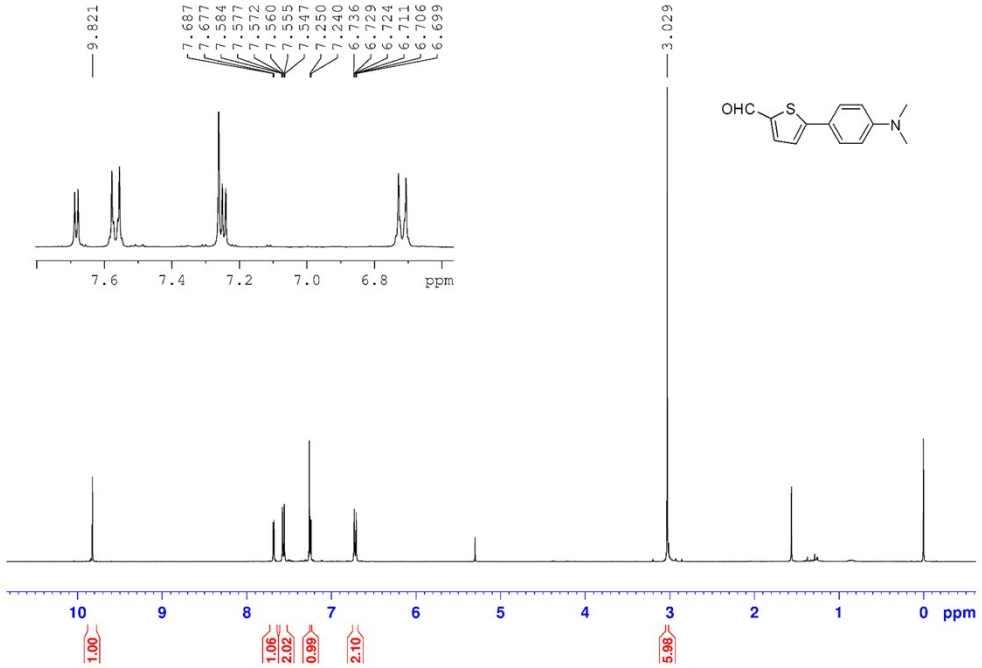

Figure S49. ^{1}H NMR spectrum of CHO-FN in $CDCl_3$

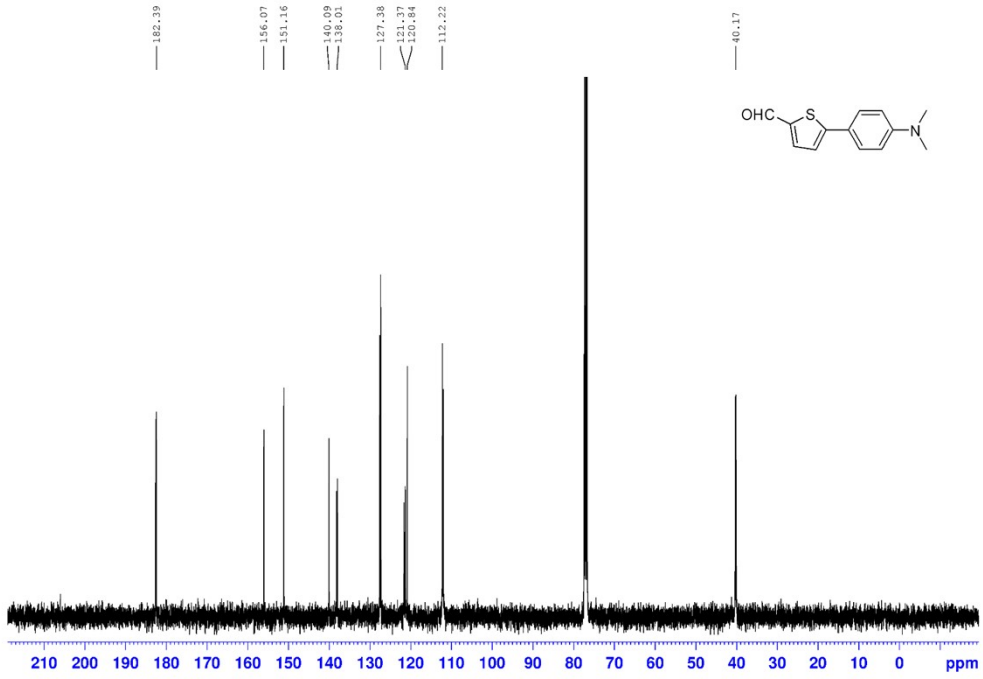

Figure S50. ^{13}C NMR spectrum of CHO-FN in $CDCl_3$

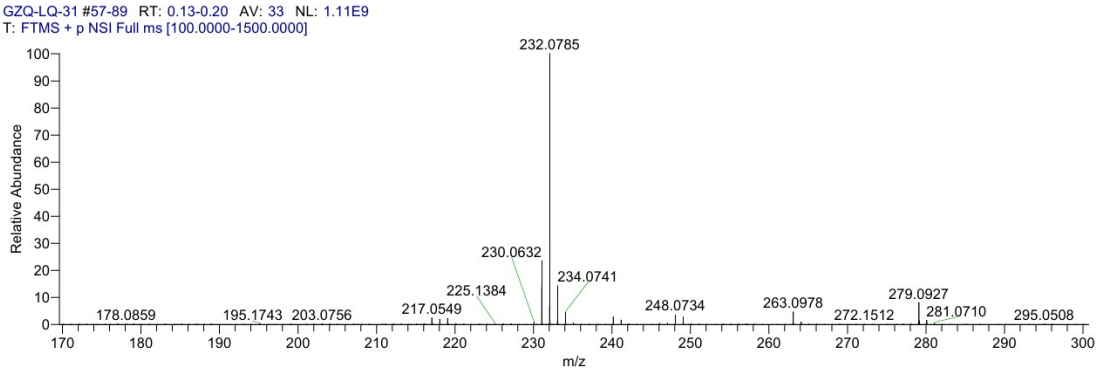

GZQ-LQ-31#57-89 RT: 0.13-0.20 AV: 33
T: FTMS + p NSI Full ms [100.0000-1500.0000]
m/z= 231.59-232.53

m/z	Intensity	Relative	Theo. Mass	Delta (ppm)	Composition
232.0785	1150020608.0	100.00	232.0791	-0.58	$C_{13}H_{14}ONS$

Figure S51. HRMS spectrum of CHO-FN

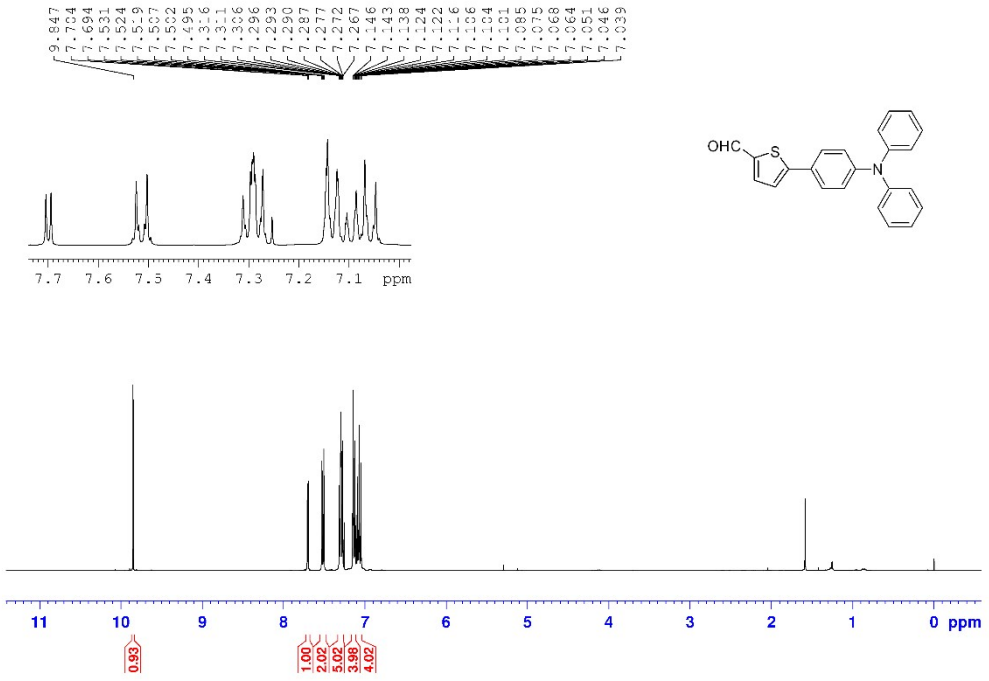

Figure S52. ^{1}H NMR spectrum of CHO-FTPA in $CDCl_3$

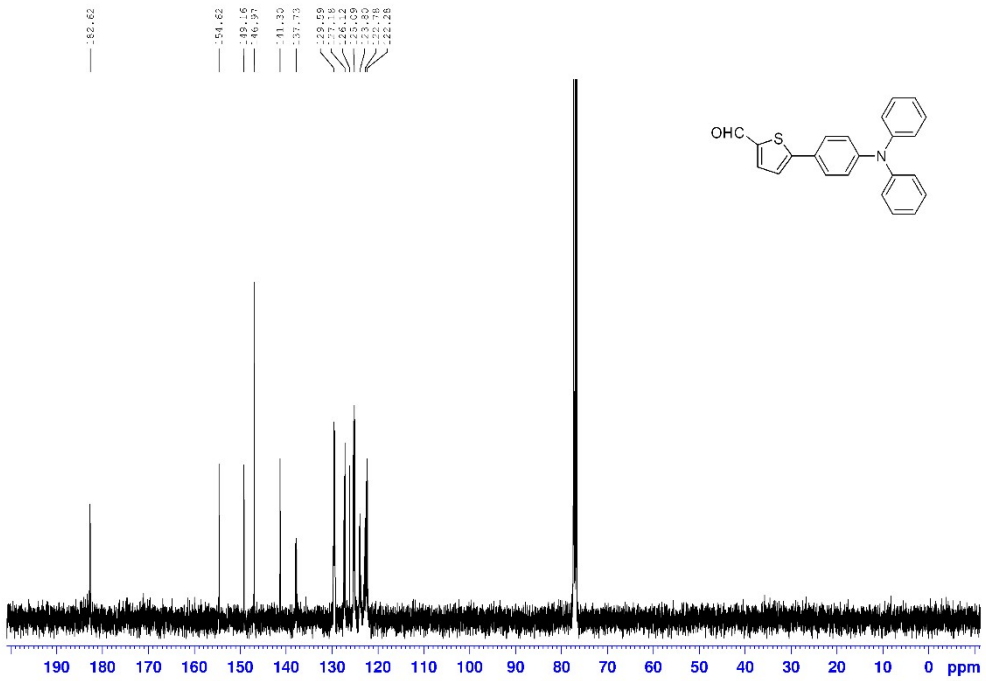

Figure S53. ^{13}C NMR spectrum of CHO-FTPA in $CDCl_3$

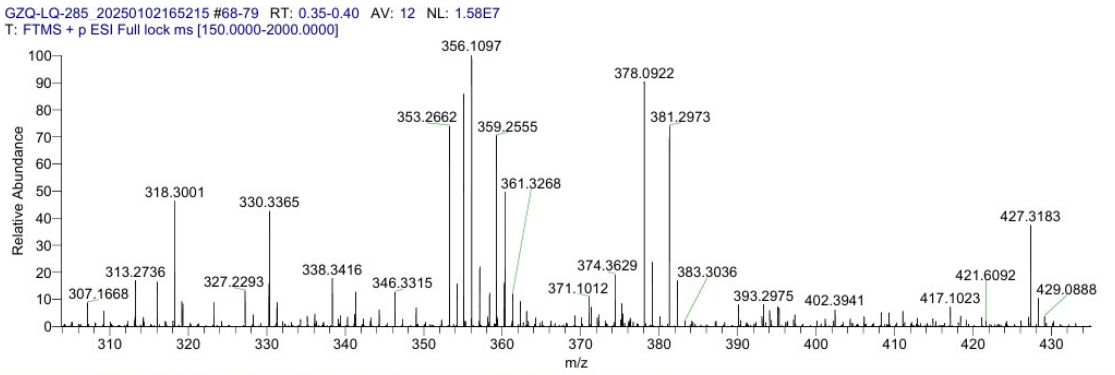

GZQ-LQ-285_20250102165215#68-79 RT: 0.35-0.40 AV: 12
T: FTMS + p ESI Full lock ms [150.0000-2000.0000]
m/z= 355.15-356.59

m/z	Intensity	Relative	Theo. Mass	Delta (ppm)	Composition
356.1097	15802384.0	100.00	356.1104	-0.65	$C_{23}H_{18}ONS$

Figure S54. HRMS spectrum of CHO-FTPA

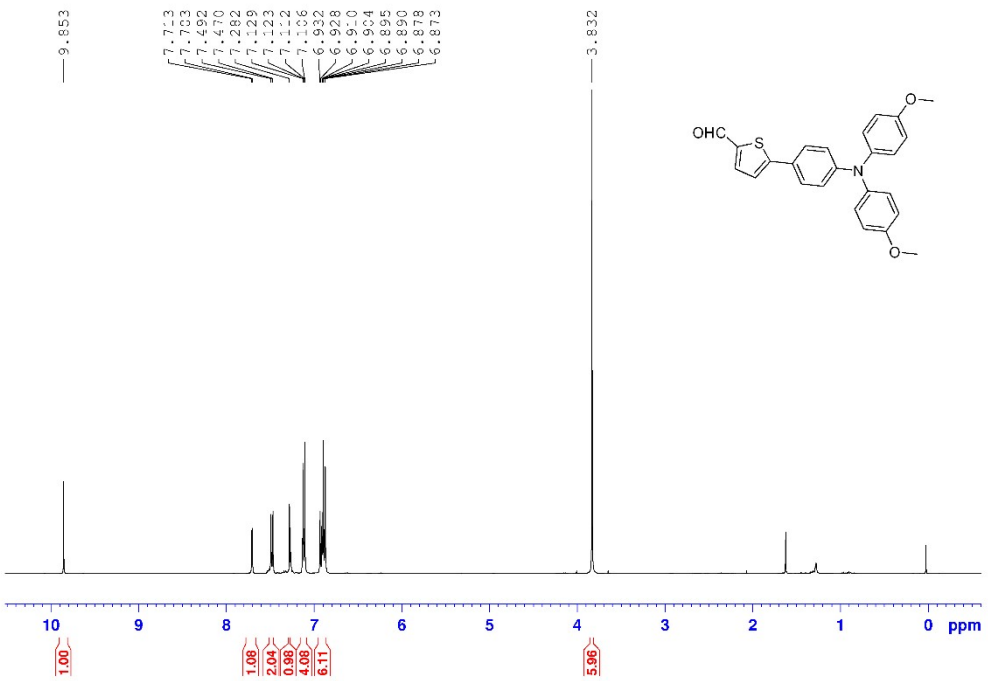

Figure S55. ^{1}H NMR spectrum of CHO-FTPA-OME in $CDCl_3$

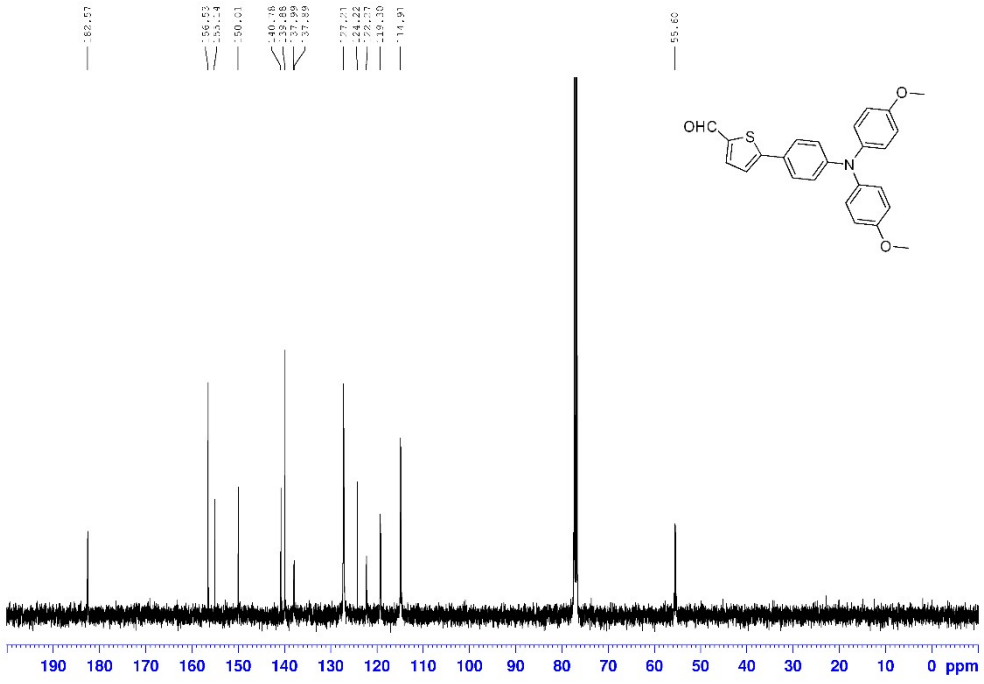

Figure S56. ^{13}C NMR spectrum of CHO-FTPA-OME in $CDCl_3$

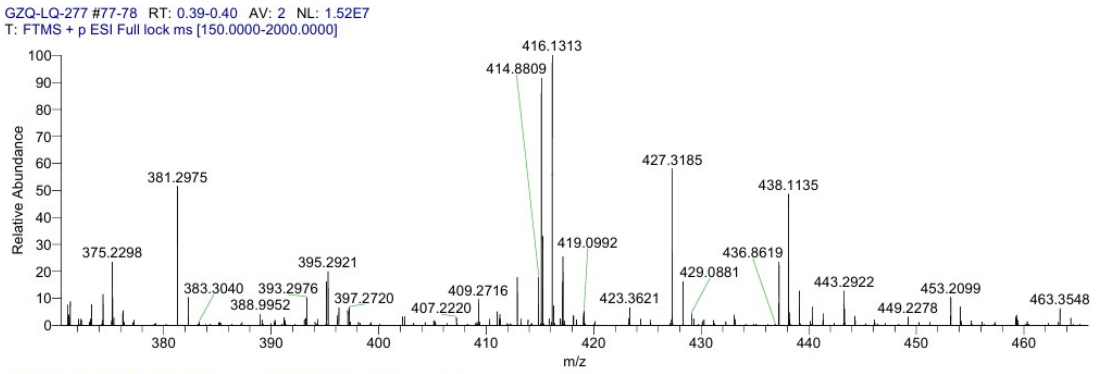

GZQ-LQ-277#77-78 RT: 0.39-0.40 AV: 2
T: FTMS + p ESI Full lock ms [150.0000-2000.0000]
m/z= 415.61-416.40

m/z	Intensity	Relative	Theo. Mass	Delta (ppm)	Composition
416.1313	15229687.0	100.00	416.1315	-0.15	$C_{25}H_{22}O_3NS$

Figure S57. HRMS spectrum of CHO-FTPA-OME

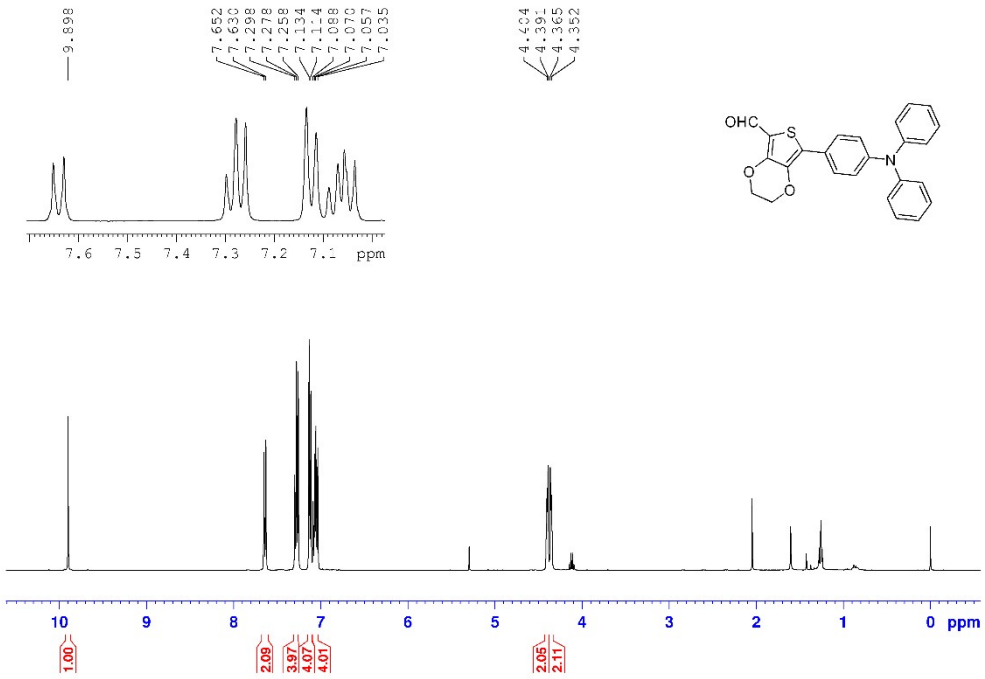

Figure S58. ^{1}H NMR spectrum of CHO-FOTPA in $CDCl_3$

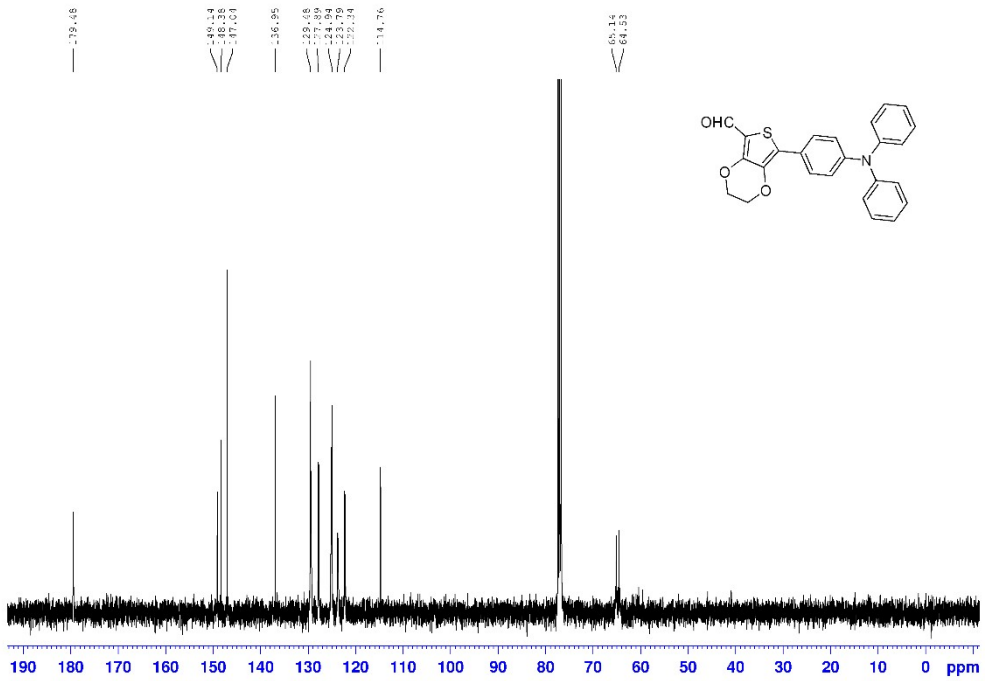

Figure S59. ^{13}C NMR spectrum of CHO-FOTPA in $CDCl_3$

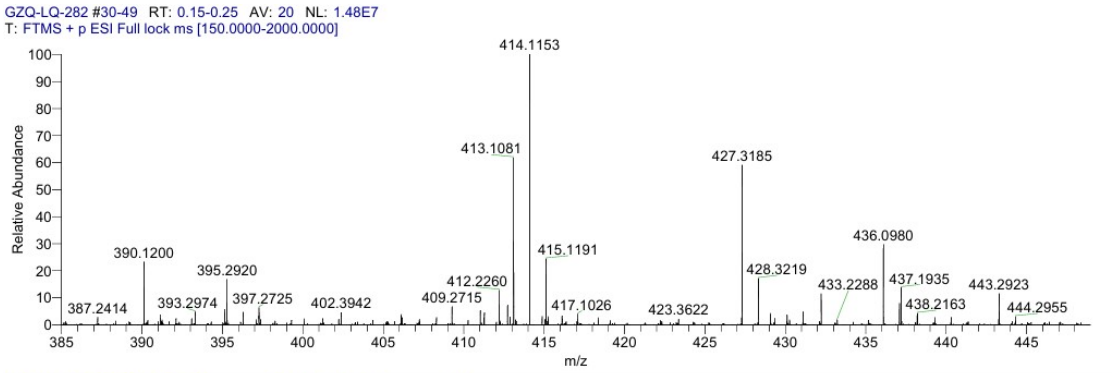

GZQ-LQ-282#29-50 RT: 0.15-0.25 AV: 22
T: FTMS + p ESI Full lock ms [150.0000-2000.0000]
m/z= 413.70-414.52

m/z	Intensity	Relative	Theo. Mass	Delta (ppm)	Composition
414.1153	15003711.0	100.00	414.1158	-0.58	$C_{25}H_{20}O_3NS$

Figure S60. HRMS spectrum of CHO-FOTPA

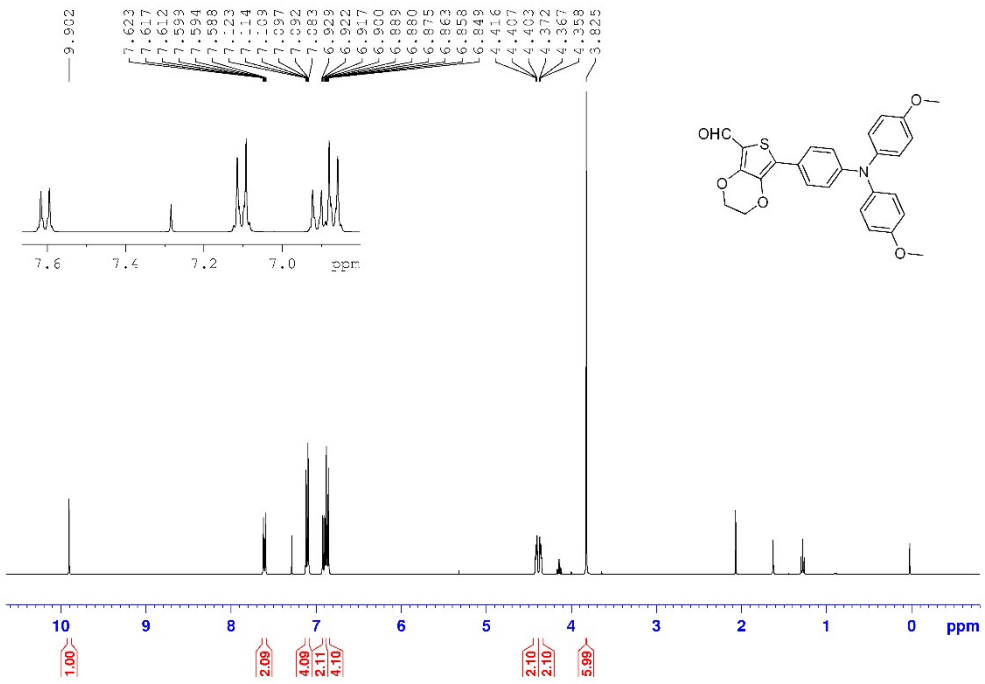

Figure S61. ^{1}H NMR spectrum of CHO-FOTPA-OME in $CDCl_3$

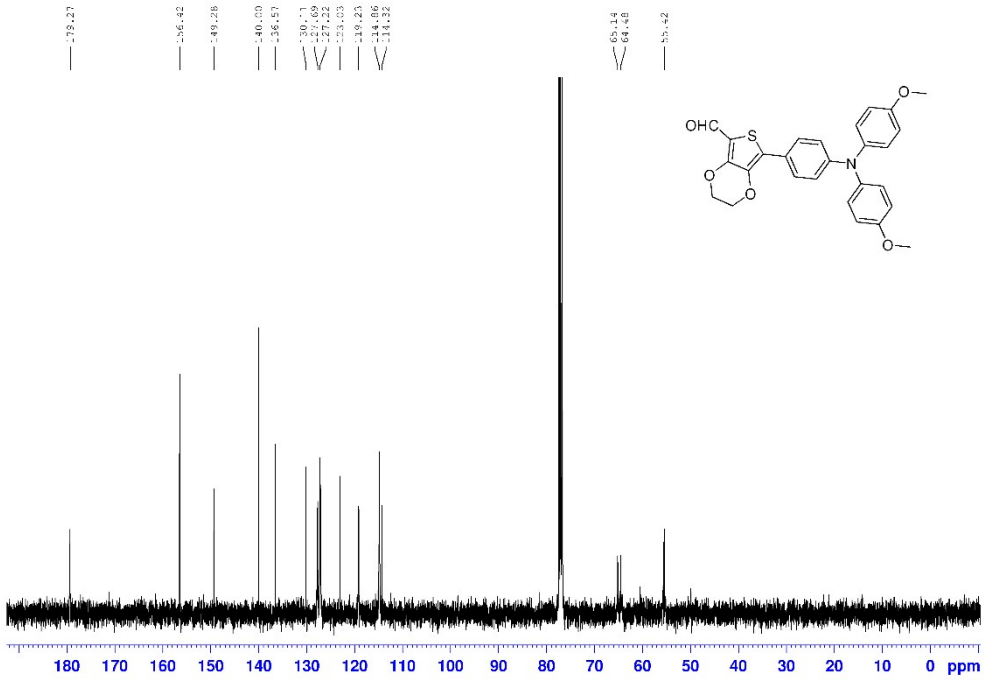

Figure S62. ^{13}C NMR spectrum of CHO-FOTPA-OME in $CDCl_3$

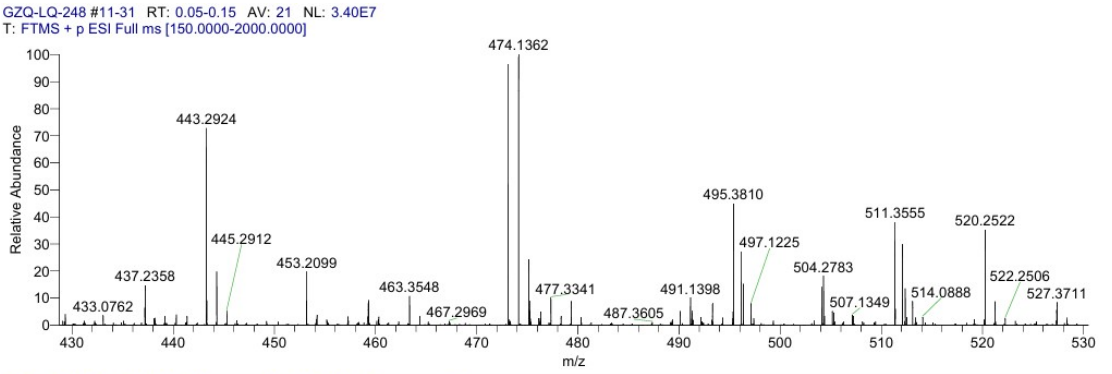

GZQ-LQ-248#10-31 RT: 0.05-0.15 AV: 22
T: FTMS + p ESI Full lock ms [150.0000-2000.0000]
m/z= 473.42-474.46

m/z	Intensity	Relative	Theo. Mass	Delta (ppm)	Composition
474.1362	34266112.0	100.00	474.1370	-0.75	$C_{27}H_{24}O_5NS$

Figure S63. HRMS spectrum of CHO-FOTPA-OME

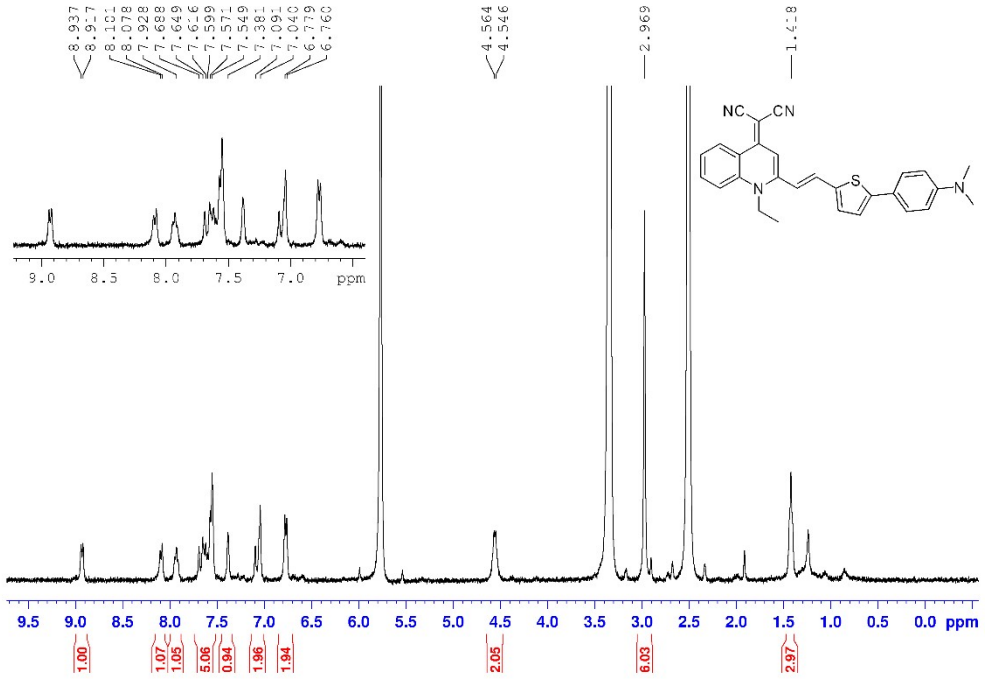

Figure S64. ^{1}H NMR spectrum of QM-FN in DMSO-d_6

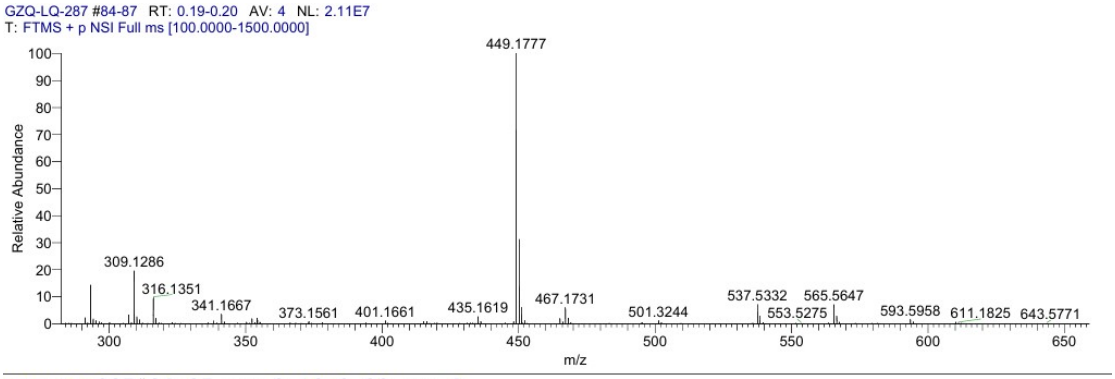

GZQ-LQ-287#84-87 RT: 0.19-0.20 AV: 4
T: FTMS + p NSI Full ms [100.0000-1500.0000]
m/z= 442.80-454.40

m/z	Intensity	Relative	Theo. Mass	Delta (ppm)	Composition
449.1777	21072218.0	100.00	449.1794	-1.79	$C_{28}H_{25}N_4S$

Figure S65. HRMS spectrum of QM-FN

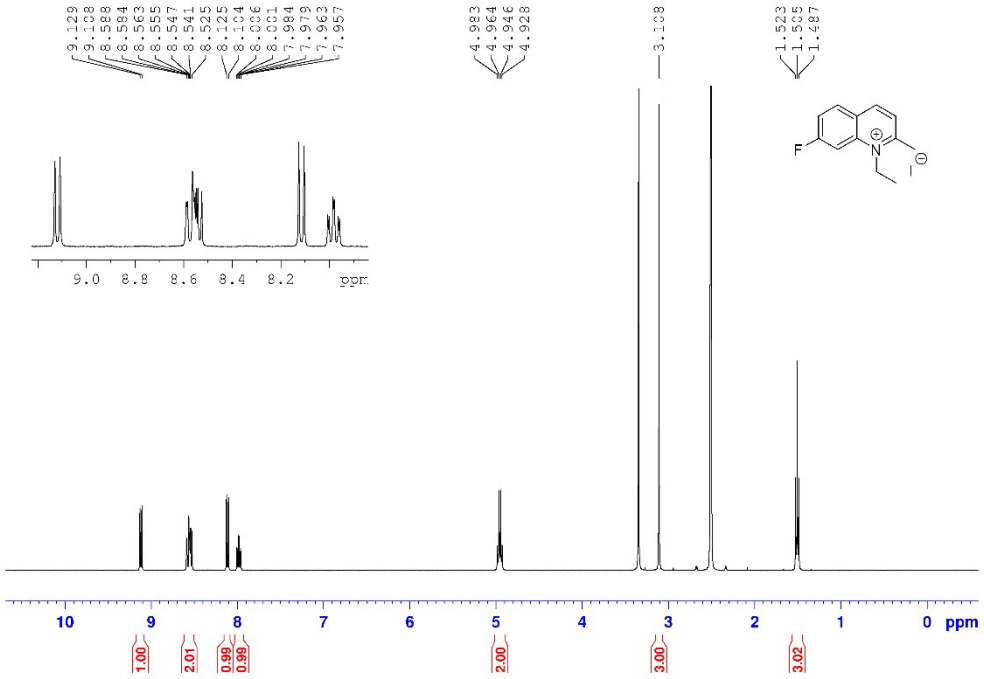

Figure S66. ^{1}H NMR spectrum of F-Q-Et in DMSO-d_6

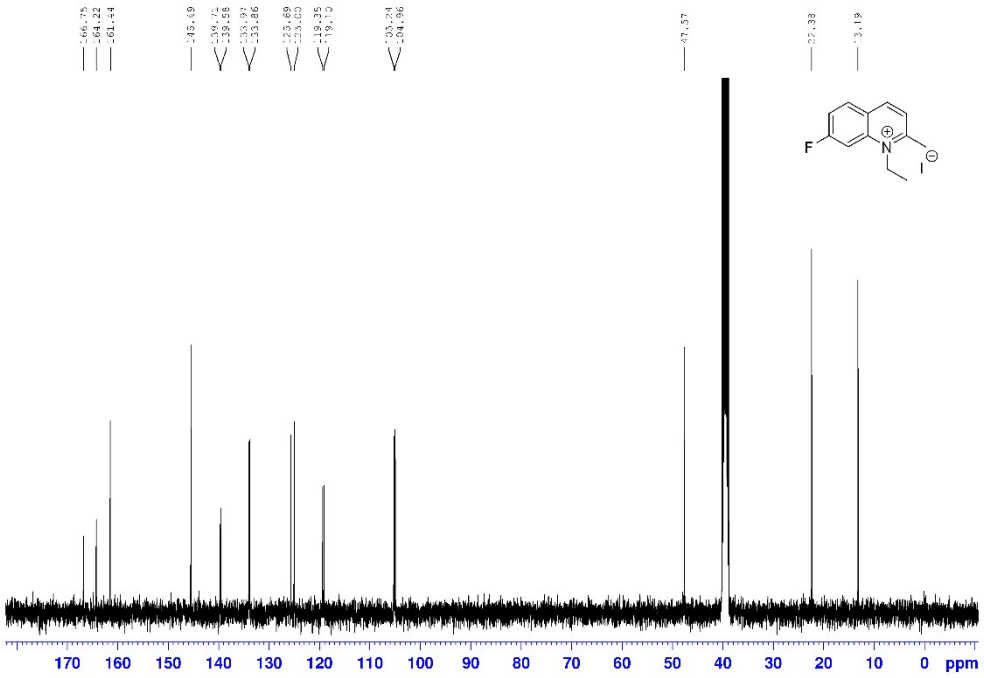

Figure S67. ^{13}C NMR spectrum of F-Q-Et in DMSO-d_6

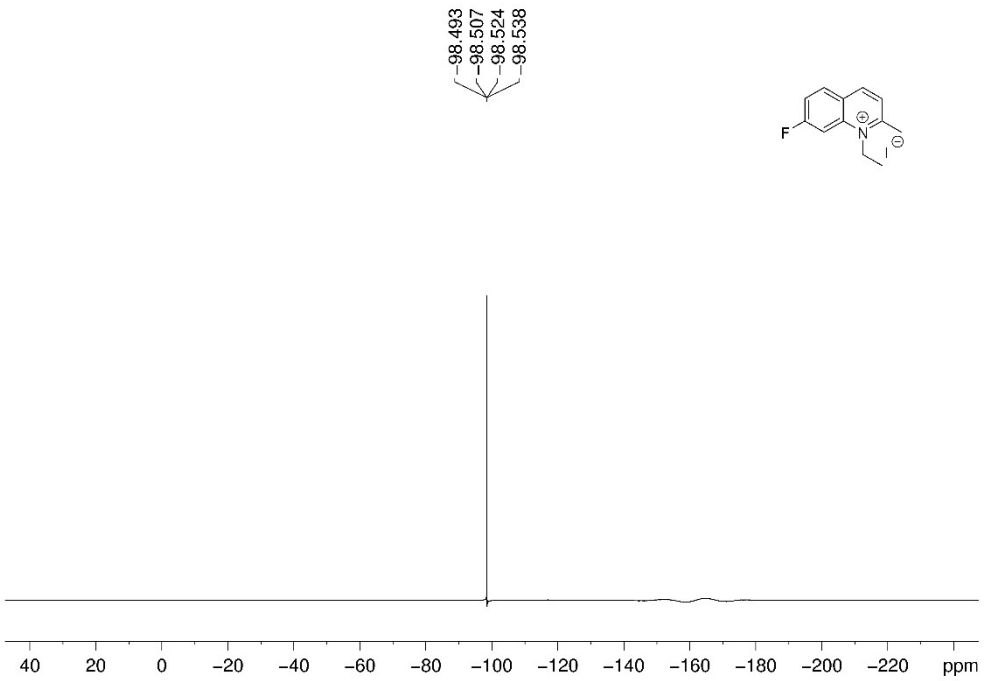

Figure S68. ^{19}F NMR spectrum of F-Q-Et in DMSO-d_6

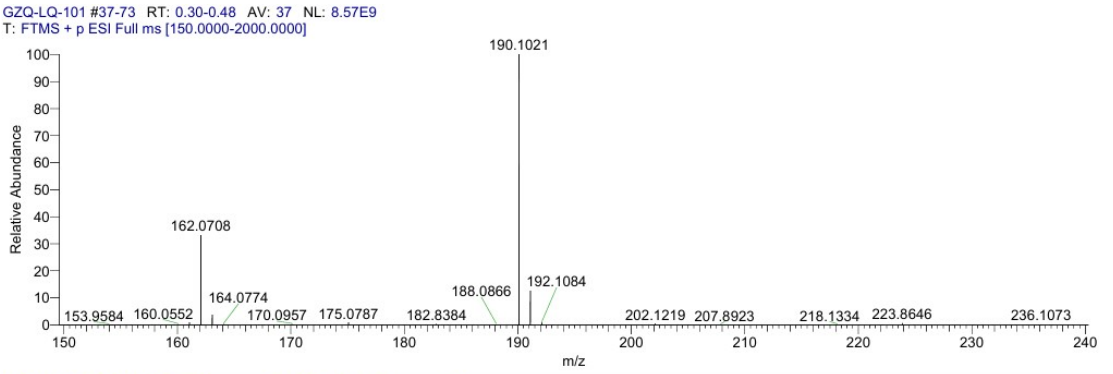

GZQ-LQ-101#49-73 RT: 0.36-0.48 AV: 25
T: FTMS + p ESI Full ms [150.0000-2000.0000]

m/z	Intensity	Relative	Theo. Mass	Delta (ppm)	Composition
190.1021	8395082752.0	100.00	190.1027	-0.58	$C_{12}H_{13}NF$

Figure S69. HRMS spectrum of F-Q-Et

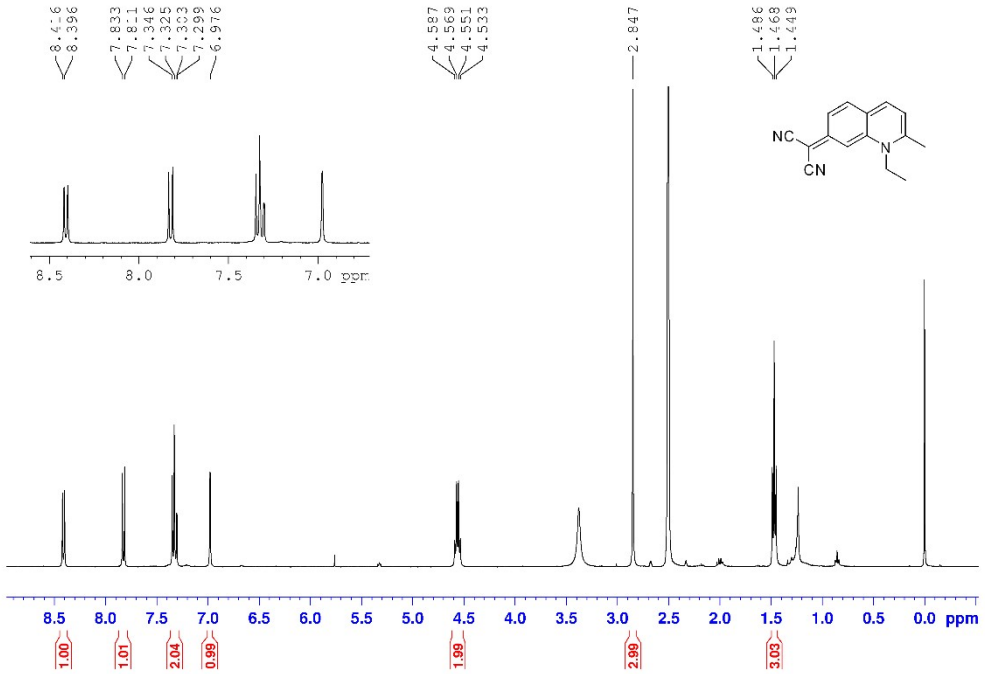

Figure S70. ^{1}H NMR spectrum of LQM in DMSO-d_6

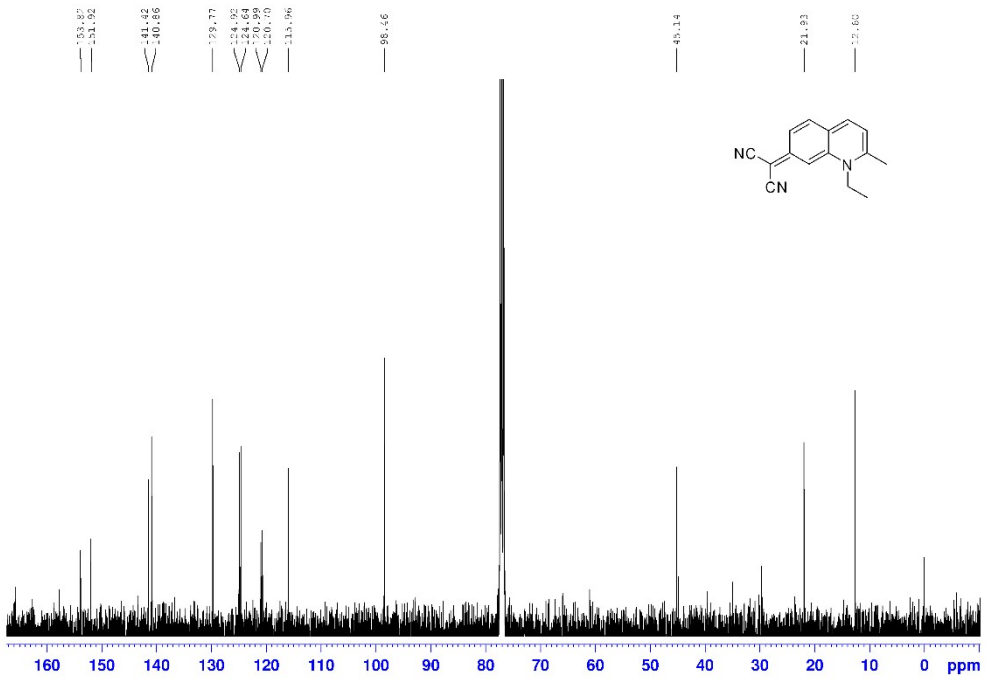

Figure S71. ^{13}C NMR spectrum of LQM in DMSO-d_6

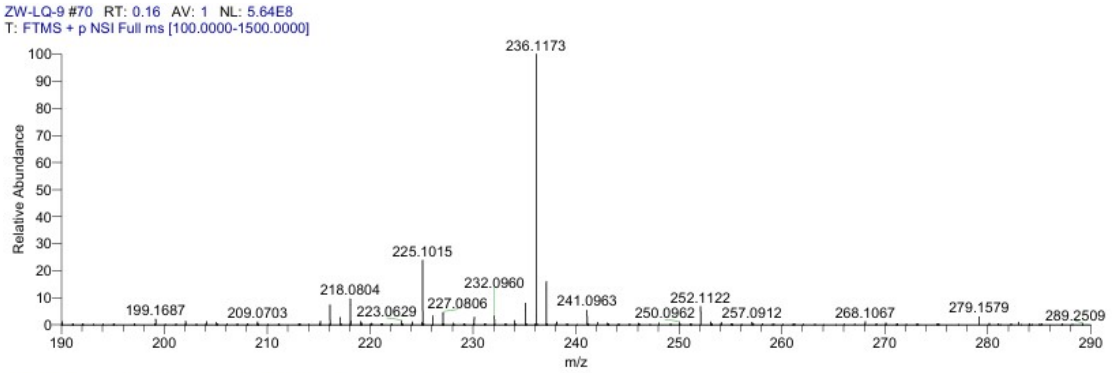

ZW-LQ-9#60-76 RT: 0.14-0.17 AV: 17
T: FTMS + p NSI Full ms [100.0000-1500.0000]
m/z= 231.86-240.13

m/z	Intensity	Relative	Theo. Mass	Delta (ppm)	Composition
236.1172	523366080.0	100.00	236.1182	-1.03	$C_{15}H_{14}N_3$

Figure S72. HRMS spectrum of LQM

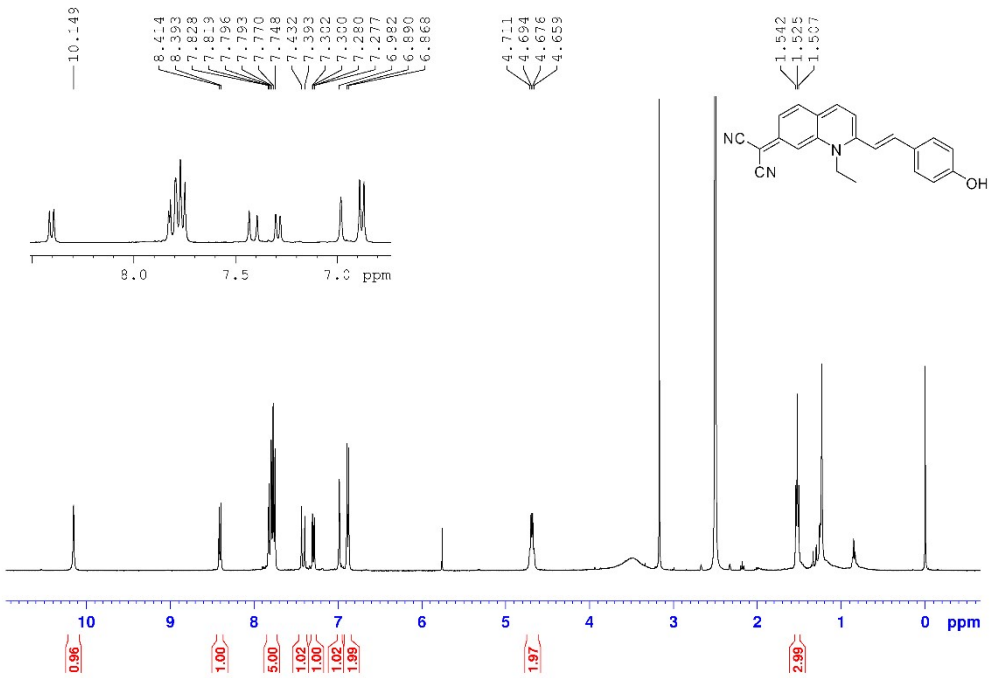

Figure S73. ^{1}H NMR spectrum of LQM-OH in DMSO-d_6

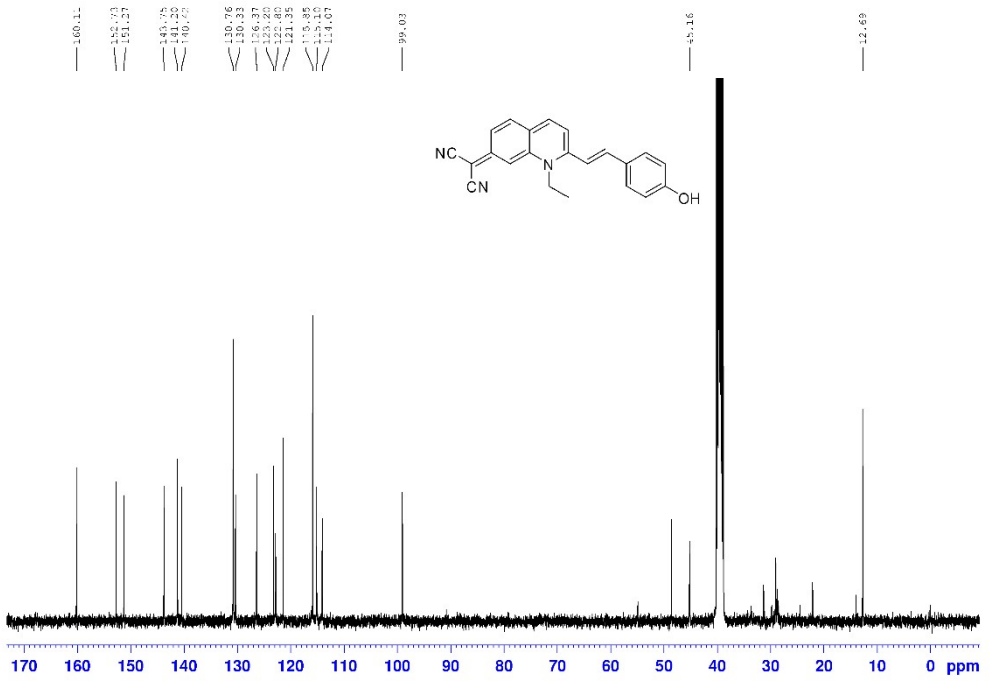

Figure S74. ^{13}C NMR spectrum of LQM-OH in DMSO-d_6

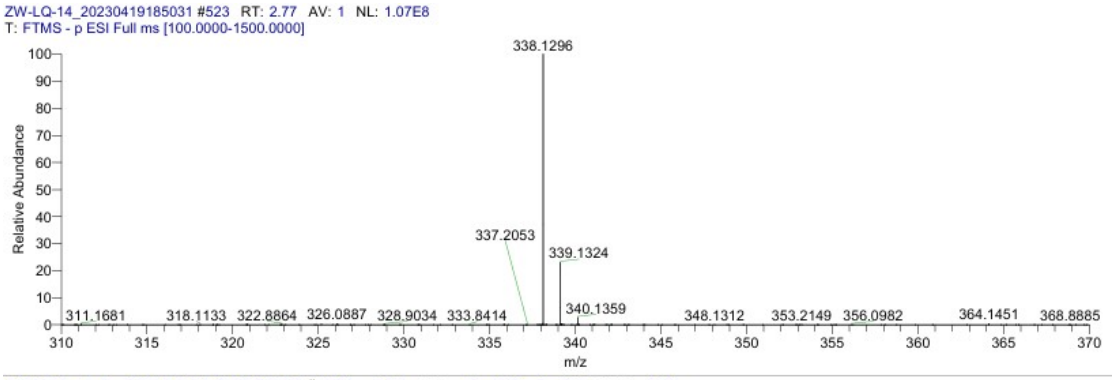

ZW-LQ-14_20230419185031#451-611 RT: 2.39-3.24 AV: 161
T: FTMS - p ESI Full ms [100.0000-1500.0000]
m/z= 337.67-338.49

m/z	Intensity	Relative	Theo. Mass	Delta (ppm)	Composition
338.1296	76250608.0	100.00	338.1288	0.84	$C_{22}H_{16}ON_3$

Figure S75. HRMS spectrum of LQM-OH

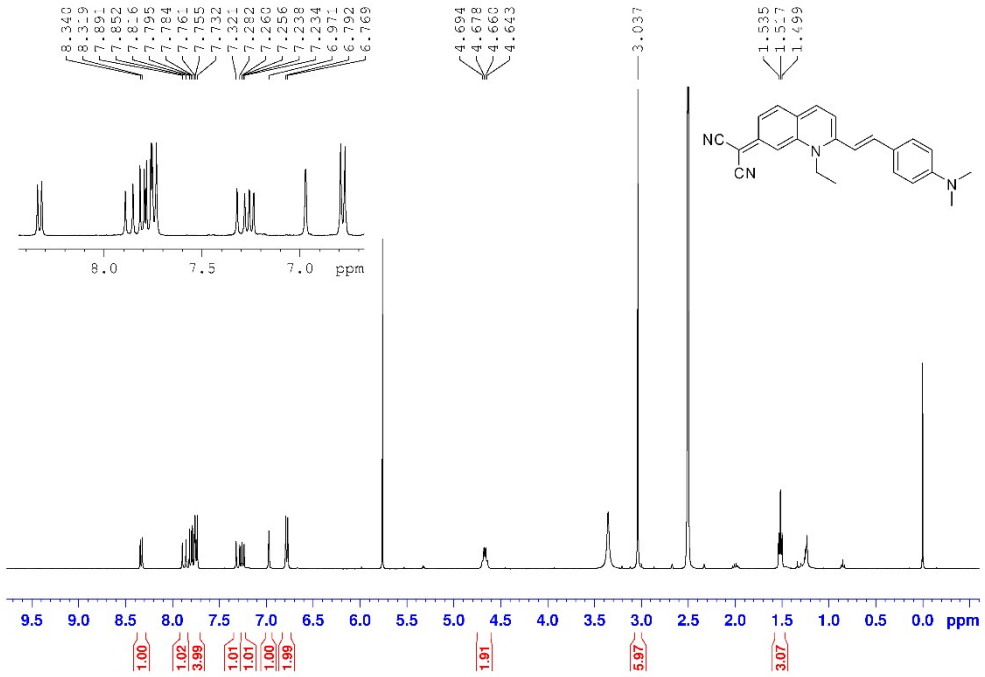

Figure S76. ^{1}H NMR spectrum of LQM-N in DMSO-d_6

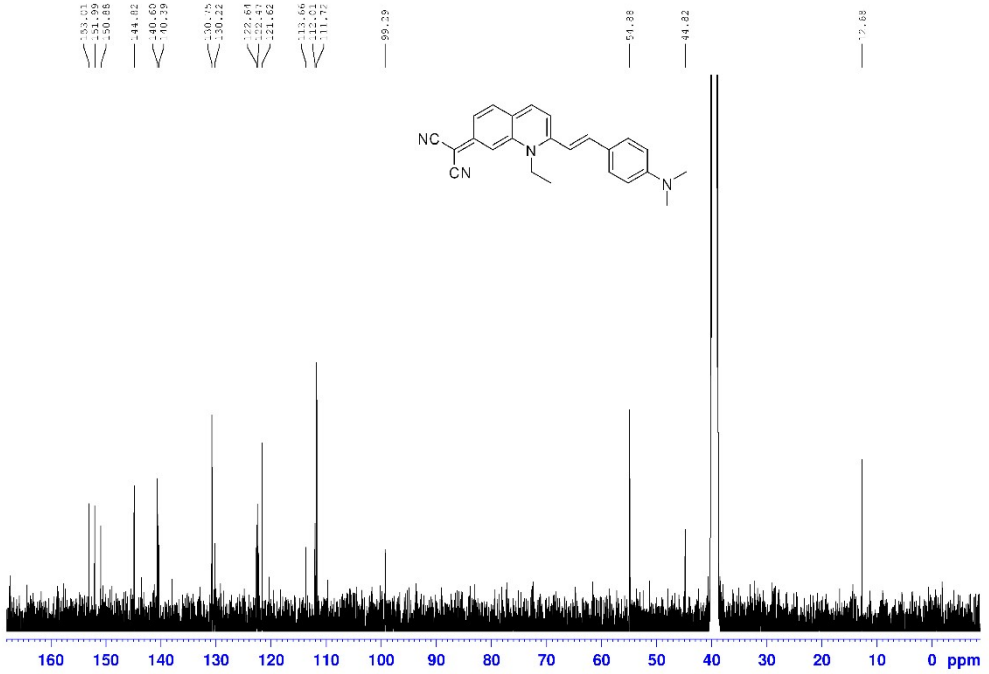

Figure S77. ^{13}C NMR spectrum of LQM-N in DMSO-d_6

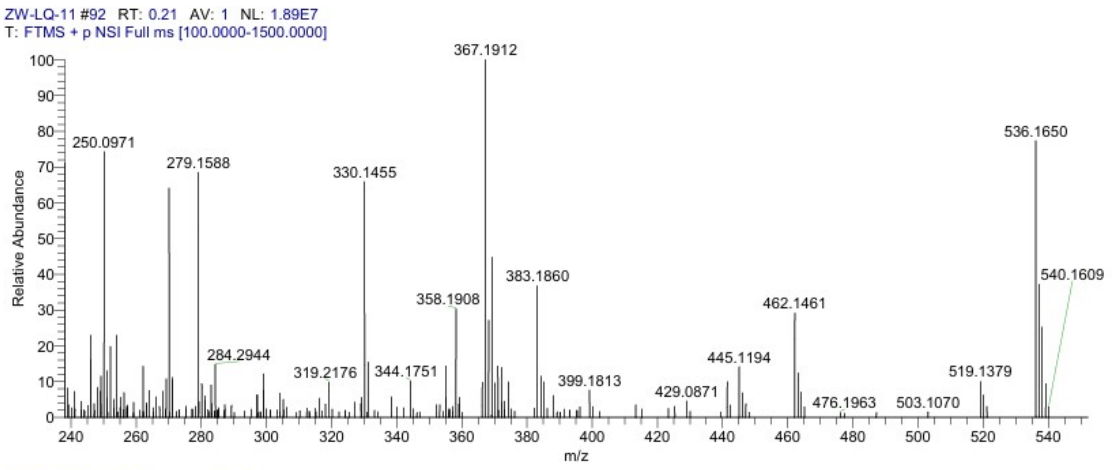

ZW-LQ-11#92 RT: 0.21
T: FTMS + p NSI Full ms [100.0000-1500.0000]
m/z= 365.89-397.55

m/z	Intensity	Relative	Theo. Mass	Delta (ppm)	Composition
367.1912	18916128.0	100.00	367.1917	-0.53	$C_{24}H_{23}N_4$

Figure S78. HRMS spectrum of LQM-N

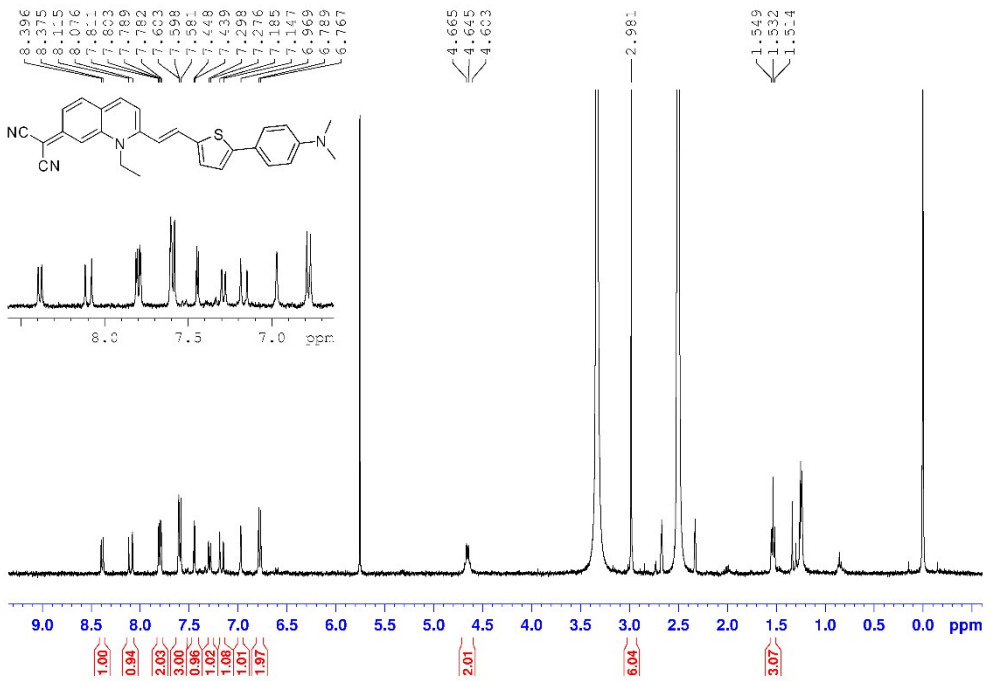

Figure S79. ^{1}H NMR spectrum of LQM-FN in DMSO-d_6

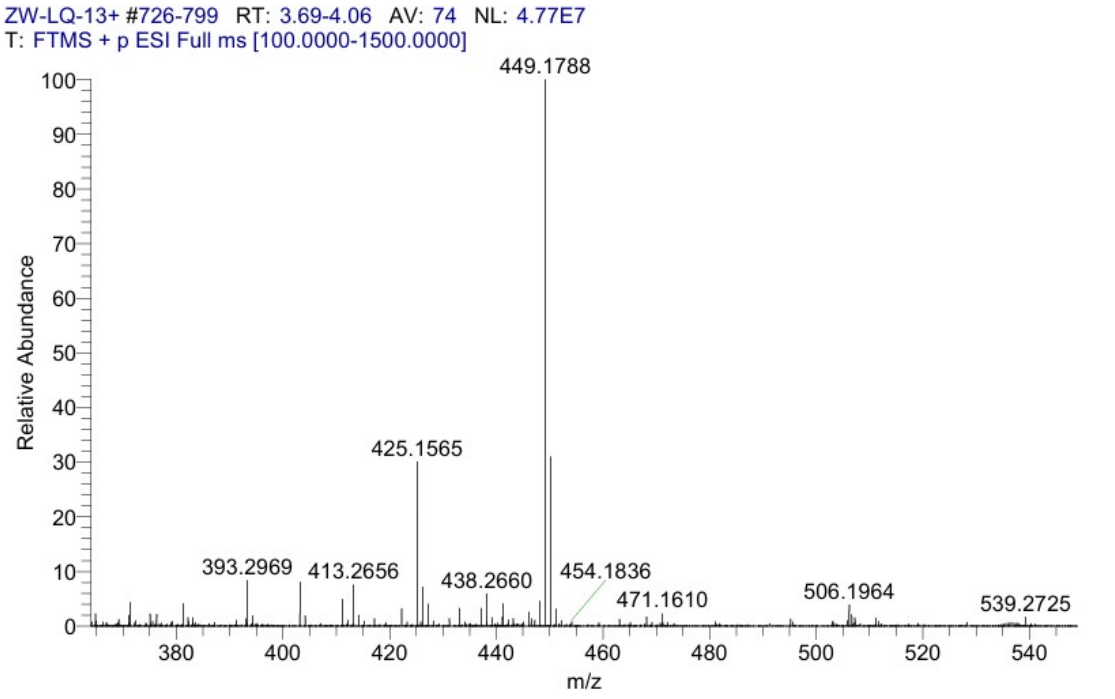

ZW-LQ-13+#746-794 RT: 3.79-4.03 AV: 49
T: FTMS + p ESI Full ms [100.0000-1500.0000]
m/z= 448.14-450.65

m/z	Intensity	Relative	Theo. Mass	Delta (ppm)	Composition
449.1788	59113424.0	100.00	449.1794	-0.60	$C_{28}H_{25}N_4S$

Figure S80. HRMS spectrum of LQM-FN

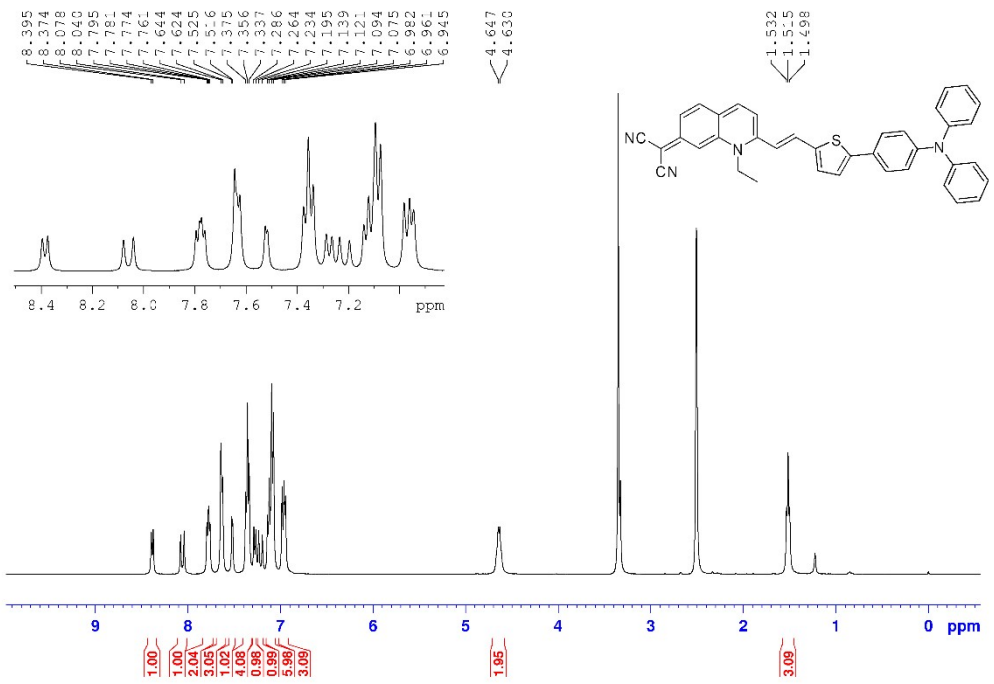

Figure S81. [1]H NMR spectrum of LQM-FT in DMSO-d_6

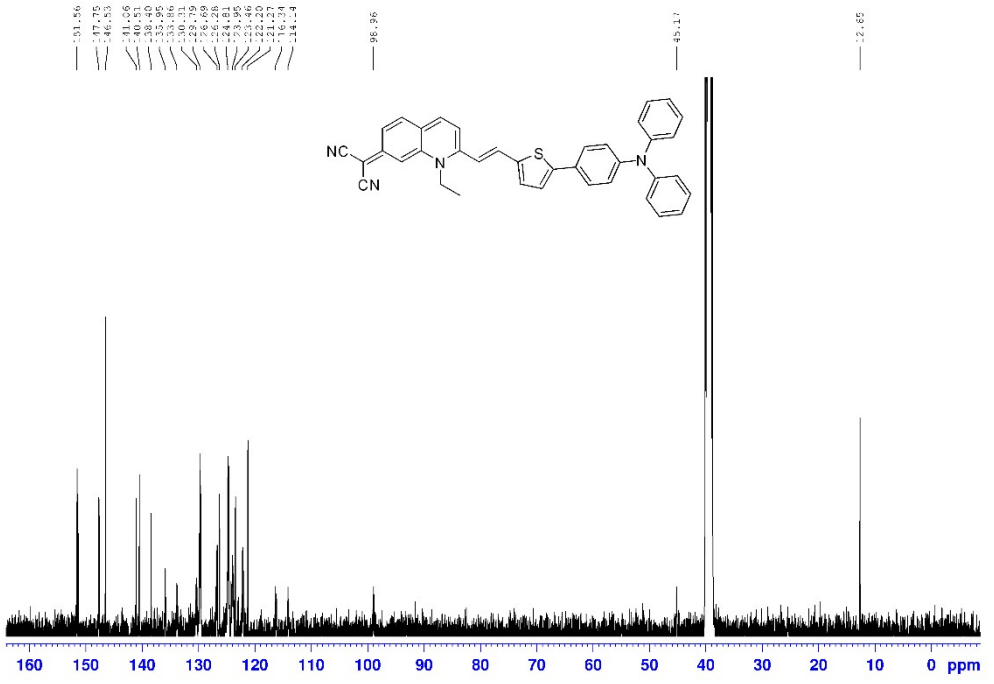

Figure S82. [13]C NMR spectrum of LQM-FT in DMSO-d_6

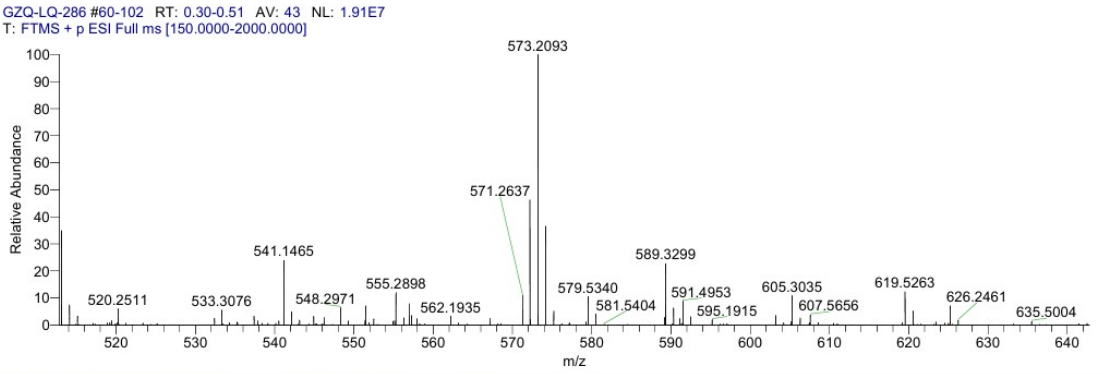

GZQ-LQ-286#60-102 RT: 0.30-0.51 AV: 43
T: FTMS + p ESI Full ms [150.0000-2000.0000]
m/z= 571.00-577.08

m/z	Intensity	Relative	Theo. Mass	Delta (ppm)	Composition
573.2093	19409938.0	100.00	573.2107	-1.41	$C_{38}H_{29}N_4S$

Figure S83. HRMS spectrum of LQM-FT

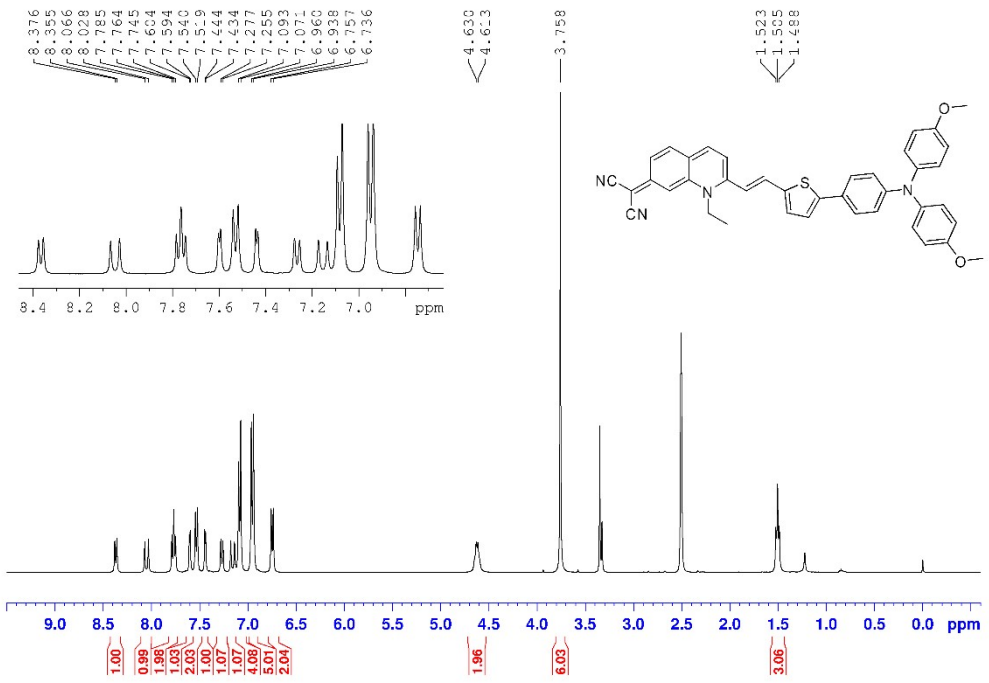

Figure S84. ^{1}H NMR spectrum of LQM-FTO in DMSO-d_6

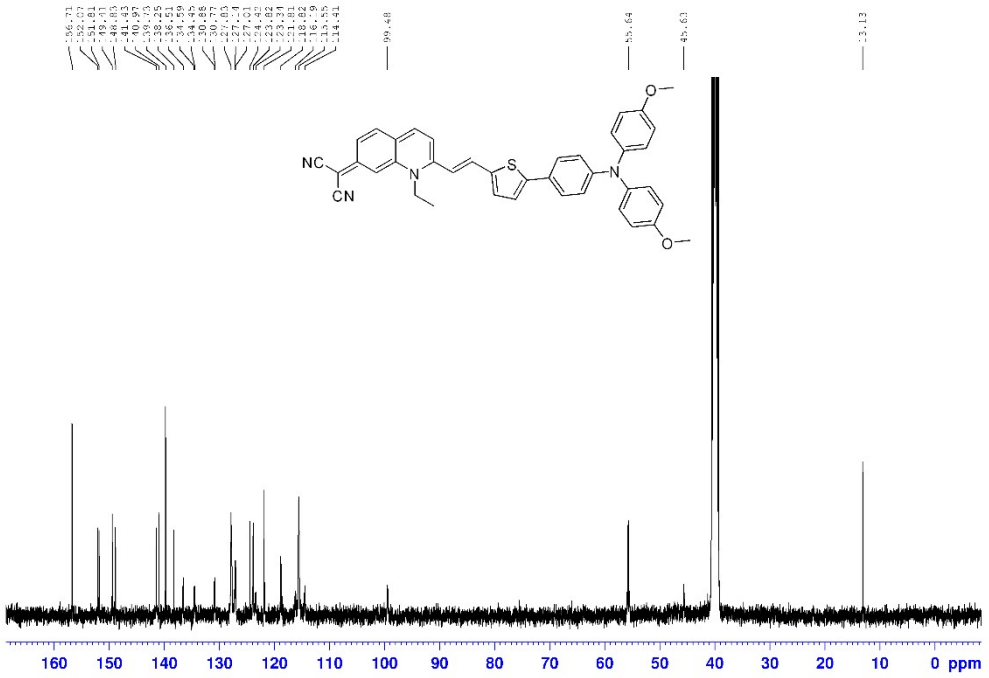

Figure S85. ^{13}C NMR spectrum of LQM-FTO in DMSO-d_6

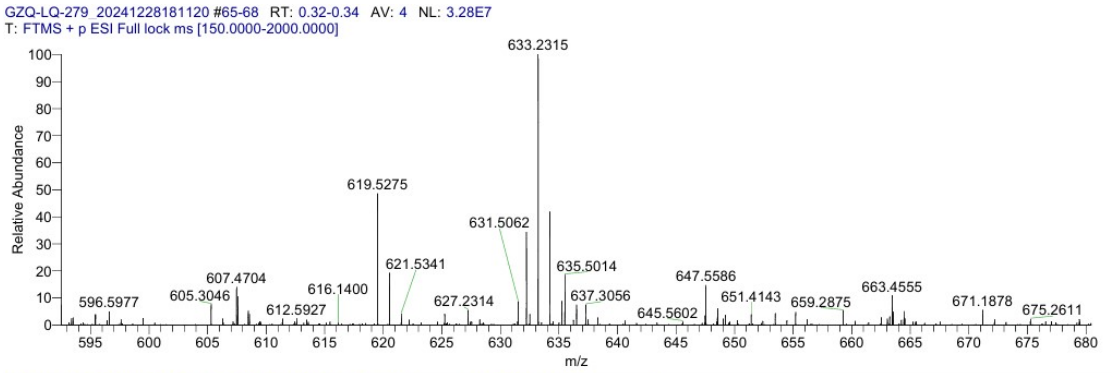

GZQ-LQ-279_20241228181120#65-68 RT: 0.32-0.34 AV: 4
T: FTMS + p ESI Full lock ms [150.0000-2000.0000]
m/z= 632.44-633.80

m/z	Intensity	Relative	Theo. Mass	Delta (ppm)	Composition
633.2315	33139320.0	100.00	633.2319	-0.34	$C_{40}H_{33}O_2N_4S$

Figure S86. HRMS spectrum of LQM-FTO

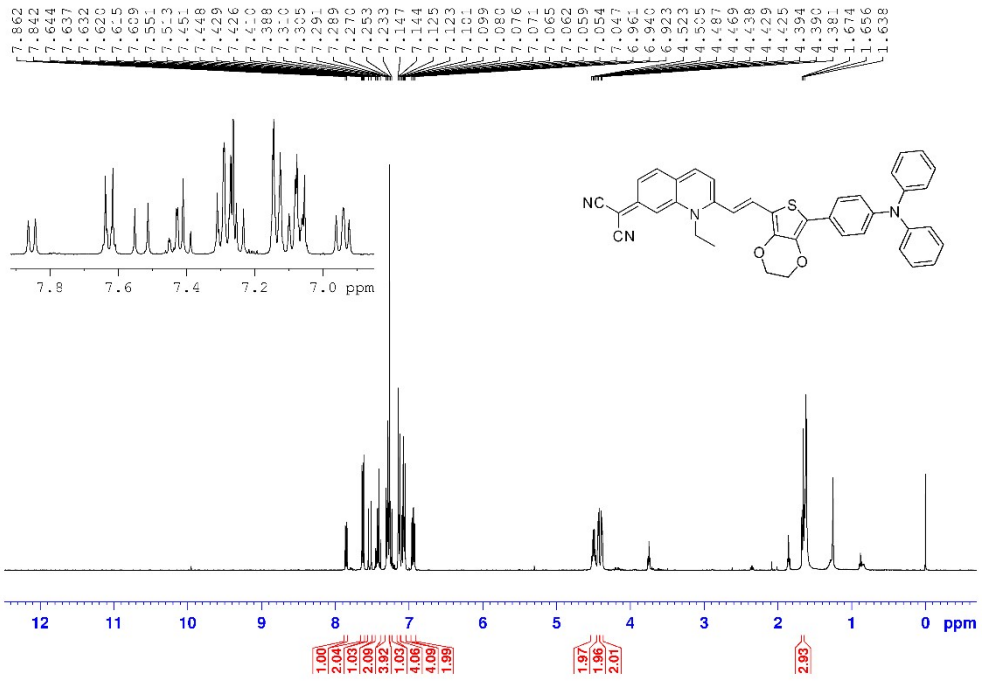

Figure S87. ^{1}H NMR spectrum of LQM-FOT in $CDCl_3$

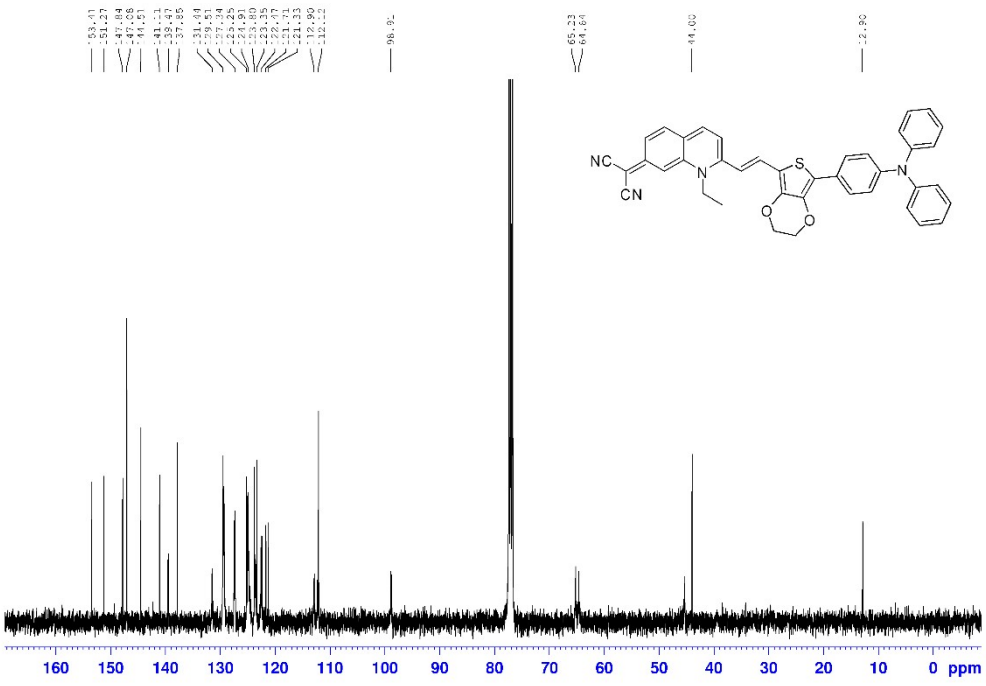

Figure S88. ^{13}C NMR spectrum of LQM-FOT in $CDCl_3$

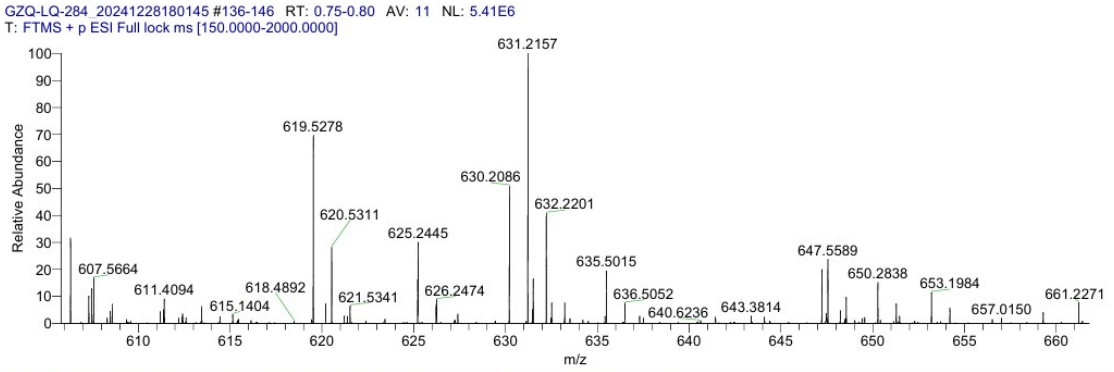

GZQ-LQ-284_20241228180145#136-147 RT: 0.75-0.80 AV: 12
T: FTMS + p ESI Full lock ms [150.0000-2000.0000]
m/z= 630.68-631.87

m/z	Intensity	Relative	Theo. Mass	Delta (ppm)	Composition
631.2157	5421407.0	100.00	631.2162	-0.50	$C_{40}H_{31}O_2N_4S$

Figure S89. HRMS spectrum of LQM-FOT

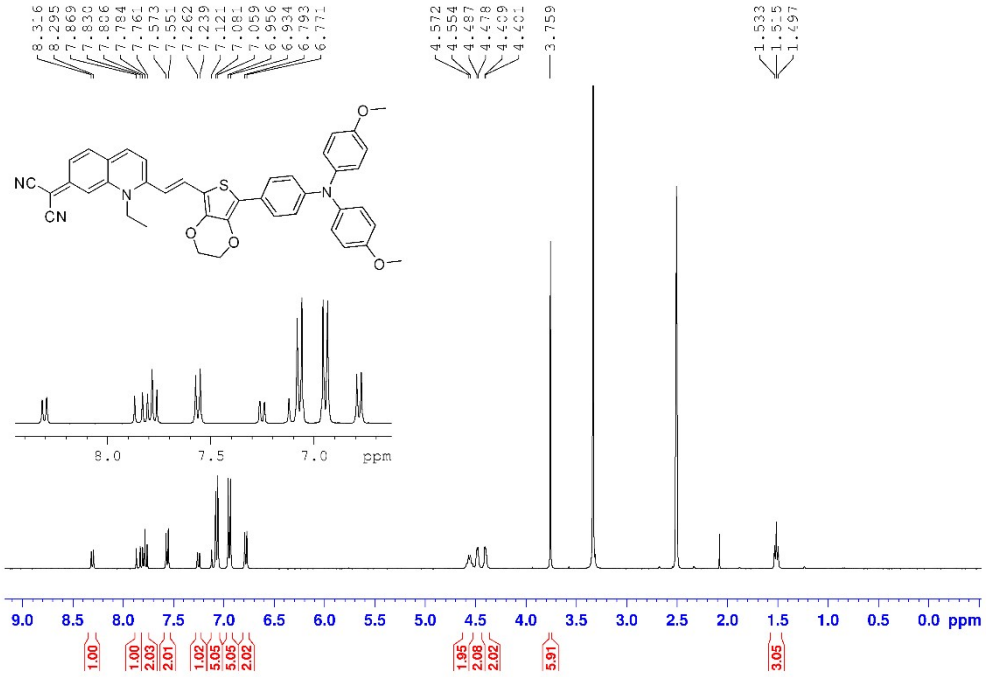

Figure S90. ^{1}H NMR spectrum of LQM-FOO in DMSO-d_6

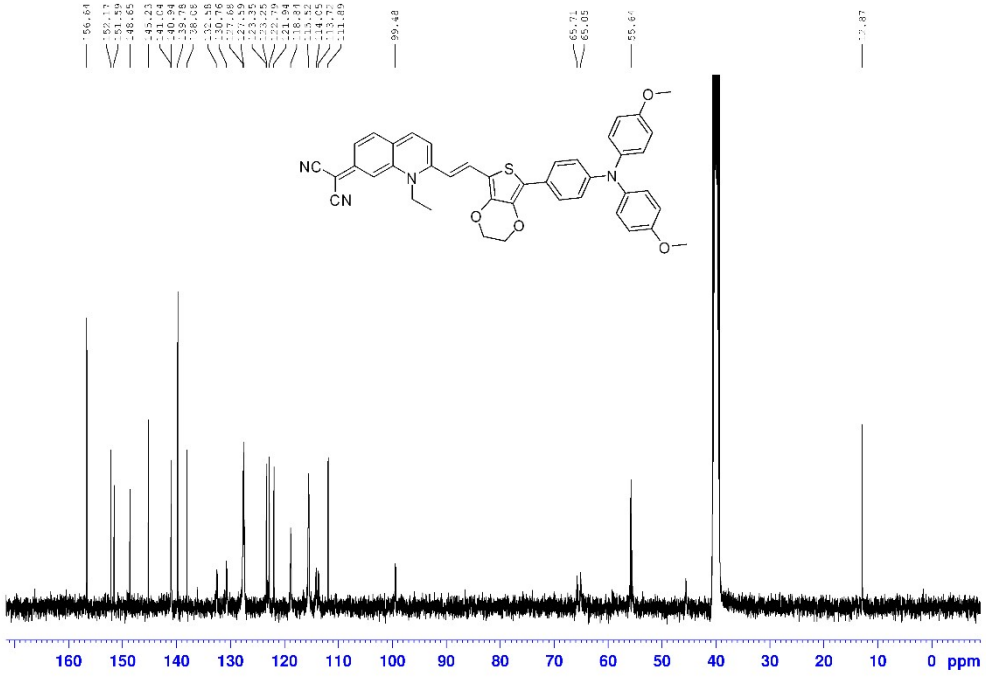

Figure S91. ^{13}C NMR spectrum of LQM-FOO in DMSO-d_6

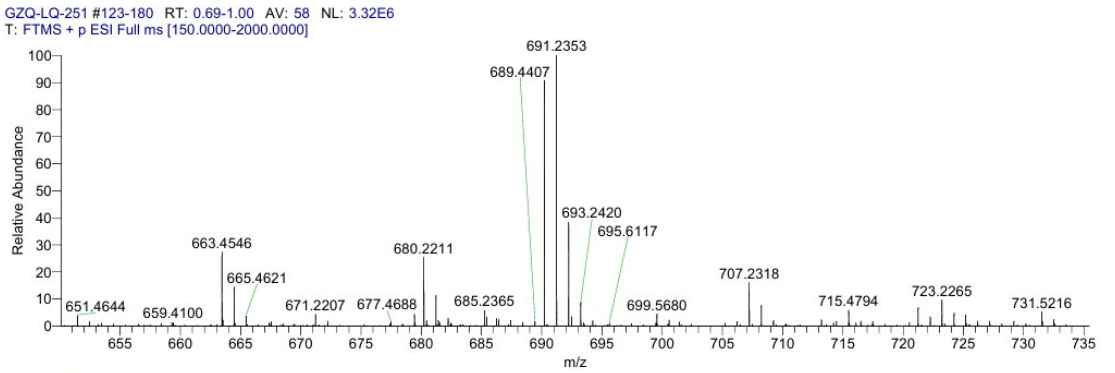

GZQ-LQ-251#123-180 RT: 0.69-1.00 AV: 58
T: FTMS + p ESI Full ms [150.0000-2000.0000]
m/z= 690.99-691.43

m/z	Intensity	Relative	Theo. Mass	Delta (ppm)	Composition
691.2353	3455705.5	100.00	691.2374	-2.10	$C_{42}H_{35}O_4N_4S$

Figure S92. HRMS spectrum of LQM-FOO

20. References

[1] Y. Yao, P. Ding, C. Yan, Y. Tao, B. Peng, W. Liu, J. Wang, M. A. Cohen Stuart and Z. Guo, *Angew. Chem., Int. Ed.,* 2023, **62**, 202218983.

[2] X. Fu, Y. Yao, Q. Liu, Z. Guo, C. Yan and W. H. Zhu, *Sci. China:Chem.,* 2025, **68**, 4497-4506.

[3] J. Huang, L. Su, C. Xu, X. Ge, R. Zhang, J. Song and K. Pu, *Nat. Mater.,* 2023, **22**, 1421-1429.

[4] S. Yao, F. Xu, Y. Wang, J. Shang, S. Li, X. Xu, Z. Liu, W. He, Z. Guo and Y. Chen, *J. Am. Chem. Soc.,* 2025, **147**, 11132-11144.

[5] H. Czili and A. Horváth, *Appl. Catal., B,* 2008, **81**, 295-302.

[6] H. Zhou, X. Zeng, A. Li, W. Zhou, L. Tang, W. Hu, Q. Fan, X. Meng, H. Deng, L. Duan, Y. Li, Z. Deng, X. Hong and Y. Xiao, *Nat. Commun.,* 2020, **11**, 6183.